1993

Flow In Tubes Of Non-circular Cross-sections

Raushan Ara Quadir

FLOW IN TUBES OF NON-CIRCULAR CROSS SECTIONS

by

Raushan A. Quadir

Department of Applied Mathematics

Submitted in partial fulfilment

of the requirements of the degree of

Doctor of Philosophy

Faculty of Graduate Studies

The University of Western Ontario

London, Ontario

April, 1993

ISBN 0-315-83992-9

Canada

ABSTRACT

In this thesis steady, laminar, viscous, incompressible flow in tubes of non-circular cross sections is investigated. The specific aims of the investigation are (a) to look at the problems of both *developing flow* and *fully developed flow*, (b) to consider non-circular cross sections in a more systematic manner than has been done in the past, and (c) to develop a relatively simple finite element technique for producing accurate numerical solutions of flow in tubes of fairly arbitrary cross sections.

Fully developed flow in tubes is governed by a Poisson type equation for the mainstream velocity. Both analytical and numerical solutions are considered. The cross sections studied include elliptic and rectangular cross sections of different aspect ratios, some triangular cross sections, and a series of crescent-shaped cross sections. The physical characteristics of the flow are examined in a systematic manner in order to determine how these characteristics are affected by certain geometrical features of the cross section. Solutions fall into three basic categories depending on the shape of the cross section. In the first category, which includes circular and elliptic cross sections, solutions are possible in closed form. In the second, including rectangular and some triangular cross sections, solutions are in the form of infinite series. In the third, including cross sections of more complicated or irregular shapes, only numerical

solutions are possible. Results of calculations of velocity profiles, flow rate, pumping power, and friction factor are presented in a way which can be useful for engineering applications.

In numerical studies of both developing and fully developed flow finite element techniques are used. Results are obtained for tubes of rectangular and elliptic cross sections of different aspect ratios, for tubes of crescent-shaped cross sections and a tube whose cross section is an oval of Cassini. For fully developed flow, results are compared with the corresponding exact solutions, where available. For rectangular and elliptic cross sections results are also compared with those obtained by using a commercial package (FIDAP). For developing flow finite element results are compared with corresponding theoretical and experimental results from previous work, where available.

To my parents

ACKNOWLEDGEMENTS

I would like to express my thanks to Dr. M. Zamir for suggesting the topic of this thesis, and for his continued interest, encouragement and guidance throughout the course of this work and in its final preparation.

I would also like to thank Dr. P.J. Sullivan and Dr. H. Rasmussen for their encouragement and help. I am also thankful to Dr. J.M. Floryan of the Mechanical Engineering Department for his valuable suggestions about FIDAP.

The Canadian Commonwealth Scholarship Agency deserves recognition for its financial support.

Much appreciation is given to the faculty, staff and fellow students of the Department of Applied Mathematics and to friends outside the department with whom I have been in contact, especially Muhit and his famlily.

I am happy at this opportunity to express my thanks to my parents, Sharif and Sitara, and my brothers and sisters for supporting me throughout my life. I owe a special thanks to my eldest brother Hanif for his enthusiasm and inspiration.

Finally, I am sincerely grateful to my husband, Shahed, whose endless love and understanding carried me through the most difficult of times.

Table of Contents

List of Figures

List of Tables

CHAPTER 1: GENERAL INTRODUCTION

1.1 Introduction

It is known that when a viscous fluid enters a tube of constant cross section, at a certain distance downstream it will assume a fully developed velocity profile which becomes invariant further downstream. While theoretically this condition is reached only asymptotically, for practical purposes an *entrance length* is usually defined as the distance downstream from entrance at which the centerline velocity attains 99% of its fully developed value. Flow in the developing region is generally referred to as the *developing* or *entry flow* and flow in the invariant region is known as the *fully developed flow*. In this thesis we consider both problems, in tubes of non-circular cross sections.

Flow in tubes is important because it has numerous applications in engineering and industry as well as in blood flow. While tubes of circular cross sections are the most common, tubes of non-circular cross sections are also fairly common in engineering and industrial applications, particularly in compact heat exchangers and in nuclear reactors. Furthermore, in installations such as these, the entrance length may be a significant part of the total length of the tube. An understanding of the velocity field is a necessary prerequisite to an understanding of the heat-transfer process. An accurate description of the velocities and pressure within the entrance region is needed to calculate pressure drop for inlets, e.g., to jet engines, and to correct data based on fully developed flow models, e.g., in viscometer studies.

The importance of determining the entrance length in engineering applications stems from the fact that the pressure difference required by entrance flow per length of tube is always higher than that required by fully developed flow. In tubes of non-circular cross sections this "penalty" is compounded by another. The pressure difference required by the flow in tubes of non-circular cross sections is always higher than that required by the corresponding flow in a tube of circular cross section. For various reasons the adverse effects of developing flow and those of non-circular cross sections have not been studied adequately *in combination*. The purpose of the present study is to do so, for tubes of a variety of non-circular cross sections.

1.2 Brief Historical Review

Flow in tubes was among the first viscous flow phenomena to be investigated both analytically and experimentally. The theory of viscous flow based on a set of general equations of motion for an incompressible fluid was first given by Navier in 1821. Based on different assumptions these equations were derived later by Poisson (1831) and Saint Venant (1843). The mathematical theory for steady laminar fully developed flow in tubes was given by Stokes (1845). Classical experimental investigations on the flow in a tube of circular cross section were carried out independently by Hagen (1839) and Poiseuille (1840). Fully developed flow in tubes has since been known as *Poiseuille or Hagen-Poiseuille flow.*

For fully developed flow it is possible to obtain exact analytical solutions for some specific cross sections. A solution for the flow in a tube of elliptic cross section was

obtained by Boussinesq (1868) and further discussion of the results were given by Greenhill (1881) and by Lees (1916). A solution for the flow in a tube of rectangular cross section was obtained by Graetz (1880). Galerkin (1919), Kolossoff (1924) and Paschoud (1924) obtained solution for the flow in a tube of right angle isosceles triangular cross section. Sheppard (1929), Taylor (1929) and Tao (1961) solved for the torsion problem in a prism whose cross section is a cardioid. Tao also obtained solution for forced convection problems of the flow in a tube of equilateral triangular cross section (1961) and a tube whose cross section is a Pascal's limacon (1962).

Clark & Kays (1953) used finite difference schemes to solve a heat-transfer problem for a tube of rectangular cross section. Schmidt & Newell (1967) used the scheme for flow in tubes of isosceles triangular and rectangular cross sections.

In the case of developing flow, because of the non-linear inertia terms in the governing equations, it is not possible to obtain exact solutions even in the simplest case of a circular cross section. Approximate methods must invariably be used in this case, consisting usually of some simplification of the Navier-Stokes equations, followed by a numerical solution of the simplified equations. The analysis of entry flow has so far been confined primarily to the case of a tube of circular cross section (Goldstein 1938, Schlichting 1968) or to that of two dimensional flow between parallel plates (Van Dyke 1970, Zamir & Camiletti 1982, Camiletti & Zamir 1984). For other cross sections, where the axial velocity component in a transverse cross section of the flow field is a function of *two* variables instead of one, there have been only a few isolated reports of theoretical or experimental work in the literature. Some of the theoretical results have been reviewed

by Shah and London (1978). The solutions are confined to selected rectangular and some triangular cross sections. Previous work on this problem can be divided into four general methods which have been used: simple matching, integral equations, linearized equations and numerical methods. These methods usually involved some form of Prandtl's boundary layer approximations, though in some cases the full Navier-Stokes equations have been used.

The matching method was first suggested by Boussinesq (1891), was used by Schlichting (1934) for the flow between parallel plates, and later by Atkinson & Goldstein (in Goldstein 1938) for the flow in a tube of circular cross section. Collins & Schowalter (1962), and Roidt & Cess (1962) improved Schlichting's solutions by utilizing additional terms in the expansion of the Blasius boundary layer function and in the perturbation of the fully developed flow. The integral method was first used by Schiller (1922) for the flow in a tube of circular cross section and for the flow between parallel plates. Later modifications and improvements of this method were made by Siegel (1953), Shapiro et al. (1954), and Campbell & Slattery (1963) for the flow in a tube of circular cross section and by Natio (1975) for the flow between parallel plates. Solutions of the linearized equation of motion were obtained by Langhaar (1942) and Targ (1951) for a tube of circular cross section, by Han for the flow in a tube of rectangular cross section (1960) and between parallel plates (1961) and by Han & Cooper (1962) for the flow in a tube of equilateral triangular cross section. Lundgren et al. (1964) used linearized equations to obtain a simple expression for the pressure drop due to flow development which requires a knowledge of only the fully developed velocity profile. McComas (1967) used the results of Lundgren et al. (1964) to predict the entrance length (but not the details of

flow development) in tubes of arbitrary cross sections. Miller & H. ר (1971) used the linearization technique for the flow in a tube of equilateral triangular cross section. Sparrow et al. (1964) used a different linearization technique to solve for the flow in a tube of circular cross section. Wiginton & Wendt (1969), Fleming & Sparrow (1969), Wiginton & Dalton (1970) and Aggarwala & Gangal (1975) extended this method to solve for the flow in tubes of rectangular and triangular cross sections.

In numerical studies of the developing flow problem mostly finite difference schemes have been used. Numerical solutions of the entry flow problem based on boundary layer equations were obtained by Bodoia & Osterle (1961) and Naito & Hishida (1972) for the flow between parallel plates and by Christiansen & Lemmon (1965), and Manohar (1969) for a tube of circular cross section. Patanker & Spalding (1972), Curr et al. (1972), Carlson & Hornbeck (1973), Briley (1974), and Garg (1983) obtained finite difference solutions for tubes of rectangular cross sections. Numerical solutions of the full Navier-Stokes equations were reported by Vrentas et al. (1966) and Friedmann et al. (1968) for a tube of circular cross section and by Wang & Longwell (1964), Gillis & Brandt (1964), and Morihara & Cheng (1973) for the flow between parallel plates.

1.3 Present Work

The purpose of this thesis is to consider the problems of developing and fully developed flow in tubes of non-circular cross sections in a more systematic manner than has been done in the past. We do this by looking at different classes of cross sections and considering the type of solution possible in each case, and by examining the full features

of the flow in each case so as to allow comparisons. The cross sections we studied include elliptic and rectangular cross sections of different aspect ratios, equilateral and right angle isosceles triangular cross sections, crescent-shaped cross sections of different thickness parameters and a cross section bounded by an *oval of Cassini*. We believe that this selection of cross sections represent an important range of cases both from the point of view of engineering and industrial applications and of solutions of the governing equations.

In Chapter 2 the derivation of the governing equations along with the boundary conditions of developing flow as well as fully developed flow is presented. The velocity profile in the entrance region of the tube is assumed to be uniform. For developing flow it is assumed that the streamwise viscous diffusion for all three velocity components are sufficiently small. For fully developed flow it is assumed that the velocity has only one component, which is in the direction of the flow.

In Chapter 3 analytical solutions for fully developed flow in tubes of some non-circular cross sections are presented. It is shown that the solutions for the mainstream velocity are unique, implying that the transverse velocity components are identically zero. We show that solutions fall into three basic categories depending on the shape of the cross section. In the first category, which includes circular, elliptic, equilateral triangular and crescent-shaped cross sections, solutions are possible in closed form. In the second, including rectangular and right angle isosceles triangular cross sections, solutions are in the form of infinite series. In the third, including cross sections of more complicated or irregular shapes, only numerical solutions are possible. Based on these

solutions we calculate and compare the results for the velocity profile, flow rate, pumping power, wall shear stress and friction factor in tubes of elliptic and rectangular cross sections of different aspect ratios, tubes of equilateral triangular and right angle isosceles triangular cross sections, and tubes of crescent-shaped cross sections. Results are presented in a way which can be useful for engineering and industrial applications. An important feature of rectangular, elliptic and crescent-shaped cross sections, which include the limiting cases of square and circular cross sections, is that they can be changed widely by changing their aspect ratios or thickness parameters. We are thus able to produce a systematic range of solutions for tubes of elliptic, rectangular and crescent-shaped cross sections. The purpose of this chapter is also to examine the physical characteristics of the flow in a representative series of cross sections to determine how these characteristics are affected by certain geometrical features of the cross section. Also, with these results we are able to examine the concept of corrective *shape factor* used in engineering and industrial applications.

In Chapter 4 finite element techniques are used to produce numerical solutions for fully developed flow in tubes of non-circular cross sections. The particular method we use is based on the *Galerkin weighted residual method*. Results are obtained for tubes of elliptic and rectangular cross sections of different aspect ratios, tubes of crescent-shaped cross sections and a tube whose cross section is an oval of Cassini. The last two cross sections are used as examples of arbitrary cross sections. These numerical results are compared with the corresponding analytical results, where available. Results for elliptic and rectangular cross sections are also compared with those obtained by using a commercial software package (FIDAP: Fluid Dynamics Analysis Package, Fluid

Dynamics International). FIDAP is a general purpose package designed for use on a mainframe only, for simulating flow problems, including the effects of heat transfer, in two-dimensional, axi-symmetric and three-dimensional geometries. The package was found to be rather inefficient because it is more comprehensive than is required by the present problem.

Solutions for developing flow in tubes of non-circular cross sections is presented in Chapter 5. This chapter first presents a review of various methods which have been used to produce solutions of this problem in the past, thus providing an opportunity to evaluate the effectiveness of these methods and the accuracy of their results. The results of these studies are also compiled and reduced to a standard format so as to allow comparison with each other and later with our own results. The main objective of this chapter is then to develop and present a finite element scheme for producing accurate numerical solutions of the governing equations for developing flow, and of comparing the results with existing theoretical and experimental results where available. Results are obtained for tubes of rectangular and elliptic cross sections of different aspect ratios, for a tube of crescent-shaped cross section and for a tube whose cross section is an oval of Cassini.

CHAPTER 2: GOVERNING EQUATIONS AND BOUNDARY CONDITIONS

2.1 Introduction

In this chapter the derivation of the governing equations along with the boundary conditions for the developing as well as fully developed flow is presented. The velocity profile in the entrance of the tube is assumed to be uniform. For developing flow it is assumed that the streamwise viscous diffusion for all three velocity components are sufficiently small. F· ·fully developed flow it is assumed that the velocity has only one component, which is in the direction of the flow.

2.2 Governing Equations for Developing Flow

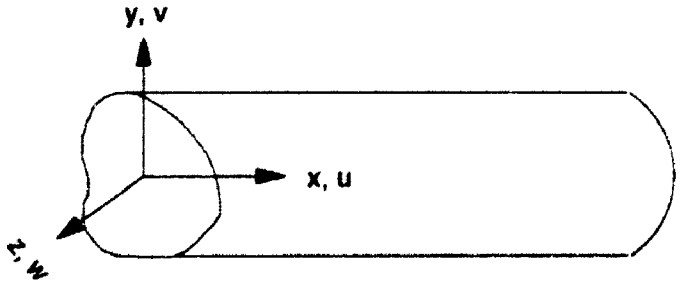

Sketch 2a: Schematic of a tube of arbitrary cross section.

Consider steady, laminar flow of a viscous, incompressible fluid in a tube of arbitrary cross section. Using rectangular Cartesian coordinates, x along the axis of the tube and

y,z in a cross section perpendicular to x (Sketch 2a). Let u,v,w be the components of velocity in the x,y,z directions, p be the pressure and μ the viscosity. The governing equations are obtained from Navier-Stokes equations

$$\rho\left(u\frac{\partial u}{\partial x}+v\frac{\partial u}{\partial y}+w\frac{\partial u}{\partial z}\right)=-\frac{\partial p}{\partial x}+\mu\left(\frac{\partial^2 u}{\partial x^2}+\frac{\partial^2 u}{\partial y^2}+\frac{\partial^2 u}{\partial z^2}\right) \qquad (2.2.1a)$$

$$\rho\left(u\frac{\partial v}{\partial x}+v\frac{\partial v}{\partial y}+w\frac{\partial v}{\partial z}\right)=-\frac{\partial p}{\partial y}+\mu\left(\frac{\partial^2 v}{\partial x^2}+\frac{\partial^2 v}{\partial y^2}+\frac{\partial^2 v}{\partial z^2}\right) \qquad (2.2.1b)$$

$$\rho\left(u\frac{\partial w}{\partial x}+v\frac{\partial w}{\partial y}+w\frac{\partial w}{\partial z}\right)=-\frac{\partial p}{\partial z}+\mu\left(\frac{\partial^2 w}{\partial x^2}+\frac{\partial^2 w}{\partial y^2}+\frac{\partial^2 w}{\partial z^2}\right) \qquad (2.2.1c)$$

and the equation of continuity

$$\frac{\partial u}{\partial x}+\frac{\partial v}{\partial y}+\frac{\partial w}{\partial z}=0 \qquad (2.2.2)$$

It is assumed that the streamwise viscous diffusion for all three velocity components are sufficiently small so that second derivatives with respect to x can be neglected compared with second derivatives in the y,z directions. With these assumptions the governing equations become

$$\rho\left(u\frac{\partial u}{\partial x}+v\frac{\partial u}{\partial y}+w\frac{\partial u}{\partial z}\right)=-\frac{\partial p}{\partial x}+\mu\left(\frac{\partial^2 u}{\partial y^2}+\frac{\partial^2 u}{\partial z^2}\right) \qquad (2.2.3a)$$

$$\rho\left(u\frac{\partial v}{\partial x}+v\frac{\partial v}{\partial y}+w\frac{\partial v}{\partial z}\right)=-\frac{\partial p}{\partial y}+\mu\left(\frac{\partial^2 v}{\partial y^2}+\frac{\partial^2 v}{\partial z^2}\right) \qquad (2.2.3b)$$

$$\rho\left(u\frac{\partial w}{\partial x}+v\frac{\partial w}{\partial y}+w\frac{\partial w}{\partial z}\right)=-\frac{\partial p}{\partial z}+\mu\left(\frac{\partial^2 w}{\partial y^2}+\frac{\partial^2 w}{\partial z^2}\right) \qquad (2.2.3c)$$

Nondimensionalizing the equations in the usual way

$$x^*=\frac{x}{D_h},\quad y^*=\frac{y}{D_h},\quad z^*=\frac{z}{D_h}$$

$$u^*=\frac{u}{\bar{u}},\quad v^*=\frac{v}{\bar{u}},\quad w^*=\frac{w}{\bar{u}},\quad p^*=\frac{p-p_o}{\rho\bar{u}^2} \qquad (2.2.4)$$

where stars denote dimensionless quantities, $\bar{u}$ is the mean axial velocity, ρ is the density, p_0 is the pressure at the tube entrance and D_h is the hydraulic diameter defined by

$$D_h=\frac{4\times cross\,sectional\,area}{perimeter}$$

Dropping the stars, the governing equations in dimensionless form thus become

$$u\frac{\partial u}{\partial x}+v\frac{\partial u}{\partial y}+w\frac{\partial u}{\partial z}=-\frac{\partial p}{\partial x}+\frac{1}{R_e}\left(\frac{\partial^2 u}{\partial y^2}+\frac{\partial^2 u}{\partial z^2}\right) \qquad (2.2.5a)$$

$$u\frac{\partial v}{\partial x}+v\frac{\partial v}{\partial y}+w\frac{\partial v}{\partial z}=-\frac{\partial p}{\partial y}+\frac{1}{R_e}\left(\frac{\partial^2 v}{\partial y^2}+\frac{\partial^2 v}{\partial z^2}\right) \qquad (2.2.5b)$$

$$u\frac{\partial w}{\partial x}+v\frac{\partial w}{\partial y}+w\frac{\partial w}{\partial z}=-\frac{\partial p}{\partial z}+\frac{1}{R_e}\left(\frac{\partial^2 w}{\partial y^2}+\frac{\partial^2 w}{\partial z^2}\right) \qquad (2.2.5c)$$

$$\frac{\partial u}{\partial x}+\frac{\partial v}{\partial y}+\frac{\partial w}{\partial z}=0 \qquad (2.2.6)$$

where R_e is the Reynolds number defined by

$$R_e=\frac{\rho \bar{u} D_h}{\mu}$$

The problem formulation is completed by specifying boundary and entry conditions. We have no-slip boundary condition on the wall of the tube. i.e.

$$u=v=w=0 \quad \text{at the tube wall} \qquad (2.2.7a)$$

An entry condition is also required and it is usually assumed that a uniform velocity profile applies at the entrance of the tube. i.e.

$$u(0,y,z)=1, \quad p(0,y,z)=0 \qquad (2.2.7b)$$

2.3 Governing Equations for Fully Developed Flow

For fully developed flow it is assumed that the flow velocity has only one component, $u(y,z)$, which is along the axis of the tube. The equation of continuity is

satisfied identically, while the y and z- momentum equations, Eqns. 2.2.1.b and 2.2.1c give

$$\frac{\partial p}{\partial y} = \frac{\partial p}{\partial z} = 0 \tag{2.3.1}$$

i.e. the pressure is constant over the cross section of the tube.

The x- momentum equation, Eqn. 2.2.1a gives

$$\frac{\partial^2 u}{\partial y^2} + \frac{\partial^2 u}{\partial z^2} = \frac{1}{\mu}\frac{dp}{dx} \tag{2.3.2}$$

Since dp/dx is a function of x alone and u is a function of y and z, the only way Eqn. 2.3.2 can be satisfied is if dp/dx is a constant. We let

$$\frac{1}{\mu}\frac{dp}{dx} = K$$

where K is a constant. Therefore Eqn. 2.3.2 becomes

$$\frac{\partial^2 u}{\partial y^2} + \frac{\partial^2 u}{\partial z^2} = \nabla^2 u = K \tag{2.3.3}$$

The statement of the problem is completed by the no-slip boundary condition, i.e.

$$u = 0 \quad \text{at the tube wall.} \tag{2.3.4}$$

The pressure distribution along the tube, must satisfy

$$p = \mu K x + k_1 \tag{2.3.5}$$

where k_1 is a constant. Thus if the pressure difference between the two ends of a tube of length l is P, the pressure gradient is usually written as

$$K = -\frac{P}{\mu l} \tag{2.3.6}$$

Finally the governing equation is

$$\frac{\partial^2 u}{\partial y^2} + \frac{\partial^2 u}{\partial z^2} = -\frac{P}{\mu l} \tag{2.3.7}$$

subject to $u = 0$ on the boundary of the tube. Because of the elliptic nature of this equation, a change in the shape of the boundary in a small region of the wall affects the solution in the entire cross section.

CHAPTER 3: ANALYTICAL SOLUTIONS FOR FULLY DEVELOPED FLOW IN TUBES OF SOME NON-CIRCULAR CROSS SECTIONS

3.1 Introduction

Fully developed flow in tubes of arbitrary cross sections is governed by a Poisson type equation (2.3.7) for the mainstream velocity component. It can be shown that solutions of this equation are unique. It can also be shown that the transverse velocity components are identically zero (Sec. 3.2).

There has been only isolated solutions of this equation for specific cross sections (Dryden et al., 1956 and Berker, 1963) and these have generally dealt with only some aspect of the flow. The purpose of this chapter is to consider the problem of fully developed flow in tubes of non-circular cross sections in a more systematic manner. We do this by looking at different classes of cross sections and considering the type of solution possible in each case, and by examining the full features of the flow in each case so as to allow comparisons.

Thus we show first that solutions fall into three basic categories depending on the shape of the cross section. In the first category, which includes circular, elliptic, equilateral triangular and crescent-shaped cross sections, solutions are possible in closed form. In

the second, including rectangular and right angle isosceles triangular cross sections, solutions are in the form of infinite series. In the third, including cross sections of more complicated or irregular shapes, only numerical solutions are possible.

Based on these solutions we then calculate and compare the results for velocity profile, maximum and average velocity, flow rate, pumping power, wall shear stress and friction factor. The cross sections we studied include elliptic and rectangular cross sections of different aspect ratios, equilateral and right angle isosceles triangular cross sections, and crescent-shaped cross sections. We believe that this selection of cross sections represent an important range of cases both from the point of view of engineering and industrial applications and of solutions of the governing equations.

3.2 Uniqueness of Solutions

A simple theorem by Chorlton (1967) establishes the uniqueness of the solution, which states that if $\nabla^2 u = f(y,z)$ at all points (y,z) of a region S in the plane Oy, Oz bounded by the closed curve C and if f is prescribed at each point (y,z) of S, and u is prescribed at each point of C, then any solution $u = u(y,z)$ satisfying these conditions is unique.

The proof proceeds by letting $u = u_1(y,z)$ and $u = u_2(y,z)$ be two solutions of $\nabla^2 u = f(y,z)$ in a closed region S in the yz-plane subject to $u_1 = 0$, $u_2 = 0$ on C.

Let $$U(y,z) = u_1(y,z) - u_2(y,z),$$

then $\nabla^2 U = 0$ in S, since each of u_1 and u_2 satisfy the governing equation (2.3.7). Also $U = 0$ on C where $u_1 = u_2 = 0$.

Consider

$$I = \int\int_S \left\{ \left(\frac{\partial U}{\partial y} \right)^2 + \left(\frac{\partial U}{\partial z} \right)^2 \right\} dy dz$$

which can be written as

$$I = \int\int_S \left\{ \left(\frac{\partial U}{\partial y} \right)^2 + \left(\frac{\partial U}{\partial z} \right)^2 + U\left(\frac{\partial^2 U}{\partial y^2} + \frac{\partial^2 U}{\partial z^2} \right) \right\} dy dz$$

$$= \int\int_S \left\{ \frac{\partial}{\partial y}\left(U \frac{\partial U}{\partial y} \right) + \frac{\partial}{\partial z}\left(U \frac{\partial U}{\partial z} \right) \right\} dy dz$$

and using Green's theorem this becomes

$$I = \oint_C \left(U \frac{\partial U}{\partial y} dz - U \frac{\partial U}{\partial z} dy \right)$$

Since $U = 0$ on C, we have $I = 0$, which shows that $(\partial U/\partial y)^2 + (\partial U/\partial z)^2 = 0$ in S. Hence $\partial U/\partial y = \partial U/\partial z = 0$ at every point of S.

It thus follows that $U =$ constant in S, and since $U = 0$ on C then it follows that $U = 0$ everywhere in S. Hence the solution is unique.

Following Maslen (1958) it can be shown directly that the transverse velocity components in fully developed flow in a tube are in fact zero everywhere.

The proof proceeds by letting v, w be the velocity components in the y and z directions, and introducing a stream function $\psi(y,z)$ such that $v = \partial\psi/\partial z$, $w = -\partial\psi/\partial y$. Using Green's theorem it can be shown that

$$\int_s (\nabla^2\psi)^2 dydz = 0$$

where S is a closed region in the yz-plane. This is only possible if $\nabla^2\psi = 0$ everywhere in S, and since $\partial\psi/\partial y = \partial\psi/\partial z = 0$ on the boundary of S, it follows that ψ is a constant and the transverse velocity components are thus zero everywhere.

3.3 Membrane and Torsion Analogies

Steady unidirectional flow in a tube of arbitrary cross section is governed by Poisson equation (2.3.7). There is thus analogy between the problem and any other phenomenon governed by the same equation. We describe briefly here the analogy with the problem of deflection of a thin elastic membrane in tension under a uniform pressure, and that of the torsion of a long solid prism .

(a) Membrane Analogy:

Here the velocity in laminar flow through a tube is analogous to the displacement of a thin membrane (stretched over a cross section) due to excess pressure on one side. This was first mentioned by Prandtl (1903), and is known as the *membrane analogy*. The equation governing the displacement ξ of the membrane in the x-direction is

$$\frac{\partial^2 \xi}{\partial y^2}+\frac{\partial^2 \xi}{\partial z^2}=-\frac{\delta p}{T} \tag{3.3.1}$$

in which δp is the difference between the pressure on the concave side and that on the convex side of the membrane, and T is the surface tension, assuming δp is not too large. Comparing this Poisson equation, with that for u (2.3.7) we see that ξ is analogous to u. The boundary conditions are also analogous, since both u and ξ vanish on the boundary of the cross section. Thus, by properly adjusting δp, u and ξ can be made to be numerically the same. This problem was solved by Griffith (1918) and Taylor (1923).

(b) Torsion Analogy:

Langlois (1964), in studying the more general problem of steady flow through a straight tube of arbitrary cross section, pointed out the analogy with the torsion problem of an elastic bar of the same cross section as the tube. For a long solid prism under torsion there exists a *torsion function*, ψ, that satisfies the equation (Sokolnikoff, 1946)

$$\frac{\partial^2 \psi}{\partial y^2}+\frac{\partial^2 \psi}{\partial z^2}=0 \tag{3.3.2}$$

and the boundary condition

$$\psi=\frac{1}{2}(y^2+z^2) \quad \text{on the boundary of the prism.} \tag{3.3.3}$$

Thus the function $\psi - \frac{1}{2}(y^2 + z^2)$ is analogous to the velocity u in the flow problem.

The cross section of the tube is same as that of the prism. This analogy was first indicated by Boussinesq (1871) and was used by Paschoud (1924).

The torsion problem can also be formulated in terms of a *stress function* ϕ, which is defined by

$$\phi = \psi(y,z) - \frac{1}{2}(y^2 + z^2) \tag{3.3.4}$$

Thus the stress function ϕ satisfies the Poisson equation

$$\frac{\partial^2 \phi}{\partial y^2} + \frac{\partial^2 \phi}{\partial z^2} = -2 \tag{3.3.5}$$

and on the boundary ϕ is zero. Thus the determination of the stress distribution over a cross section of a twisted bar consists in finding a function ϕ that satisfies Eqn. 3.3.5 and is zero at the boundary. The shear stress at any point in the cross section is given by the gradient of this stress function. Some solutions of the torsion problem for non-circular cross sections were first given by Saint-Venant (1855). Solutions of the torsion of elliptic, rectangular and triangular prisms are reviewed by Love (1944) and Sokolnikoff (1946).

It was shown by Polya (1948) that if beams were to be designed to withstand torsional loads alone, then of all cross sections of a given area, the circle has the maximum

torsional rigidity. Also, among all quadrilaterals of a given area, the square has maximum torsional rigidity. We show later that these properties of the circular and square cross sections are analogous to unique flow properties in tubes of such cross sections.

3.4 Solution for Elliptic Cross Sections

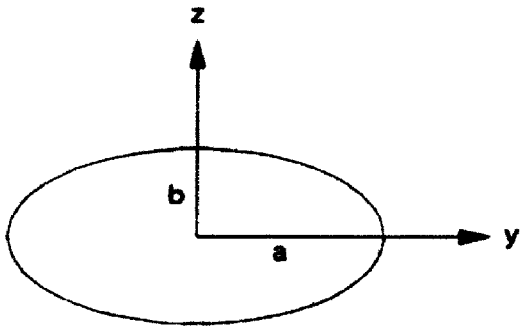

Sketch 3a: Elliptic cross section.

For a tube of elliptic cross section (Sketch 3a) of major and minor axes $2a, 2b$ respectively, the function $y^2/a^2 + z^2/b^2 - 1$ is zero on the boundary.

We thus seek a solution in the form (Panton, 1984)

$$u = Ay^2 + Bz^2 + C \tag{3.4.1}$$

The constants A, B, C are determined from the requirement that this expression must satisfy the boundary condition $u = 0$ on the circumference of the ellipse.

From Eqns. 3.4.1 and 2.3.7

$$2A + 2B = -\frac{P}{\mu l} \tag{3.4.2}$$

and from the condition $u = 0$ on the boundary $y^2/a^2 + z^2/b^2 - 1 = 0$, we have

$$A = \frac{M}{a^2}, \qquad B = \frac{M}{b^2} \qquad \text{and} \qquad C = -M \tag{3.4.3}$$

where M is any constant.

Inserting Eqn. 3.4.3 into (3.4.2) and solving for M we get

$$M = -\frac{P}{2\mu l}\frac{a^2 b^2}{(a^2 + b^2)}$$

Thus the arbitrary constants are given by

$$A = -\frac{P}{2\mu l}\frac{b^2}{(a^2 + b^2)},$$

$$B = -\frac{P}{2\mu l}\frac{a^2}{(a^2 + b^2)}$$

$$C = \frac{P}{2\mu l}\frac{a^2 b^2}{(a^2 + b^2)}.$$

Using these expressions in Eqn. 3.4.1, we have the following solution for the velocity in a tube of elliptic cross section

$$u = \frac{P}{2\mu l}\frac{a^2b^2}{(a^2+b^2)}\left[1-\frac{y^2}{a^2}-\frac{z^2}{b^2}\right] \tag{3.4.4}$$

Basic Properties of the Flow

The maximum velocity, which is obtained at the center of the tube is given by

$$\hat{u} = \frac{P}{2\mu l}\frac{a^2b^2}{(a^2+b^2)} \tag{3.4.5}$$

The volume rate of flow is given by

$$\begin{aligned} Q_v &= 4\int_0^b \int_0^{a\sqrt{(1-z^2/b^2)}} u\,dy\,dz \\ &= \frac{2P}{\mu l}\frac{a^2b^2}{(a^2+b^2)}\int_0^b \int_0^{a\sqrt{(1-z^2/b^2)}}\left[1-\frac{y^2}{a^2}-\frac{z^2}{b^2}\right]dy\,dz \\ &= \frac{\pi P}{4\mu l}\frac{a^3b^3}{(a^2+b^2)} \\ &= \frac{Pa^4}{\mu l}\frac{\pi\alpha^3}{4(1+\alpha^2)}, \quad \alpha = \frac{b}{a} \end{aligned} \tag{3.4.6}$$

and the mean velocity

$$\tilde{u} = \frac{Q}{\pi a b}$$

$$= \frac{P}{4\mu l}\frac{a^2 b^2}{(a^2+b^2)}$$

$$= \frac{\hat{u}}{2} \tag{3.4.7}$$

Thus the mean velocity is one-half of the maximum velocity for all values of the aspect ratios α, which is a unique property of elliptic cross sections.

The pumping power required to drive the flow is

$$H_r = PQ$$

$$= \frac{4\mu l}{\pi}\frac{(a^2+b^2)}{a^3 b^3}Q^2$$

$$= \frac{4\mu l}{\pi a b}\left(1+\frac{1}{\alpha^2}\right)\frac{Q^2}{a^2} \tag{3.4.8}$$

The shear stress at a point (y_1, z_1) on the wall is given by (Lees, 1916)

$$\tau_r = \mu\frac{du}{d\eta}$$

where η is the normal at a point (y_1, z_1) on the boundary and $du/d\eta$ is the directional derivative at that point. Since

$$\frac{du}{d\eta} = \left[\left(\frac{\partial u}{\partial y}\right)^2 + \left(\frac{\partial u}{\partial z}\right)^2\right]^{1/2}$$

then
$$\tau_r = \mu\left[\left(\frac{\partial u}{\partial y}\right)^2 + \left(\frac{\partial u}{\partial z}\right)^2\right]^{1/2}$$
$$= 4\mu\tilde{u}\sqrt{(y_1^2/a^4 + z_1^2/b^4)}$$
$$= 4\mu\tilde{u}/h \qquad (3.4.9)$$

The shear stress at a point on the surface varies inversely with the perpendicular distance, h, from the center of the ellipse to the tangent line at that point.

3.5 Solution for an Equilateral Triangular Cross Section

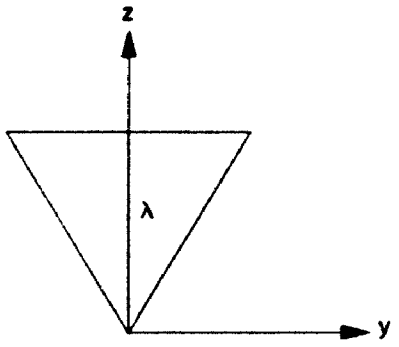

Sketch 3b: Equilateral triangular cross section.

For an equilateral triangular cross section (Sketch 3b) bounded by the lines $z = \lambda, z = \pm y\sqrt{3}$, the function

$$u = C(z - \lambda)(y^2 - z^2/3) \qquad (3.5.1)$$

is zero on the boundary, where C is a constant. From (3.5.1)

$$\frac{\partial^2 u}{\partial y^2} = 2C(z-\lambda)$$

and

$$\frac{\partial^2 u}{\partial z^2} = 2C\left(\frac{1}{3}\lambda - z\right)$$

Substituting these expressions in Eqn. 2.3.7 and solving for C we get

$$C = \frac{3}{4\lambda}\frac{P}{\mu l}$$

Hence the velocity in a tube of equilateral triangular cross section is given by

$$u = \frac{P}{\mu l}\frac{3}{4\lambda}(z-\lambda)\left(y^2 - \frac{z^2}{3}\right)$$

$$= \frac{P}{\mu l}\frac{1}{4\lambda}(z-\lambda)(3y^2 - z^2) \qquad (3.5.2)$$

Basic Properties of the Flow

The maximum velocity, which occurs at the center of gravity of the cross section i.e. $y = 0, z = 2\lambda/3$ is given by

$$\hat{u} = \frac{P}{\mu l}\frac{\lambda^2}{27} \qquad (3.5.3)$$

The flow rate is given by

$$Q_{et} = 2\int_0^{\lambda}\int_0^{z/\sqrt{3}} u\,dydz$$

$$= \frac{P}{2\mu l\lambda}\int_0^{\lambda}\int_0^{z/\sqrt{3}} (z-\lambda)(3y^2 - z^2)dydz$$

$$= \frac{P\lambda^4}{\mu l}\frac{\sqrt{3}}{180} \qquad (3.5.4)$$

and the mean velocity is

$$\tilde{u} = \frac{Q}{\lambda^2/\sqrt{3}}$$

$$= \frac{P\lambda^2}{60\mu l}$$

$$= \frac{9}{20}\hat{u} \qquad (3.5.5)$$

The pumping power required to drive the flow is given by

$$H_{et} = 60\sqrt{3}\frac{\mu l}{\lambda^4}Q^2$$

$$= \frac{60\mu l}{(\lambda^2/\sqrt{3})}\frac{Q^2}{\lambda^2} \qquad (3.5.6)$$

The shear stress at a general point on the base of the triangle is given by

$$\tau_{et} = \frac{15}{\lambda}\tilde{u}\left(1 - 3\frac{y^2}{\lambda^2}\right) \qquad (3.5.7)$$

where the base extends from $y = -\lambda/\sqrt{3}$ to $y = \lambda/\sqrt{3}$.

3.6 Solution for Rectangular Cross Sections

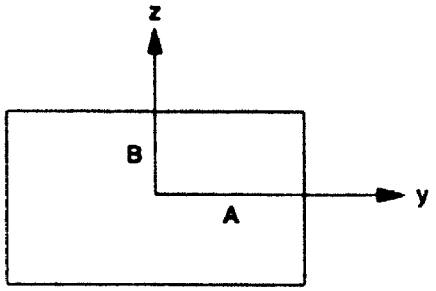

Sketch 3c: Rectangular cross section.

For a rectangular cross section (Sketch 3c) bounded by $y = \pm A, z = \pm B$, a particular integral of the governing equation (Eqn. 2.3.7) satisfying $u = 0$ on $z = \pm B$ is

$$u_1(y,z) = \frac{P}{2\mu l}(B^2 - z^2) \tag{3.6.1}$$

Separation of variables then yields the following general solution of the homogeneous equation

$$u_2(y,z) = \sum_{n=0}^{\infty} C_n \cosh(My)\cos(Mz) \tag{3.6.2}$$

where $M = (2n+1)\pi/2B, \quad n = 0, 1, 2, \ldots$

By superposition, a general solution satisfying the no-slip boundary condition at $z = \pm B$ is given by

$$u(y,z) = \frac{P}{2\mu l}(B^2 - z^2) + \sum_{n=0}^{\infty} C_n \cosh(My)\cos(Mz) \tag{3.6.3}$$

We find C_n such that the no-slip boundary condition at $y = \pm A$ is satisfied . This requires that

$$-\frac{P}{2\mu l}(B^2 - z^2) = \sum_{n=0}^{\infty} C_n \cosh(MA)\cos(Mz)$$

for $-B \le z \le B$.

The right hand side is a Fourier series expansion for the function $-(P/2\mu l)(B^2 - z^2)$. Multiplying both sides by $\cos(Mz)$ and integrating from $z = -B$ to $z = B$, we find

$$C_n = \frac{(-1)^{n+1}32B^2}{(2n+1)^3\pi^3\cosh(MA)}\frac{P}{2\mu l} \tag{3.6.4}$$

Hence the velocity in a tube of rectangular cross section is given by

$$u(y,z) = \frac{P}{2\mu l}\left[B^2 - z^2 - \frac{4}{B}\sum_{n=0}^{\infty}(-1)^n \frac{\cosh(My)\cos(Mz)}{M^3\cosh(MA)}\right] \tag{3.6.5}$$

Basic Properties of the Flow

The maximum velocity, which occurs at the center of the tube is given by

$$\hat{u} = \frac{P}{2\mu l}\left[B^2 - \frac{4}{B}\sum_{n=0}^{\infty}(-1)^n M^{-3} sech(MA)\right] \tag{3.6.6}$$

The volume rate of flow is given by

$$\begin{aligned} Q_r &= 4\int_0^B \int_0^A u\,dy\,dz \\ &= \frac{2P}{\mu l}\int_0^B \int_0^A \left[B^2 - z^2 - \frac{32B^2}{\pi^3}\sum_{n=0}^{\infty}\frac{(-1)^n \cosh(My)\cos(Mz)}{(2n+1)^3\cosh(MA)}\right]dy\,dz \\ &= \frac{P}{\mu l}\left[\frac{4}{3}B^3 A - \frac{8}{B}\sum_{n=0}^{\infty} M^{-5}\tanh(MA)\right] \\ &= \frac{PA^4}{\mu l}\left[\frac{4}{3}\beta^3 - \frac{256}{\pi^5}\beta^4\sum_{n=0}^{\infty}\frac{\tanh(MA)}{(2n+1)^5}\right], \quad \beta = \frac{B}{A} \end{aligned} \tag{3.6.7}$$

and the mean velocity is in the form

$$\begin{aligned} \tilde{u} &= \frac{Q}{4AB} \\ &= \frac{P}{\mu l}\left[\frac{1}{3}B^2 - \frac{2}{B^2 A}\sum_{n=0}^{\infty} M^{-5}\tanh(MA)\right] \end{aligned} \tag{3.6.8}$$

The ratio of maximum to mean velocity is clearly not a constant as it is in the case of elliptic cross sections. Here it depends on the aspect ratio $\beta = B/A$.

The pumping power is obtained as

$$H_r = \mu l\left[\frac{4}{3}B^3A - \frac{8}{B}\sum_{n=0}^{\infty} M^{-5}\tanh(MA)\right]^{-1} Q^2$$

$$= \frac{\mu l}{4AB}\left[\frac{\beta^2}{3} - \frac{2}{A^7\beta^4}\sum_{n=0}^{\infty} M^{-5}\tanh(MA)\right]^{-1}\frac{Q^2}{A^2} \qquad (3.6.9)$$

3.7 Solution for a Right Angle Isosceles Triangular Cross Section

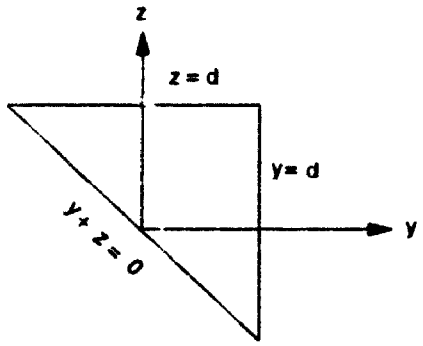

Sketch 3d: Right angle isosceles triangle.

Following Kolossoff (1924), the solution for a right angle isosceles triangular cross section (Sketch 3d) can be constructed in a similar way to that for a rectangular cross section.

If the cross section of the tube is bounded by the lines $y = d, z = d, y + z = 0$, we consider the harmonic functions

$$u_1 = \frac{P}{2\mu l}\left[d^2 + \frac{1}{2}(z^2 - y^2) - (y - d)(z - d) - 4d^2\left(\frac{2}{\pi}\right)^3 F_1\right] \qquad (3.7.1a)$$

$$u_2 = \frac{P}{2\mu l}\left[d^2 + \frac{1}{2}(y^2 - z^2) - (y - d)(z - d) - 4d^2\left(\frac{2}{\pi}\right)^3 F_2\right] \qquad (3.7.1b)$$

where
$$F_1 = \sum_{n=0}^{\infty} \frac{(-1)^n}{(2n+1)^3} \frac{\sinh\{(2n+1)\pi z/2d\}\cos\{(2n+1)\pi y/2d\}}{\sinh\{(2n+1)\pi/2\}} \qquad (3.7.2a)$$

and
$$F_2 = \sum_{n=0}^{\infty} \frac{(-1)^n}{(2n+1)^3} \frac{\sinh\{(2n+1)\pi y/2d\}\cos\{(2n+1)\pi z/2d\}}{\sinh\{(2n+1)\pi/2\}} \qquad (3.7.2b)$$

In order to satisfy no-slip boundary condition we require

$$u = \frac{P}{2\mu l}\left[\frac{1}{2}(u_1+u_2) - \frac{1}{2}(y^2+z^2)\right] \qquad (3.7.3)$$

and the solution for the velocity in a tube of right angle isosceles triangular cross section is thus given by

$$u = \frac{P}{2\mu l}\left[-yz + d(y+z) - \frac{1}{2}(y^2+z^2) - 2\left(\frac{2}{\pi}\right)^3 d^2 F(y,z)\right] \qquad (3.7.4)$$

where

$$F(y,z) = \sum_{n=0}^{\infty} \frac{(-1)^n \sinh(Nz)\cos(Ny) + \sinh(Ny)\cos(Nz)}{(2n+1)^3 \sinh(Nd)}$$

and
$$N = \frac{(2n+1)\pi}{2d} \qquad (3.7.5)$$

Basic Properties of the Flow

The maximum velocity, which occurs when $y = z = 3d/8$ is given by

$$\hat{u} = \frac{P}{2\mu l}\left[\frac{15d^2}{32} - \frac{32d^2}{\pi^3}\sum_{n=0}^{\infty}\frac{(-1)^n \sinh\left(\frac{3}{8}Nd\right)\cos\left(\frac{3}{8}Nd\right)}{(2n+1)^3\sinh(Nd)}\right] \tag{3.7.6}$$

The volume rate of flow is obtained as

$$\begin{aligned} Q_{it} &= \int_{-d}^{d}\int_{d}^{-z} u\,dy\,dz \\ &= \frac{P}{\mu l}\left[\frac{d^4}{3} - \frac{2^6 d^4}{\pi^5}\sum_{n=0}^{\infty}\frac{\coth(Nd)}{(2n+1)^5}\right] \\ &= \frac{Pd^4}{\mu l}\left[\frac{1}{3} - \frac{64}{\pi^5}\sum_{n=0}^{\infty}\frac{\coth(Nd)}{(2n+1)^5}\right] \end{aligned} \tag{3.7.7}$$

and the mean velocity is given by

$$\begin{aligned} \tilde{u} &= \frac{Q}{2d^2} \\ &= \frac{P}{\mu l}\left[\frac{d^2}{6} - \frac{2^5 d^2}{\pi^5}\sum_{n=0}^{\infty}\frac{\coth(Nd)}{(2n+1)^5}\right] \end{aligned} \tag{3.7.8}$$

The pumping power is in the form

$$\begin{aligned} H_{it} &= \frac{\mu l}{d^4}\left[\frac{1}{3} - \frac{2^6}{\pi^5}\sum_{n=0}^{\infty}\frac{\coth(Nd)}{(2n+1)^5}\right]^{-1} Q^2 \\ &= \frac{\mu l}{2d^2}\left[\frac{1}{6} - \left(\frac{2}{\pi}\right)^5\sum_{n=0}^{\infty}\frac{\coth(Nd)}{(2n+1)^5}\right]^{-1}\frac{Q^2}{d^2} \end{aligned} \tag{3.7.9}$$

3.8 Solution for Crescent-Shaped Cross Sections

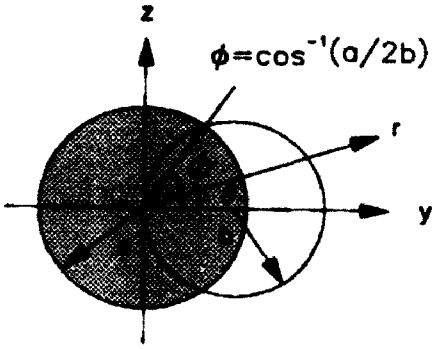

Sketch 3e: Crescent-shaped cross section.

Solution for a tube of crescent-shaped cross section can be obtained by using the analogy with the torsion problem (Timoshenko & Goodier 1970) for straight bars. For a crescent-shaped cross section (the unshaded region in Sketch 3e) bounded by two circular arcs in which the first circle is $y^2+z^2=a^2$ and the second circle is $(y-b)^2+z^2=b^2$, the function

$$u = C(y^2+z^2-a^2)\left(1-\frac{2by}{y^2+z^2}\right) \tag{3.8.1}$$

is zero on the boundary, where C is a constant. From (3.8.1) we have

$$\frac{\partial^2 u}{\partial y^2} = C\left[2+\frac{4a^2by(y^2-3z^2)}{(y^2+z^2)^3}\right]$$

$$\frac{\partial^2 u}{\partial z^2} = C\left[2-\frac{4a^2by(y^2-3z^2)}{(y^2+z^2)^3}\right]$$

Substituting these expressions in Eqn. 2.3.7 and solving for C we get

$$C = -\frac{P}{4\mu l}$$

Hence the solution (in *Cartesian coordinate* system) for the velocity in a tube of crescent-shaped cross section is given by

$$u(y,z) = \frac{P}{4\mu l}(a^2 - y^2 - z^2)\left(1 - \frac{2by}{y^2+z^2}\right) \tag{3.8.2}$$

and in *polar coordinates*

$$u(r,\theta) = \frac{P}{4\mu l}(a^2 - r^2)\left(1 - \frac{2b\cos\theta}{r}\right) \tag{3.8.3}$$

Basic Properties of the Flow

The crescent-shaped cross section has the following geometric properties:

Area:

$$\begin{aligned} A_r &= \int_0^{\phi} (4b^2\cos^2\theta - a^2)d\theta \\ &= (2b^2 - a^2)\phi + b^2\sin 2\phi \\ &= b^2[(2-\varepsilon^2)\phi + \sin 2\phi] \end{aligned}$$

where $\varepsilon = a/b$ and $\phi = \cos^{-1}(\varepsilon/2)$, which determines the thickness of the cross section and its value acts as a thickness parameter.

Perimeter:

$$L_r = \int_0^{2\phi} (a + 2b)\,d\theta$$

$$= 2(a + 2b)\phi$$

$$= 2b(\varepsilon + 2)\phi$$

Hydraulic diameter:

$$D_h = \frac{4 \times area}{perimeter}$$

$$= \frac{2b[(2 - \varepsilon^2)\phi + \sin 2\phi]}{(2 + \varepsilon)\phi}$$

The line of maximum velocity occurs at $r = r_1$ as defined below, which is found to be close to the convex side of the cross section

$$r_1(\theta) = \left[\frac{1}{2} a^2 b \cos\theta + \frac{b^3}{27} \cos^3\theta + \frac{ab\cos\theta}{18} \sqrt{3(27a^2 + 4b^2\cos^2\theta)} \right]^{\frac{1}{3}}$$

$$+ \left[\frac{1}{2} a^2 b \cos\theta + \frac{b^3}{27} \cos^3\theta - \frac{ab\cos\theta}{18} \sqrt{3(27a^2 + 4b^2\cos^2\theta)} \right]^{\frac{1}{3}} + \frac{1}{3} b \cos\theta$$

and the velocity on the line of maximum velocity is

$$\bar{u} = \frac{P}{4\mu l}\left[(a^2 - r_1^2)\left(1 - \frac{2b\cos\theta}{r_1}\right)\right] \tag{3.8.4}$$

where the range of θ is

for $\phi < \pi/2$, $-\phi \le \theta \le \phi$ and for $\phi = \pi/2$, $\theta = 0$.

The maximum velocity $\hat{u}$ occurs at $r = r_1, \theta = 0$.

The volume rate of flow is given by

$$Q_r = 2\int_0^{\phi}\int_a^{2b\cos\theta} u(r,\theta) r\,dr\,d\theta$$

$$= \frac{P}{4\mu l}\left[\left(b^4 - 2a^2b^2 - \frac{1}{2}a^4\right)\phi + \frac{8}{3}a^3 b\sin\phi - \left(a^2b^2 - \frac{2}{3}b^4\right)\sin 2\phi + \frac{b^4}{12}\sin 4\phi\right]$$

$$= \frac{Pb^4}{48\mu l}[6(2 - 4\varepsilon^2 - \varepsilon^4)\phi + 32\varepsilon^3\sin\phi - 4(3\varepsilon^2 - 2)\sin 2\phi + \sin 4\phi] \tag{3.8.5}$$

and the mean velocity is obtained as

$$\tilde{u} = \frac{Q}{b^2[(2 - \varepsilon^2)\phi + \sin 2\phi]}$$

$$= \frac{Pb^2}{48\mu l}\left[\frac{6(2 - 4\varepsilon^2 - \varepsilon^4)\phi + 32\varepsilon^3\sin\phi - 4(3\varepsilon^2 - 2)\sin 2\phi + \sin 4\phi}{(2 - \varepsilon^2)\phi + \sin 2\phi}\right] \tag{3.8.6}$$

The pumping power is obtained as

$$H_{cr} = \frac{48\mu l}{b^4}[6(2-4\varepsilon^2-\varepsilon^4)\phi + 32\varepsilon^3 \sin\phi - 4(3\varepsilon^2-2)\sin 2\phi + \sin 4\phi]^{-1} Q^2 \quad (3.8.7)$$

3.9 Results and Discussions

In what follows we compare the properties of the flow in tubes having the cross sections considered in this chapter with each other. For a meaningful comparison, the cross sections being compared are assumed to have the same cross sectional area or the same perimeter length. The circular cross section is used as a reference in all cases. Geometrical factors are given in Tables 3.1 and 3.2.

Cross section	If $A = A_c$	L/L_c
Ellipse with $\alpha = 0.4$	$ab = R^2$	1.20
Equilateral triangle	$\lambda^2/\sqrt{3} = \pi R^2$	1.28
Rectangle with $\beta = 0.4$	$4AB = \pi R^2$	1.24
Square	$4A^2 = \pi R^2$	1.12
Right angle isosceles triangle	$2d^2 = \pi R^2$	1.36
Crescent shaped with $\phi = \pi/4$	$b^2[(2-\varepsilon^2)\phi + \sin 2\phi] = \pi R^2$	1.51

Table 3.1: Comparisons of cross sections having the same cross sectional area as a circular cross section (subscript c).

Cross section	If $L = L_c$	A/A_c
Ellipse with $\alpha = 0.4$	$a^2(1+\alpha^2) = 2R^2$	0.68
Equilateral triangle	$\lambda\sqrt{3} = \pi R$	0.60
Rectangle with $\beta = 0.4$	$2(A+B) = \pi R$	0.64
Square	$4A = \pi R$	0.78
Right angle isosceles triangle	$(2+\sqrt{2})d = \pi R$	0.53
Crescent shaped with $\phi = \pi/4$	$b(\varepsilon+2)\phi = \pi R$	0.43

Table 3.2: Comparisons of cross sections having the same perimeter length as a circular cross section (subscript c).

3.9.1 Velocity Profiles

Elliptic Cross Sections:

The velocity distribution on the two axes of an ellipse can be written in the form

$$\frac{u_a}{(P/2\mu l)} = \frac{\alpha^2}{1+\alpha^2}(1-y^2)$$

$$\frac{u_b}{(P/2\mu l)} = \frac{1}{1+\alpha^2}(\alpha^2 - z^2)$$

where $\alpha = b/a$, and u_a, u_b are the profiles on the major and the minor axes respectively.

Velocity profiles along the axes of elliptical cross sections with $\alpha = 1$ (circle), $\alpha = 0.5$ and $\alpha = 0.2$ are shown in Fig. 3.1. In this figure the broken lines are for elliptic cross sections and the solid curve is for a circular cross section. While the velocity profiles remain parabolic, the maximum velocity is reduced considerably as ellipticity increases. In particular, the maximum velocity in a tube of elliptic cross section with aspect ratio 0.5 is reduced by 60%. It is evident that the velocity gradient at the end of the minor axis is greater than that at the end of the major axis.

Contours of constant velocity, $\alpha = 0.5$, are shown in Fig. 3.2. The contour lines shown represent constant values of $u/\hat{u}$. A unique feature of the flow in a tube of elliptic cross section is that these contour lines are themselves ellipses *of the same aspect ratio as the bounding ellipse*. This is clear from the expression for the velocity u:

$$\frac{y^2}{a^2} + \frac{z^2}{b^2} = 1 - \frac{u}{\hat{u}}$$

Equilateral Triangular Cross Section:

The velocity distribution over the cross section of an equilateral triangle is given by

$$\frac{u}{\hat{u}} = 6.75(\nu^2 - \nu^3 - \sigma^2 + \nu\sigma^2)$$

where $\nu = z/\lambda$ and $\sigma = y\sqrt{3}/\lambda$.

Some velocity profiles are shown in Fig 3.3. The velocities are non-dimensionalized in terms of maximum velocity. From this figure it is observed that the velocity gradient at the apex of the triangle is zero.

Rectangular Cross Sections:

Velocity distribution over the cross section of a rectangle is only available in the form of infinite series (Eqn. 3.6.5)

$$\frac{u}{\hat{u}} = \frac{[1 - \delta^2 - 32G_2/\pi^3]}{[1 - 32G_1/\pi^3]}$$

where

$$G_1 = \sum_{n=0}^{\infty} \frac{(-1)^n sech(M_1/\beta)}{(2n+1)^3} \qquad (3.9.1a)$$

$$G_2 = \sum_{n=0}^{\infty} \frac{(-1)^n \cosh(M_1\gamma/\beta)\cos(M_1\delta)}{(2n+1)^3 \cosh(M_1/\beta)} \qquad (3.9.1b)$$

$$M_1 = \frac{(2n+1)\pi}{2},$$

$$\text{and} \quad \beta = \frac{B}{A}, \quad \gamma = \frac{z}{B}, \quad \delta = \frac{y}{A}$$

These series are rapidly convergent, however, and can be evaluated numerically. The velocity profiles on the axes of rectangular cross sections with different aspect ratios, β, are plotted on Fig. 3.4. The broken lines are for rectangular cross sections and the solid curve is for the limiting case of a square cross section ($\beta = 1.0$). We observe that in the xy-plane, as the aspect ratio increases the profiles become more and more flattened, in non-dimensional form. Velocity profiles in planes parallel to the coordinate planes are shown in Figs. 3.5 and 3.6 for $\beta = 0.2$ and 1.0 (square). These figures indicate that the variations of velocity are quite gradual away from the wall but are quite rapid near the wall. Comparisons of Figs. 3.5 and 3.6, illustrate that velocity profiles are more rounded for the case of square. Velocity profiles for $\beta = 0.2$ in the xz-plane are more flattened than the profiles in the xy-plane.

Information about the flow pattern near the corner can be obtained from the velocity profile along a diagonal which is given by

$$\frac{u_{rd}}{\hat{u}} = \frac{[1 - \delta^2 - 32G_3/\pi^3]}{[1 - 32G_1/\pi^3]}$$

where

$$G_3 = \sum_{n=0}^{\infty} \frac{(-1)^n \cosh(M_1\delta/\beta)\cos(M_1\delta)}{(2n+1)^3 \cosh(M_1/\beta)}$$

and G_i is as defined in Eqn. 3.9.1a.

Velocity profiles along a diagonal of tubes of rectangular cross sections are plotted in Fig. 3.7 for different values of the parameters β and δ. It is clear from this figure that the velocity gradient in the corner of the rectangle evaluated at the wall is zero, as expected. The shear stress is zero in the corner.

Contours of constant velocity for a tube of rectangular cross section with $\beta = 0.5$ are shown in Fig. 3.8. Inspection of these contours shows that the sharp corners of the rectangle become rounded by the contour lines which becomes elliptic near the center of the cross section. This is consistent with the velocity gradients being higher near the mid-points of the boundary and approaching zero near the corner.

The effects of aspect ratio on the maximum velocity is shown in Fig. 3.9, both for elliptic and rectangular cross sections. The maximum velocity increases to a maximum value as the aspect ratio increases to 1.0.

Right Angle Isosceles Triangular Cross Section:

Velocity profile in a tube of a right angle isosceles triangular cross section is available in the form of infinite series (Eqn. 3.7.5)

$$\frac{u}{\hat{u}} = \frac{[-(\phi+\psi)^2/2 + (\phi+\psi) - 16F_4/\pi^3]}{[15/32 - 32F_3/\pi^3]}$$

where
$$F_3 = \sum_{n=0}^{\infty} \frac{(-1)^n}{(2n+1)^3} \frac{\sinh(3Nd/8)\cos(3Nd/8)}{\sinh(Nd)} \qquad (3.9.2a)$$

$$F_4 = \sum_{n=0}^{\infty} \frac{(-1)^n}{(2n+1)^3} \frac{F(\phi,\psi)}{\sinh(Nd)} \qquad (3.9.2b)$$

and
$$F(\phi,\psi) = \sinh(Nd\psi)\cos(Nd\phi) + \sinh(Nd\phi)\cos(Nd\psi)$$

$$N = \frac{(2n+1)\pi}{2d}, \quad \phi = \frac{y}{d} \quad \text{and} \quad \psi = \frac{z}{d}$$

Both of these series are rapidly convergent, however, and can be evaluated numerically. Fig 3.10 shows the variations of velocity in planes parallel to xy-plane. Velocity profiles in the neighbourhood of the side wall are fairly shallow. The profile becomes peaked on the two axes of the cross section. The flow pattern near the corner can be obtained from the velocity profile along a diagonal, which is given by

$$\frac{u}{\hat{u}} = \frac{[2\phi(1-\phi) - 4F_5(2/\pi)^3]}{[15/32 - 32F_4\pi^3]}$$

where
$$F_5 = \sum_{n=0}^{\infty} \frac{(-1)^n \sinh(Nd\phi)\cos(Nd\phi)}{(2n+1)^3 \sinh(Nd)}$$

and F_3 is as defined in Eqn. 3.9.2a.

Velocity profile along a diagonal of the cross section is plotted in Fig. 3.11. From this figure it is clear that the gradient of velocity at the apex of the triangle evaluated at the wall is zero, as expected. The shear stress is zero at the apex.

Crescent-Shaped Cross Sections:

Velocity profiles for tubes of crescent-shaped cross sections, measured on the axis of symmetry, with different values of the thickness parameter $\phi = \cos^{-1}(a/2b)$ are shown in Fig. 3.12. In the limiting case ($\phi = \pi/2$) the result corresponds to that of a circle. Fig. 3.13 shows the variations of velocity profile in planes corresponding to different values of θ and with $\phi = \pi/3$. Velocity in the neighbourhood of the cusps ($\theta = \pm\phi$) is very low, and near the plane of symmetry ($\theta = 0.0$) is highest.

In Fig. 3.14 velocity profiles along the line of maximum velocity for crescent-shaped cross section with different thickness parameters are shown. It is clear from this figure that the maximum velocity occurs on the axis of symmetry (i.e. $\theta = 0.0$), as indicated before. The velocity gradient in the cusps of the crescent evaluated at the wall, is zero, as expected, indicating that the shear stress is zero there.

The line of maximum velocity and the mid-line chord for $\phi = \pi/3$, and $\phi = \pi/6$ are shown in Figs. 3.15 and 3.16. Comparison of these figures shows that as the crescent becomes thicker the line of maximum velocity moves closer to the convex side of the crescent and as the crescent becomes thinner the line of maximum velocity almost

coincides with the mid-line chord. The effect of thickness on maximum velocity is shown in Fig. 3.17. The maximum velocity increases as the crescent becomes thicker. When the cross section becomes circular the maximum normalized velocity is equal to 1.0.

3.9.2 Shape Factors

In engineering applications the flow rate in a tube of non-circular cross section is often expressed in the form (Duncan et al. 1970)

$$Q = \frac{C_1 P D^4}{\mu l}$$

where C_1 is a "*shape factor*", a constant whose value depends on the shape of the cross section, and D is a *characteristic linear dimension* of that cross section. In what follows we give exact values of D and C_1 for the cross sections considered in this chapter.

Circular Cross Section

$$D = R(\text{radius})$$

$$C_1 = \pi/8$$

Elliptic Cross Section

$$D = a(\text{major axis})$$

$$C_1 = \pi\alpha^3/[4(1+\alpha^2)]$$

Equilateral Triangular Cross Section

$$D = \lambda(\text{height})$$

$$C_1 = \sqrt{3}/180$$

Rectangular Cross Section

$$D = A(\text{longer side})$$

$$C_1 = \frac{4}{3}\beta^3 - \frac{256}{\pi^5}\beta^4 \sum_{n=0}^{\infty} \frac{\tanh(MA)}{(2n+1)^5}$$

Right Angle Isosceles Triangular Cross Section

$$D = d(\text{height})$$

$$C_1 = \frac{1}{3} - \frac{64}{\pi^5} \sum_{n=0}^{\infty} \frac{\coth(Nd)}{(2n+1)^5}$$

Crescent-Shaped Cross Section

$$D = b(\text{radius of the fixed circle})$$

$$C_1 = \frac{1}{48}[6(2-4\varepsilon^2-\varepsilon^4)\phi + 32\varepsilon^3 \sin\phi - 4(3\varepsilon^2-2)\sin 2\phi + \sin 4\phi]$$

3.9.3 Boussinesq Coefficients

The flow rate Q, maximum velocity $\hat{u}$ and the mean velocity $\bar{u}$ may also be expressed by the relations

$$Q = \bar{u}A_r = k_1 K A_r^2$$

$$\hat{u} = k_2 K A_r$$

where k_1 and k_2 are coefficients introduced by Boussinesq (1868). Here A_r is the cross-sectional area of the tube and K is the pressure gradient. In what follows we give the values of the *Boussinesq coefficients* k_1 and k_2 for the cross sections considered in this chapter.

Circular Cross Section

$$k_1 = 1/8\pi$$
$$k_2 = 1/4\pi$$

Elliptic Cross Sections

$$k_1 = \alpha/[4\pi(1+\alpha^2)]$$
$$k_2 = \alpha/[2\pi(1+\alpha^2)]$$

Equilateral Triangular Cross Section

$$k_1 = \sqrt{3}/60$$
$$k_2 = \sqrt{3}/27$$

Rectangular Cross Sections

$$k_1 = \frac{\beta}{12} - \frac{16\beta^2}{\pi^5}\sum_{n=0}^{\infty}\frac{\tanh(MA)}{(2n+1)^5}$$

$$k_2 = \frac{\beta}{8} - \frac{4\beta}{\pi^5}\sum_{n=0}^{\infty}\frac{(-1)^n sech(MA)}{(2n+1)^3}$$

Right Angle Isosceles Triangular Cross Section

$$k_1 = \frac{1}{12} - \frac{2^4}{\pi^5} \sum_{n=0}^{\infty} \frac{\coth(Nd)}{(2n+1)^5}$$

$$k_2 = \frac{15}{128} - \frac{8}{\pi^3} \sum_{n=0}^{\infty} \frac{(-1)^n \sinh(3Nd/8)\cos(3Nd/8)}{(2n+1)^3 \sinh(Nd)}$$

Crescent-Shaped Cross Sections

$$k_1 = \frac{[6(2-4\varepsilon^2-\varepsilon^4)\phi + 32\varepsilon^3 \sin\phi - 4(3\varepsilon^2-2)\sin 2\phi + \sin 4\phi]}{48[(2-\varepsilon^2)\phi + \sin 2\phi]^2}$$

$$k_2 = \frac{(a^2 - r_2^2)(r_2 - 2b)}{b^2 r_2[(2-\varepsilon^2)\phi + \sin 2\phi]}$$

where

$$r_2 = \left[\frac{1}{2}a^2 b + \frac{b^3}{27} + \frac{ab}{18}\sqrt{3(27a^2+4b^2)}\right]^{\frac{1}{3}}$$

$$+\left[\frac{1}{2}a^2 b + \frac{b^3}{27} - \frac{ab}{18}\sqrt{3(27a^2+4b^2)}\right]^{\frac{1}{3}} + \frac{1}{3}b$$

3.9.4 Comparisons of Flow Rates

In what follows the flow rates for the cross sections considered here are compared with each other, using the case of circular cross section as a reference. The tubes being compared are assumed to have the same driving pressure gradient and either (a) the same cross sectional area, or (b) the same perimeter length.

Elliptic Cross Sections

If the areas of tubes of elliptical and circular cross sections are equal and if the flow in both tubes is under the same pressure gradient, then the ratio of the two flow rates is given by

$$\frac{Q_e}{Q_c} = \frac{2\alpha}{1+\alpha^2}, \quad \alpha = \frac{b}{a}$$

If both tubes have the same perimeter and pressure gradient, the ratio of flow rates is given by

$$\frac{Q_e}{Q_c} = \frac{8\alpha^3}{(1+\alpha^2)^3}$$

In Fig. 3.18 the flow rate in tubes of elliptic cross sections of aspect ratios α is compared with that in a tube of circular cross section. The two tubes have the same cross-sectional area in one case and the same perimeter length in the other. It is seen that increasing ellipticity reduces the total flow rate in both cases. The ratio of flow rate for the same area is higher than that for the same perimeter. We see that for $\alpha = 0.2$, there is 61% decrease in the flow when both tubes have the same area and there is 94% decrease in the flow when both have the same perimeter. In general, the flow rate in a tube of circular cross section is greater than that in a tube of elliptic cross section whether the tubes have the same area or have the same perimeter.

The flow rate in a tube of elliptic cross section can be rewritten as

$$Q_e = \frac{\pi P}{4\mu l}\frac{a^2 b^2 \alpha}{(1+\alpha^2)} = \frac{PA_r^2}{4\pi\mu l}\frac{\alpha}{(1+\alpha^2)} \qquad (3.9.3a)$$

where $A_r = \pi a b$ is the area of the ellipse. Differentiating Q_r with respect to α we get

$$\frac{\partial Q_r}{\partial \alpha} = \frac{PA_r^2}{4\pi\mu l}\frac{1-\alpha^2}{(1+\alpha^2)^2} \qquad (3.9.3b)$$

Hence if μ, l, P, A_r are all fixed, Q_r has an extremum at $\alpha = 1.0$, which is easily shown to be a maximum. Thus a tube of circular cross section is more efficient than a tube of elliptic cross section, in the sense that a circular tube produces a greater volume of flow for a fixed pressure gradient than does an elliptic tube of the same cross-sectional area.

Equilateral Triangular Cross Section

If tubes of equilateral triangular and circular cross sections have the same area and if the flow in both tubes is driven by the same pressure gradient, then using Eqns. 3.5.6 (with $\alpha = 1.0$) and 3.6.5, the ratio of the two flow rates is calculated as

$$\frac{Q_{et}}{Q_e} = 0.725$$

If the perimeters are the same, the flow rates are in the ratio

$$\frac{Q_{et}}{Q_e} = 0.2652$$

which shows that the flow rate in a tube of circular cross section is considerably greater than that in a tube of equilateral triangular cross section, particularly when the tubes being compared have the same perimeter length.

Rectangular Cross Sections

If the areas of tubes of rectangular and elliptic cross sections are equal, then $4AB = \pi ab$, and if the flow in both tubes is under the same pressure gradient, the ratio of the flow rates is given by

$$\frac{Q_r}{Q_e} = \frac{\pi}{4}\beta^2\left(\alpha + \frac{1}{\alpha}\right)\left[\frac{4}{3\beta} - \frac{256}{\pi^5}\sum_{n=0}^{\infty}\frac{\tanh(M_1/\beta)}{(2n+1)^5}\right]$$

The series on the right hand side is rapidly convergent, and for a given β, can be evaluated numerically.

If both tubes have the same perimeter, then $4(A+B) = \pi a\sqrt{\frac{1}{2}(1+\alpha^2)}$, and if the flow in both tubes is driven by the same pressure gradient, the ratio of the two flow rates is given by

$$\frac{Q_r}{Q_e} = \frac{\pi^3\beta^4}{16(1+\beta)^4}\left(\alpha + \frac{1}{\alpha}\right)^3\left[\frac{4}{3\beta} - \frac{256}{\pi^5}\sum_{n=0}^{\infty}\frac{\tanh(M_1/\beta)}{(2n+1)^5}\right]$$

In Fig. 3.19 the flow rate in tubes of rectangular cross sections of aspect ratio β is compared with that in tubes of elliptic cross sections of aspect ratio α, by taking α constant

and varying β. The two tubes have the same cross sectional area in one case and the same perimeter in the other. It is clear from the figure that the ratio of flow rates increases with an increase in β, whereas the ratio decreases with increasing α. In particular we see that for $\alpha = 1.0, \beta = 0.1$ the flow rate of an elongated rectangular cross section is less than that of a circular cross section. Again for $\alpha = 0.1, \beta = 1.0$ the flow rate in square cross section is greater than that of an elongated elliptic cross section. Since circular and square cross sections are limiting cases of elliptic and rectangular cross sections, we are thus able to compare the flow rates in tubes of circular and square cross sections. For $\alpha = 1.0, \beta = 1.0$ the flow rate in a tube of square cross section is less than that in a tube of circular cross section. In this case, value of the ratio is equal to 0.883 (for the same cross-sectional area) and 0.544 (for the same perimeter length). Thus the flow rates in tubes of rectangular cross sections are less than that in a tube of circular cross section. The reduction of the flow rate is due to the sharp corners of the rectangle.

Right Angle Isosceles Triangular Cross Section

If the cross-sectional areas of tubes of right angle isosceles triangular and elliptic cross sections are the same, $2d^2 = \pi ab$, and if the flow in both tubes is under the same pressure gradient, then ratio of the two flow rates is given by

$$\frac{Q_{is}}{Q_e} = \pi\left(\alpha + \frac{1}{\alpha}\right)\left[\frac{1}{3} - \frac{64}{\pi^5}\sum_{n=0}^{\infty}\frac{\coth\left(\frac{(2n+1)\pi}{2}\right)}{(2n+1)^5}\right]$$

If the cross-sectional areas of right angle isosceles triangular and square cross sections are equal ($2d^2 = 4d^2$), then we have

$$\frac{Q_{is}}{Q_{sq}} = 0.7423$$

where

$$Q_{is} = \frac{1}{3} - \frac{64}{\pi} \sum_{n=0}^{\infty} \frac{\coth(2n+1)\frac{\pi}{2}}{(2n+1)^5}$$

and

$$Q_{sq} = \frac{4}{3} - \frac{256}{\pi^5} \sum_{n=0}^{\infty} \frac{\tanh(2n+1)\frac{\pi}{2}}{(2n+1)^5}$$

A tube of square cross section produces more flow in both cases.

If we compare flow rates in tubes of right angle isosceles triangular and equilateral triangular cross sections of the same cross-sectional area, $2d^2 = \lambda^2/\sqrt{3}$, and the same pressure gradient, then the ratio of the flow rates becomes

$$\frac{Q_{is}}{Q_{et}} = \frac{15}{\sqrt{3}}\left[\frac{1}{3} - \frac{64}{\pi^5} \sum_{n=0}^{\infty} \frac{\coth(2n+1)\frac{\pi}{2}}{(2n+1)^5}\right]$$

$$= 0.9038$$

Thus the flow rate in an isosceles triangular cross section is less than that in an equilateral triangular cross section.

If the perimeters of tubes of right angle isosceles triangular and elliptic cross sections are the same, $4(3+2\sqrt{2})d^2 = \pi^2 a^2(1+\alpha^2)$, and if the flow in both tubes is driven by the same pressure gradient, then we have

$$\frac{Q_{is}}{Q_{e}} = \frac{\pi^3}{(2+\sqrt{2})^4}\left(\alpha + \frac{1}{\alpha}\right)^3\left[\frac{1}{3} - \frac{64}{\pi^5} \sum_{n=0}^{\infty} \frac{\coth(Nd)}{(2n+1)^5}\right]$$

In Fig. 3.20 the flow rate in a tube of right angle isosceles triangular cross section is compared with that in tubes of elliptic cross sections of different aspect ratios α. The two tubes have the same cross-sectional area in one case and the same perimeter in the other. It is seen than the flow decreases as α increases. In particular for $\alpha = 1.0$ (i.e. circle) when the tubes have the same area, the ratio of the flow rates is

$$\frac{Q_{is}}{Q_c} = 0.6557$$

and when the tubes have the same perimeter, the ratio is

$$\frac{Q_{is}}{Q_c} = 0.1905$$

Hence in both cases the flow rate in a tube of circular cross section is considerably higher than that in a tube of right angle isosceles triangular cross section.

Crescent-Shaped Cross Sections

In Fig. 3.21 the flow rate in a tube of crescent-shaped cross section of different thickness parameters is compared with that in a tube of circular cross section. The two tubes have the same cross-sectional area in one case and the same perimeter in the other. Flow rate for crescent-shaped cross section decreases more if both tubes have the same perimeter. In particular for $\phi = \pi/3$, there is 35% decrease in flow rate when both tubes have the same cross-sectional area, whereas there is 76% decrease when both have the

same cross-sectional perimeter. Thus a tube of circular cross section again produces considerably greater volume of flow for the same pressure gradient than does a crescent-shaped tube of the same cross-sectional area or perimeter.

3.9.5 Pumping Power

Power Coefficients

The pumping power for the flow in a tube of non-circular cross section can be expressed in the form

$$H = \frac{\mu l}{A_r C_2 D^2} Q^2$$

where A_r is the area of the cross section of the tube, C_2 is a constant whose value depends on the shape of the cross section and D is a characteristic linear dimension of that cross section. In what follows we give the exact values of C_2 for the cross sections considered in this chapter. The values of D were given in Section 3.9.2.

Circular Cross Section

$$C_2 = 1/8$$

Elliptic Cross Sections

$$C_2 = \alpha^2/[4(1+\alpha^2)]$$

Equilateral Triangular Cross Section

$$C_2 = 1/60$$

Rectangular Cross Sections

$$C_2 = \frac{\beta^2}{3} - \frac{2}{A^7\beta^4}\sum_{n=0}^{\infty}\frac{\tanh(MA)}{M^5}$$

Right Angle Isosceles Triangular Cross Section

$$C_2 = \frac{1}{6} - \left(\frac{2}{\pi}\right)^5 \sum_{n=0}^{\infty}\frac{\coth(Nd)}{(2n+1)^5}$$

Crescent-Shaped Cross Sections

$$C_2 = \frac{6(2-3\varepsilon^4)\phi + 32\varepsilon^3\sin\phi + 8\sin 2\phi + \sin 4\phi}{(2-\varepsilon^2)\phi + \sin 2\phi} - 12\varepsilon^2$$

Comparisons

In what follows the pumping power for the cross sections considered in this chapter are compared with each other, using the case of a circular cross section as a reference. The tubes being compared are assumed to have the same flow rate and either (a) the same cross-sectional area, or (b) the same cross -sectional perimeter.

Elliptic Cross Sections

If the cross-sectional areas of tubes of elliptic and circular cross sections are the same and if both tubes have the same flow rate, then the ratios of the two powers is given by

$$\frac{H_e}{H_c} = \frac{1+\alpha^2}{2\alpha}$$

If the two tubes have the same perimeter and flow rate, the ratio of powers is given by

$$\frac{H_e}{H_c} = \frac{(1+\alpha^2)^3}{8\alpha^3}$$

Power in a tube of elliptic cross section of aspect ratio α, compared with that in a tube of circular cross section is shown in Fig. 3.22. The two tubes have the same cross-sectional area in one case and the same perimeter in the other. It is observed that power increases dramatically with increasing ellipticity. In particular for $\alpha = 0.2$ the power increases by a factor of 2.6 when both tubes have the same area and a factor of 17.57 when both have the same perimeter. A tube of elliptic cross section requires considerably more power to drive the flow than a tube of circular cross section.

Equilateral Triangular Cross Section

The ratio of powers in tubes of equilateral triangular and circular cross sections of the same cross-sectional area and the same flow rate, obtained from Eqns. 3.4.7 and 3.5.7, is

$$\frac{H_{el}}{H_c} = 1.378$$

and for the same perimeter and flow rate the ratio is given by (Eqns. 3.4.8 and 3.5.5)

$$\frac{H_{el}}{H_c} = 3.77$$

Thus the power in a tube of circular cross section is less than that in a tube of equilateral triangular cross section.

Rectangular Cross Sections

If the areas of tubes of rectangular and elliptic cross sections are the same and if both tubes have the same flow rate then the ratio of powers becomes

$$\frac{H_r}{H_e} = \frac{4\alpha}{\pi\beta^2(1+\alpha^2)}\left[\frac{4}{3\beta} - \frac{256}{\pi^5}\sum_{n=0}^{\infty}\frac{\tanh(M_1/\beta)}{(2n+1)^5}\right]^{-1}$$

If both tubes have the same perimeter and the same flow rate, the ratio of the two powers is given by

$$\frac{H_r}{H_e} = \frac{8(1+\beta)^4}{\pi^3\alpha^3(1+\alpha^2)}\left[\frac{4}{3}\beta^3 - \frac{256}{\pi^5}\beta^4\sum_{n=0}^{\infty}\frac{\tanh(M_1/\beta)}{(2n+1)^5}\right]^{-1}$$

In Fig. 3.23 pumping power in tubes of rectangular cross sections of aspect ratio β is compared with that in tubes of elliptic cross sections of aspect ratio α, by taking α

constant and varying β. The two tubes have the same cross-sectional area in one case and the same perimeter in the other. In both cases we observe that the increasing ellipticity decreases the ratio of pumping powers whereas the ratio increases with an increase in β. A tube of rectangular cross section requires more power to drive the flow than a tube of circular cross section of the same area or perimeter and the same flow rate, much more so as the aspect ratio decreases (Fig. 3.23, $\alpha = 1.0$).

Right Angle Isosceles Triangular Cross Section

Pumping power in a tube of right angle isosceles triangular cross section, compared with that in tubes of elliptic cross sections of aspect ratio α is shown in Fig. 3.24. The two tubes have the same cross -sectional area in one case and the same perimeter in the other. It is seen that the ratio of the two powers decreases with increasing ellipticity. If the cross-sectional areas of right angle isosceles triangular and circular cross sections are the same and if both tubes have the same flow rate then the ratio of powers is equal to

$$\frac{H_{is}}{H_c} = 1.52$$

and if both tubes have the same perimeter and the same flow rate, the ratio of powers is given by

$$\frac{H_{is}}{H_c} = 5.25$$

which shows that the power in a tube of triangular cross section is considerably higher than that in a tube of circular cross section, particularly when the tubes being compared have the same perimeter length.

Crescent-Shaped Cross Sections

In Fig. 3.25 power in tubes of crescent-shaped cross sections of different thickness parameters $\phi = \cos^{-1}(\varepsilon/2)$ is compared with that in a tube of circular cross section. The two tubes have the same cross-sectional area in one case and the same cross-sectional perimeter in the other. Power for crescent-shaped cross section increases more if both tubes have the same perimeter. In particular for $\phi = \pi/3$, there is 154% increase in power when both tubes have the same cross-sectional area, whereas there is 415% increase when both have the same perimeter length. Thus a tube of circular cross section again requires considerably less pumping power to drive the flow than a tube of crescent-shaped cross section of the same cross -sectional area or perimeter.

3.9.6 Wall Shear Stress

In this section the shear stresses for the cross sections considered in this chapter are compared with each other, using the shear stress in a tube of circular cross section as a reference. The tubes being compared are assumed to have the same flow rate and either (a) same cross-sectional area, or (b) same cross-sectional perimeter.

In polar coordinates the shear stress for an ellipse is given by

$$\tau_e = \frac{4\mu\bar{u}R}{a^2b^2}\sqrt{b^4\cos^2\theta + a^4\sin^2\theta}$$

$$= \frac{4\mu\bar{u}R}{b^2}\sqrt{\alpha^4\cos^2\theta + \sin^2\theta}$$

If the areas of tubes of elliptic and circular cross sections are the same and if both tubes have the same flow rate , then the ratio of the shear stresses is given by

$$\frac{\tau_e}{\tau_c} = \sqrt{\alpha^2\cos^2\theta + \frac{\sin^2\theta}{\alpha^2}}$$

If both tubes have the same perimeter and flow rate then the ratio of the shear stresses is given by

$$\frac{\tau_e}{\tau_c} = \frac{1}{2}\left(1 + \frac{1}{\alpha^2}\right)\sqrt{\alpha^2\cos^2\theta + \sin^2\theta}$$

In Fig. 3.26 the non-dimensional shear stress on tubes of elliptic cross sections is plotted for $0 \le \alpha \le 1$ and $0 \le \theta \le \pi$, using the shear stress on a tube of circular cross section as a reference. The solid lines are for the same cross-sectional area and the lines with circles are for the same perimeter. The broken line is for circular cross section. The maximum shear acting on the wall is at $\theta = \pi/2$, that is, at the end of the minor axis, as expected, and the minimum shear is at $\theta = 0$, that is, at the end of the major axis.

If tubes of equilateral triangular and circular cross sections have the same area and the same flow rate, the ratio of the two shear stresses is given by

$$\frac{\tau_{el}}{\tau_c} = \frac{15}{4}\sqrt{\frac{1}{\pi\sqrt{3}}}(1-\sigma^2)$$

And, if both tubes have the same perimeter and the same flow rate, the ratio of shear stresses is given by

$$\frac{\tau_{el}}{\tau_c} = \frac{15\sqrt{3}}{4\pi}(1-\sigma^2)$$

The shear stress along a side in a tube of equilateral triangular cross section, compared with that in a tube of circular cross section is shown in Fig. 3.27. The two tubes have the same cross-sectional area in one case, the same perimeter in the other. The broken line is for the same area and the solid curve is for the same perimeter. The maximum shear stress is found to be at the middle of the sides of an equilateral triangle. At the apex of the triangle the shear stress is zero, as expected. The ratio of shear stresses for the same perimeter is higher than the ratio for the same area. When both tubes have the same perimeter, the maximum value of the ratio is 2.067 and when both have the same area, the maximum value becomes 1.608.

The values and the positions of maximum wall shear stress for the non-circular cross sections considered in this chapter are shown in Table 3.3, using the shear stress in a circular cross section as a reference. The tubes being compared are assumed to have the same flow rate and the same cross -sectional area.

Cross section	τ_{max}/τ_c	Position of maximum shear stress
Ellipse with α =0.2	5.000	end of minor axis
Equilateral triangle	1.608	mid-point of a side
Rectangle with β =0.4	5.439	mid-point of the longer side
Square	4.257	mid-point of a side
Right angle isosceles triangle	2.428	mid point of the hypotenuse
Crescent-shaped with $\phi = \pi/4$	1.131	peak of convex side

Table 3.3: Values and positions of maximum wall shear stress, compared with that in a circular cross section. The tubes being compared are assumed to have the same cross-sectional area and flow rate.

3.9.7 Friction Factor

In engineering applications it is common to express the pressure gradient (pressure drop per unit length l of the tube) in the form

$$\frac{P}{l} = \frac{f_F}{D_h}\left(\frac{1}{2}\rho u^2\right) \tag{3.9.4}$$

where f_F is the *friction factor*, ($\rho\bar{u}^2/2$) is the dynamic pressure of the mean flow, and D_h is the hydraulic diameter.

Eqn. 3.9.4 can be rewritten, in terms of the Reynolds number $R_e = \bar{u}D_h/\nu$, so that

$$f_F R_e = \frac{P}{2\mu l}\frac{D_h^2}{\bar{u}} \tag{3.9.5}$$

This equation defines the so called *Fanning friction factor* for tubes of non-circular cross sections.

The so called "large" or Darcy friction factor f is also used in the literature, where

$$f = 4f_F \tag{3.9.6}$$

f is also known as *Darcy-Weisbach friction factor.*

Darcy's friction factor is more widely used, and we use it in what follows as the basis of comparison. It can also be expressed in the form

$$f = \frac{S}{R_e} \tag{3.10.7}$$

where the constant, S, is a characteristic of the cross section whose value depends on the shape of the cross section. The values of the constant S for the non-circular cross sections considered in this chapter are given below.

Elliptic Cross Sections:

For tubes of elliptic cross sections the friction factor can be expressed in the form

$$fR_e = 8(1+\alpha^2)\left[\frac{\pi}{E(k)}\right]^2, \quad \alpha = \frac{b}{a}$$

where E(k) is the complete elliptic integral of the second kind, i.e.,

$$E(k) = \int_0^{\pi/2} \sqrt{1-k^2\sin^2\theta}\, d\theta, \quad k = \sqrt{1-\alpha^2}$$

Table 3.4 gives the values of friction factors for elliptic cross sections of different aspect ratios.

α	$S = fR_e$
1.0	64.000
0.8	64.392
0.6	65.916
0.5	67.328
0.4	69.176
0.2	74.408

Table 3.4: Friction factors for tubes of elliptic cross sections of aspect ratio α.

Equilateral Triangular Cross Section:

The friction factor for equilateral triangular cross section is given by (using Eqns. 3.10.7, 3.6.5 and $D_h = 4\lambda/3$)

$$fR_e = 53.332$$

Rectangular Cross Section:

For tubes of rectangular cross sections the friction factor can be expressed in the form

$$fR_e = \frac{96}{(1+\beta)^2}\left[1 - \frac{192\beta}{\pi^5}\sum_{n=0}^{\infty}\frac{\tanh\{(2n+1)\pi/2\beta\}}{(2n+1)^5}\right]^{-1}, \quad \beta = \frac{B}{A}$$

The friction factors fR_e and the ratio of the maximum over the mean velocity $\hat{u}/\bar{u}$ are presented in Table 3.5 for rectangular cross sections of different aspect ratios.

β	$\hat{u}/\tilde{u}$	$S = fR_r$
1.0	2.0913	56.9080
0.8	2.0836	57.5112
0.6	2.0377	57.9196
0.5	1.9918	62.1920
0.4	1.9236	65.4724
0.2	1.7150	76.2820
0.0	1.5000	96.0000

Table 3.5: $\hat{u}/\tilde{u}$ and friction factors for tubes of rectangular cross sections of aspect ratio β.

It may be noted that in one limiting case ($\beta = 0$), the result corresponds to that of flow between parallel plates and in the other limiting case ($\beta = 1$) the result corresponds to that in a tube of a square cross section.

Right Angle Isosceles Triangular Cross Section:

The friction factor for a tube of right angle isosceles triangular cross section is given by

$$fR_e = \frac{16}{3+2\sqrt{2}}\left[\frac{1}{6} - \left(\frac{2}{\pi}\right)^5 \sum_{n=0}^{\infty} \coth\frac{(Nd)}{(2n+1)^5}\right]^{-1}$$

$$= 52.6104$$

Crescent-Shaped Cross Section:

For tubes of crescent-shaped cross sections the friction factor can be expressed in the form

$$fR_e = \frac{96[(2-\varepsilon^2)\phi + \sin 2\phi]^3}{(2+\varepsilon)^2\phi^2}\frac{1}{G_1}$$

where $G_1 = 6(2-4\varepsilon^2-\varepsilon^4)\phi + 32\varepsilon^3\sin\phi - 4(3\varepsilon^2-2)\sin 2\phi + \sin 4\phi$

The values of the friction factor fR_e for different $\phi = \cos^{-1}(a/2b)$ are given in Table 3.6.

ϕ	$\hat{u}/\tilde{u}$	$S = fR_e$
10	2.1326	60.6456
15	2.1818	62.0262
30	2.1721	61.6522
45	2.1517	60.9551
60	2.1200	60.1077
75	2.0696	59.7483
80	2.0455	60.1487
85	2.0177	61.2830
90	2.0000	64.0000

Table 3.6: Friction factor for tubes of crescent-shaped cross sections with different values of the thickness parameter, ϕ.

In the limiting case ($\phi = 90$) the result corresponds to that of a circle.

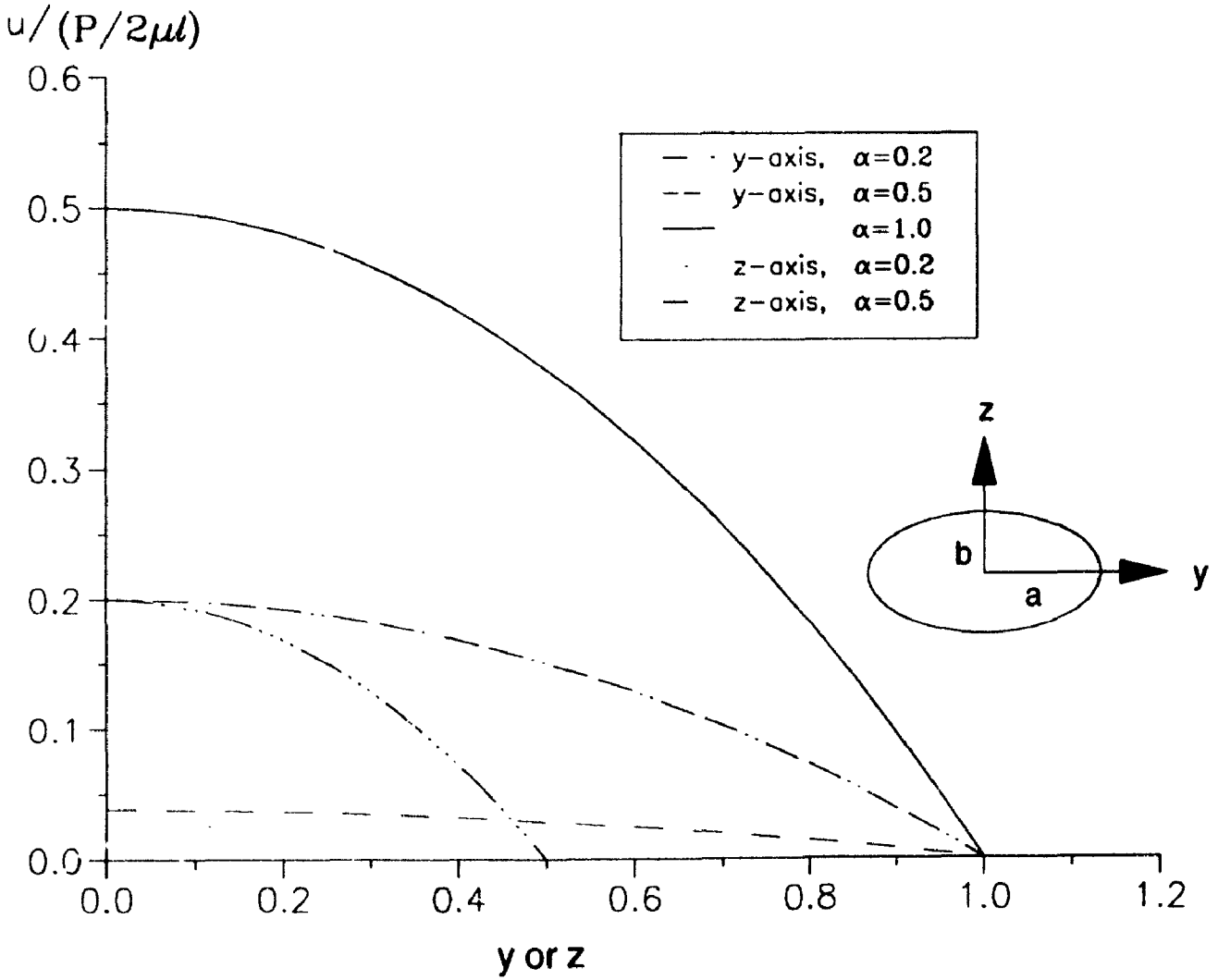

Fig. 3.1: Velocity profiles along the axes of tubes of elliptic cross sections.

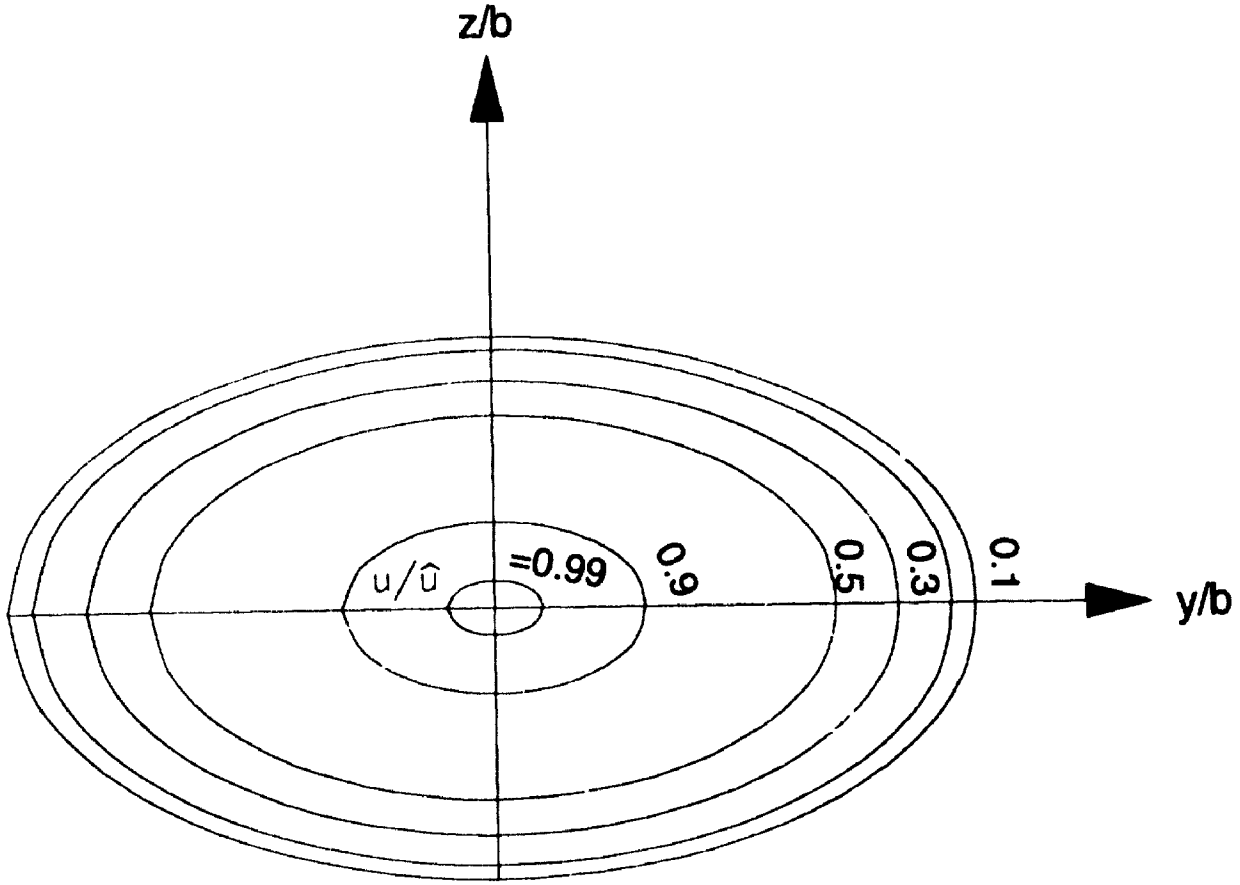

Fig. 3.2: Contours of constant velocity for a tube of elliptic cross section with aspect ratio 0.5.

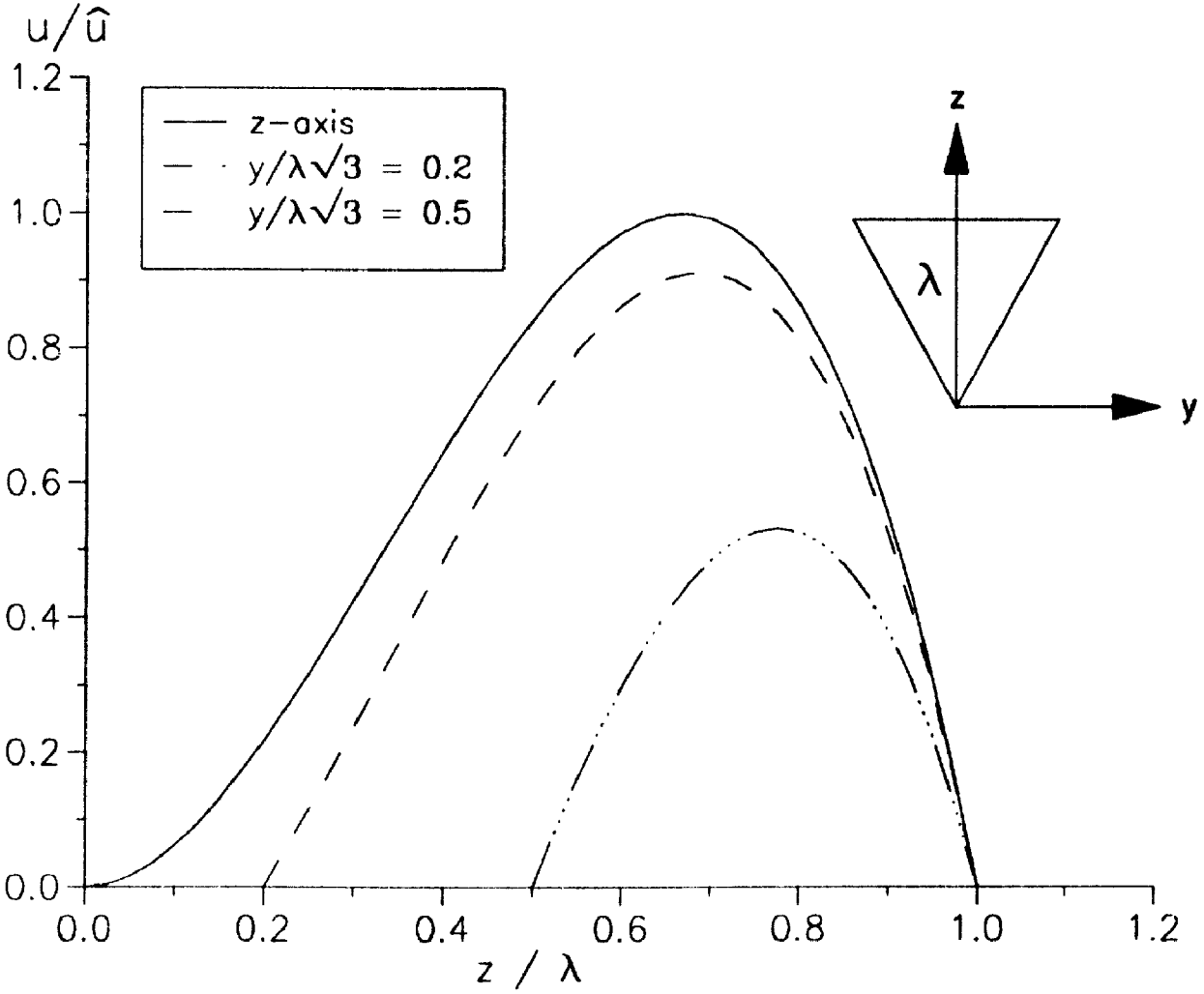

Fig. 3.3 : Velocity profiles in xz-planes in a tube of equilateral triangular cross section.

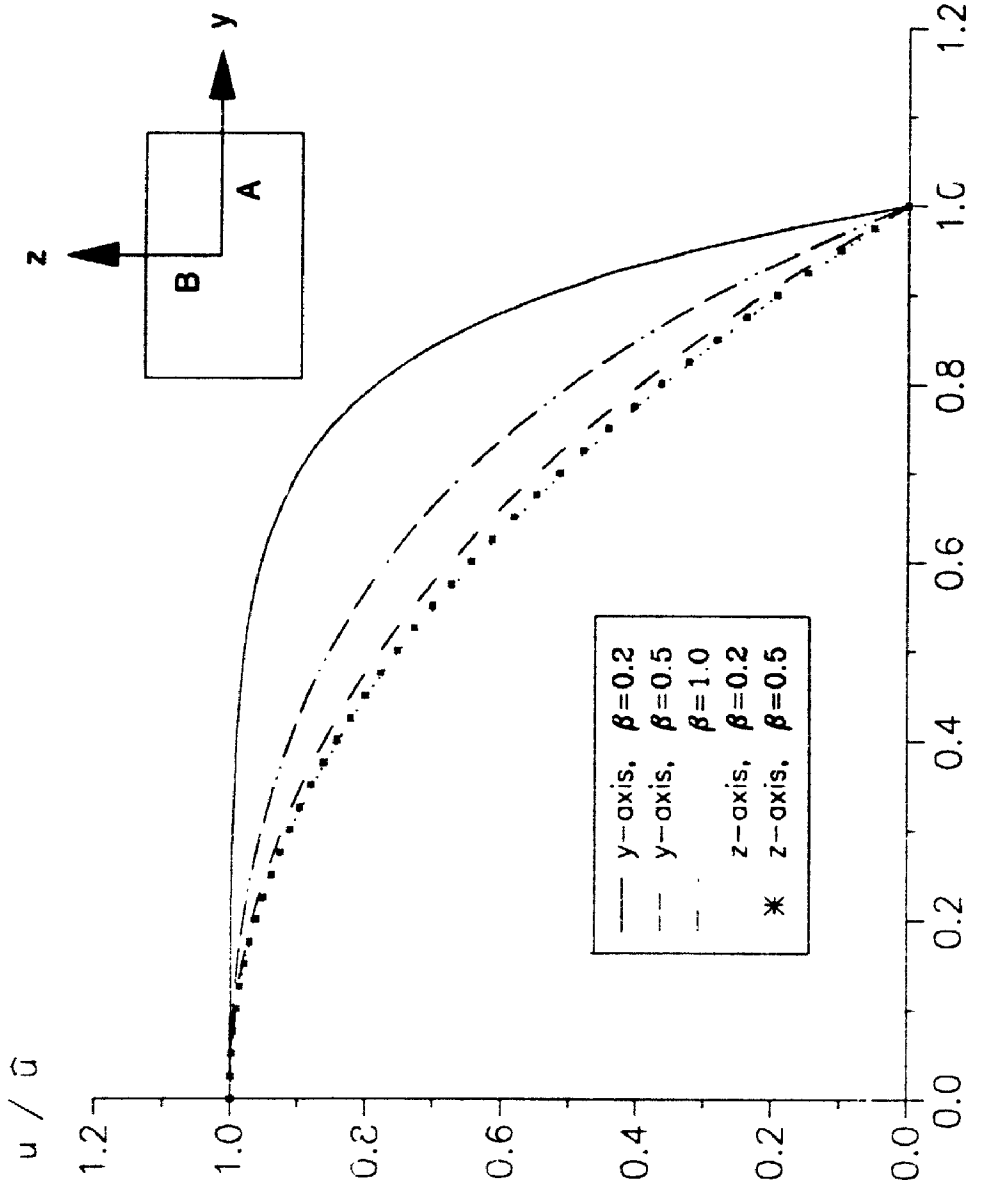

Fig. 3.4: Velocity profiles on the axes of tubes of rectangular cross sections with aspect ratio β.

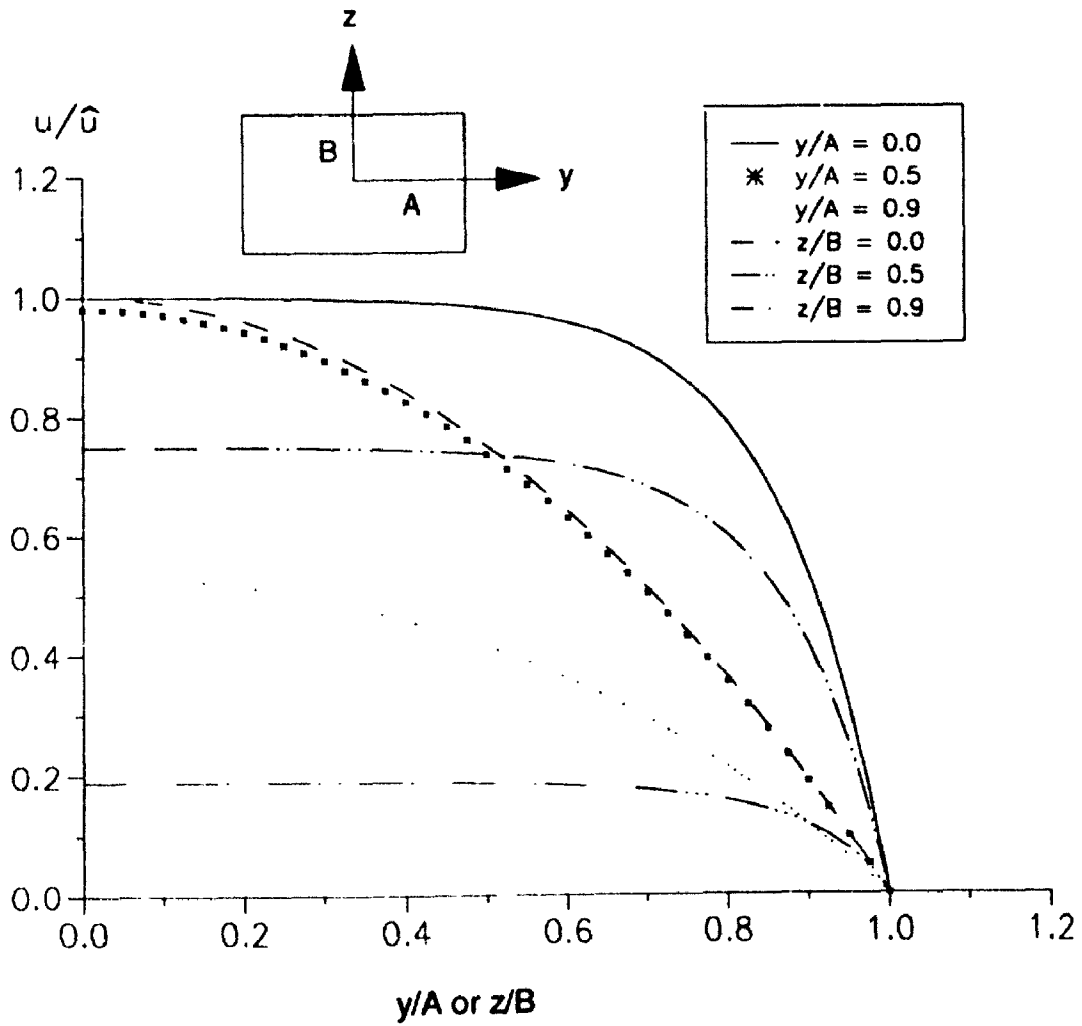

Fig. 3.5: Velocity profiles in the xz- and xy-plane of a tube of rectangular cross section with aspect ratio 0.2.

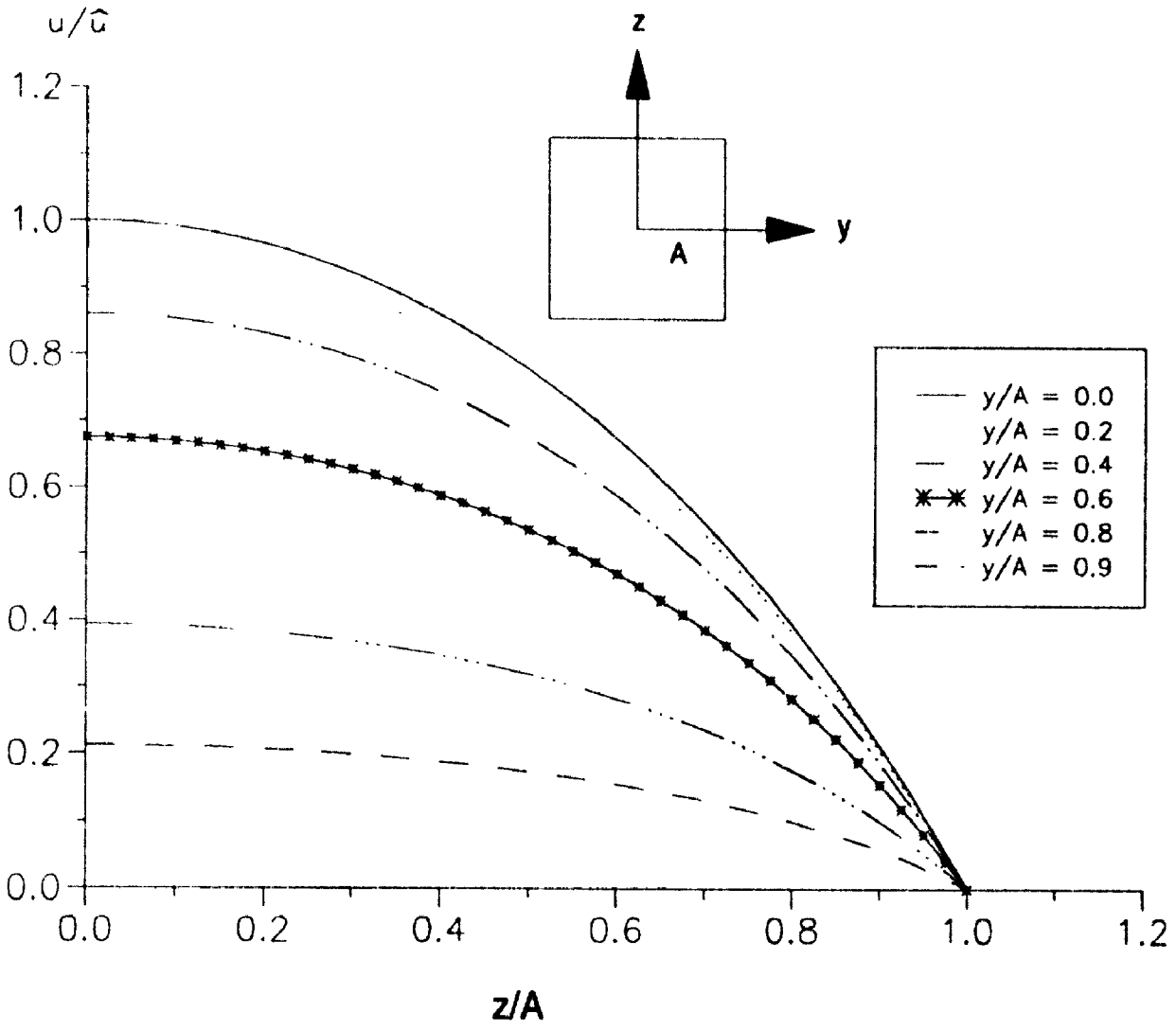

Fig. 3.6: Velocity profiles in a tube of square cross section.

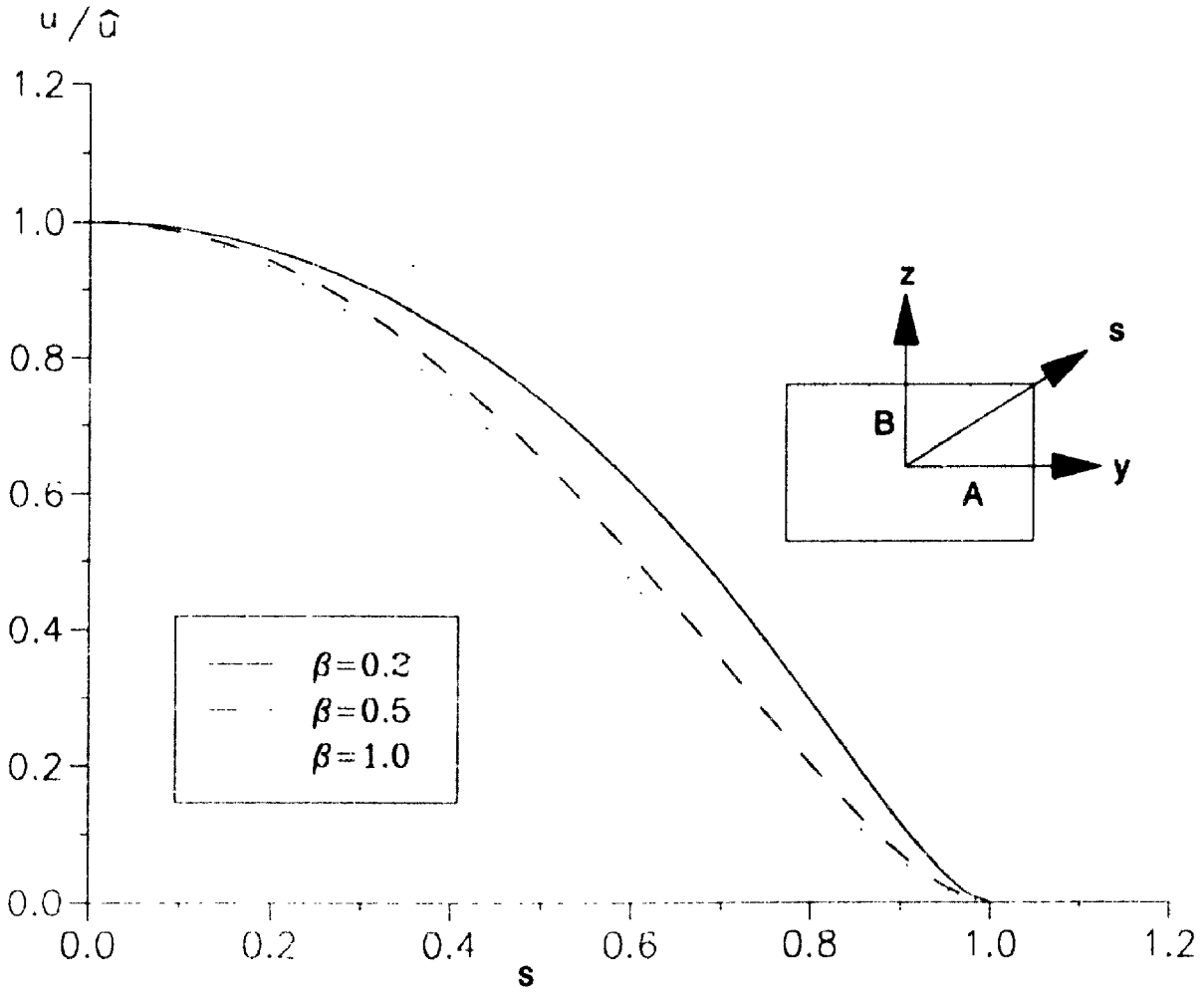

Fig. 3.7: Velocity profile along a diagonal in tubes of rectangular cross sections of different aspect ratios.

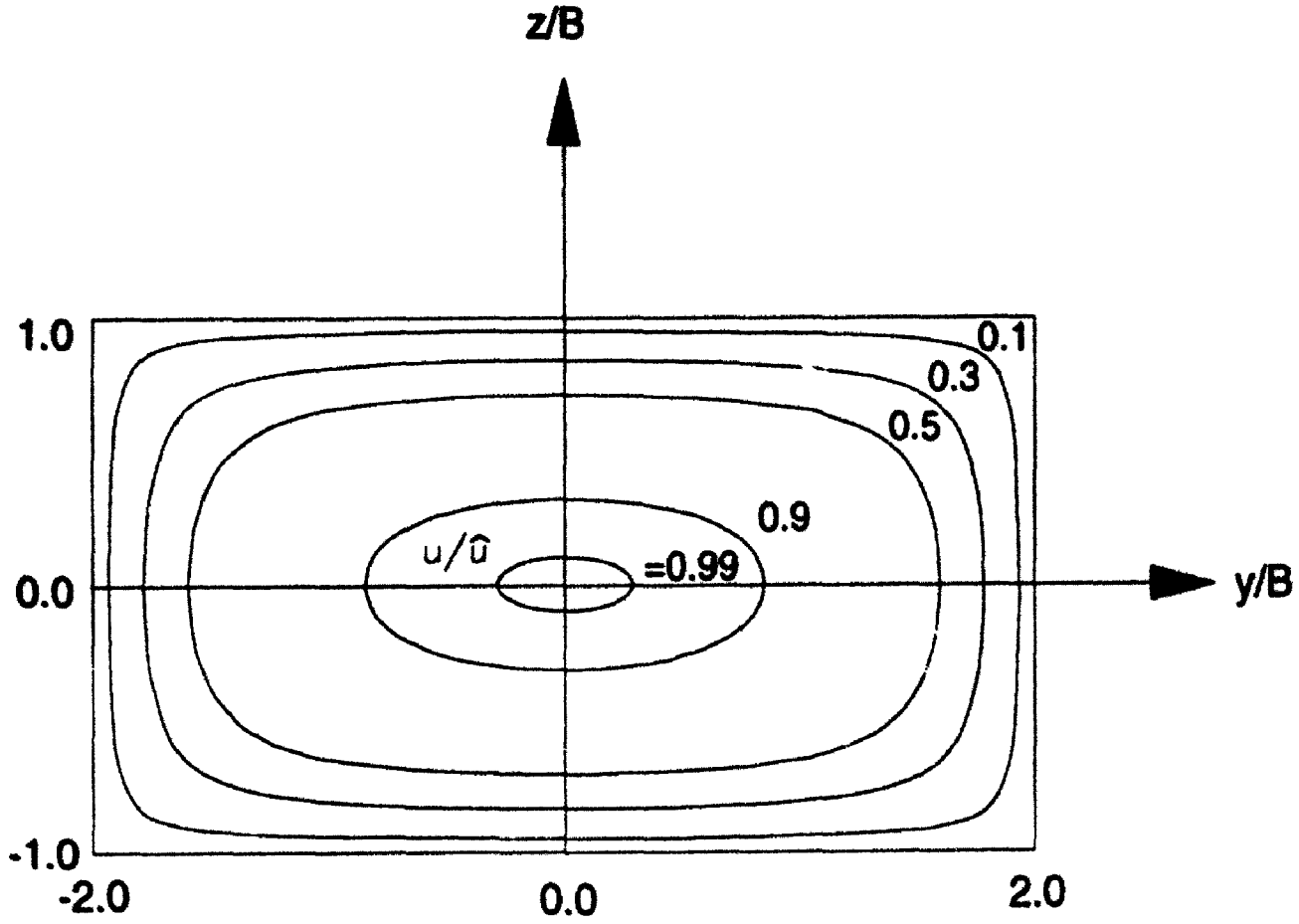

Fig. 3.8: Contours of constant velocity for a tube of rectangular cross section with aspect ratio 0.5.

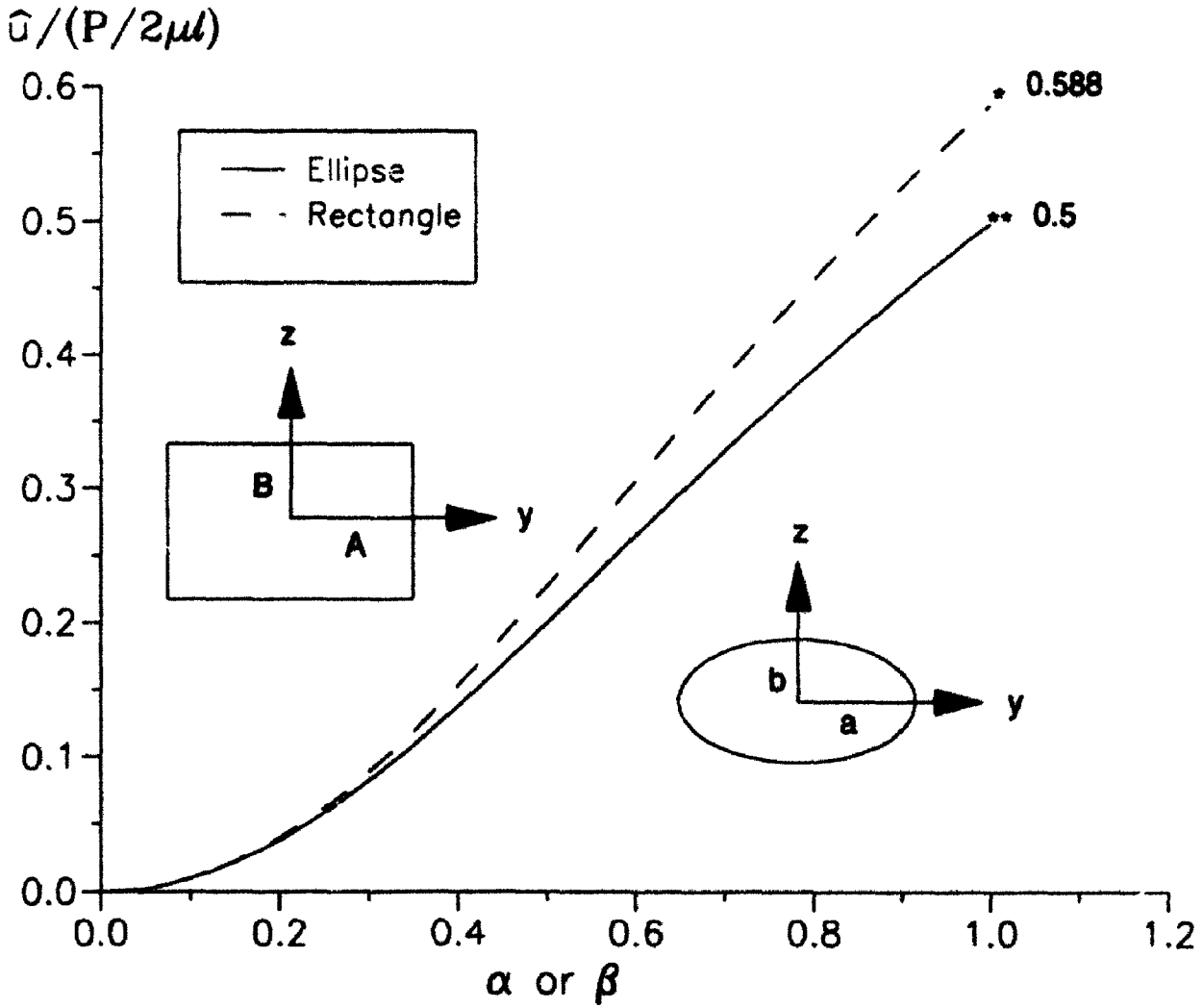

Fig. 3.9: Maximum velocity in tubes of elliptic and rectangular cross sections with different aspect ratios (* square, ** circle).

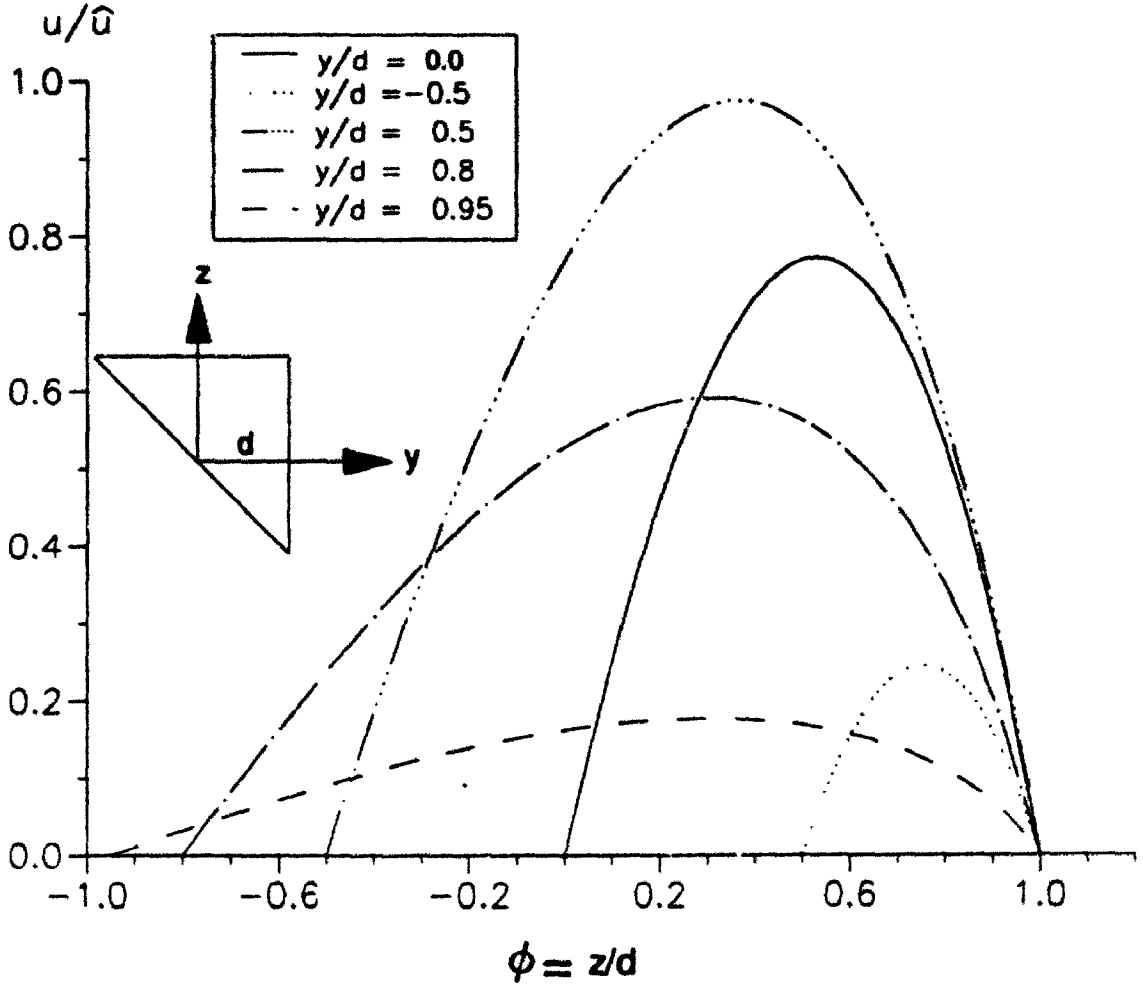

Fig. 3.10 : Velocity profiles in planes parallel to xz-plane of a tube of right angle isosceles triangular cross section.

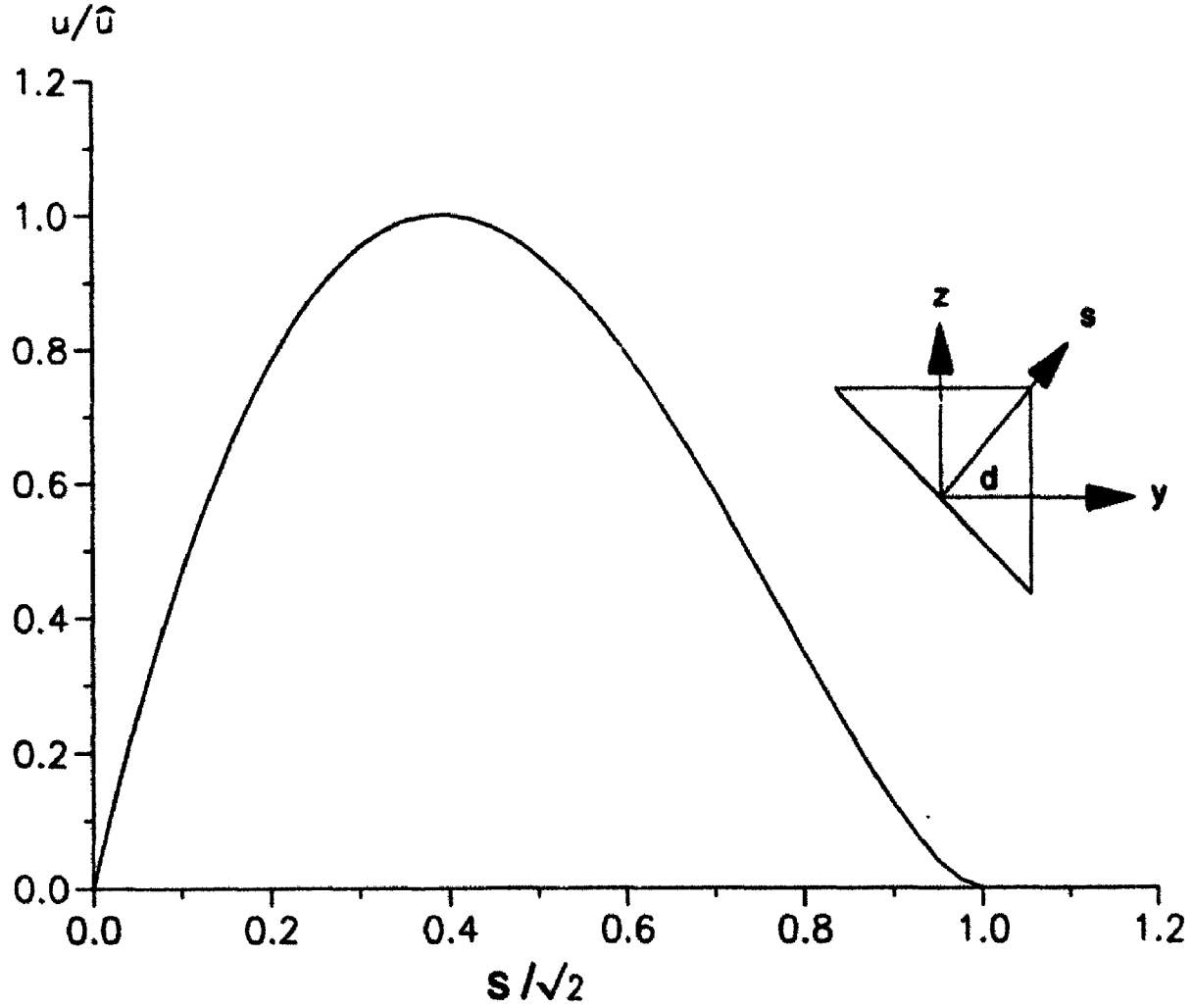

Fig. 3.11: Diagonal velocity profile in a tube of right angle isosceles triangular cross section.

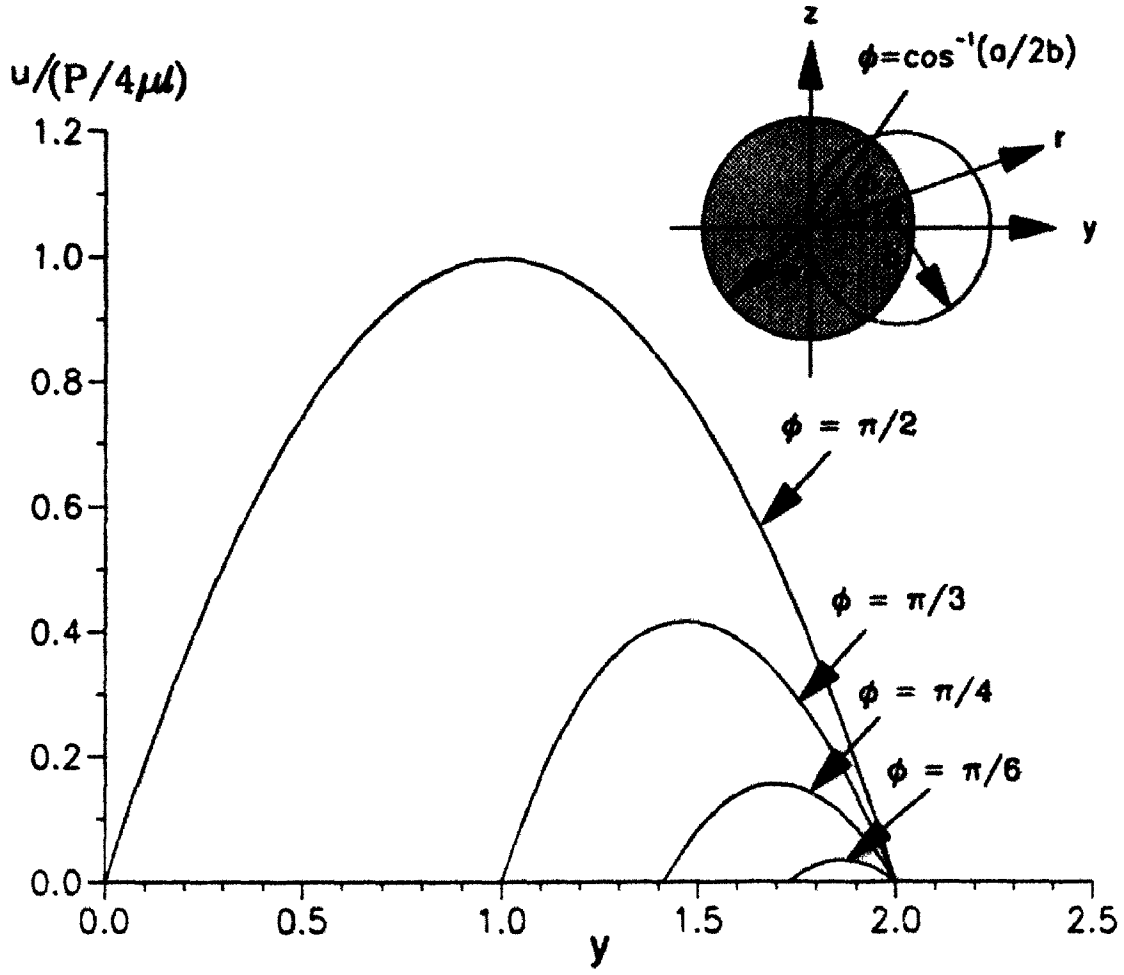

Fig. 3.12: Velocity profiles along the axis of symmetry in tubes of crescent-shaped cross sections with different values of the thickness parameter ϕ

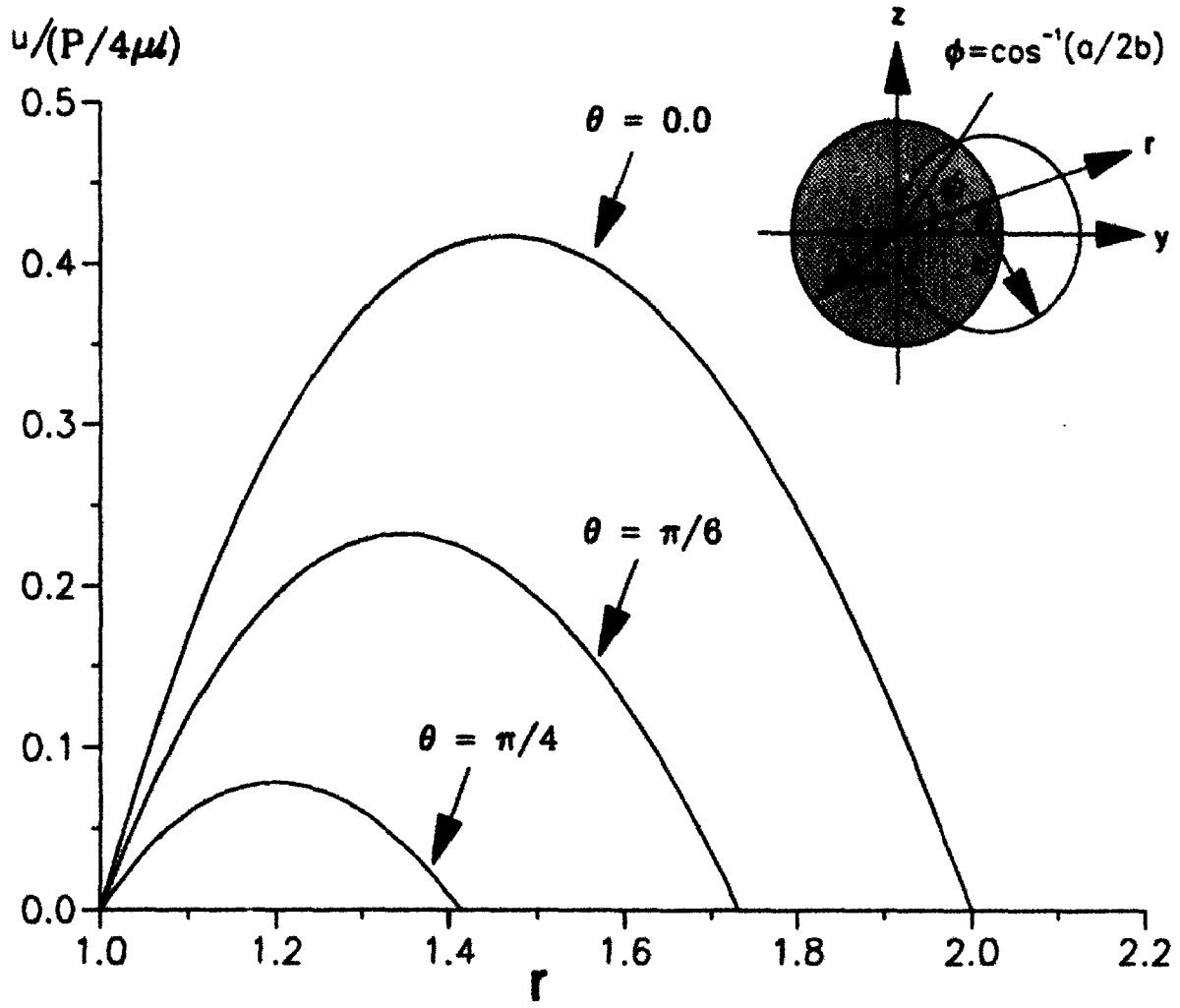

Fig. 3.13: Velocity profiles in a tube of crescent-shaped cross section with $\phi = \pi/3$

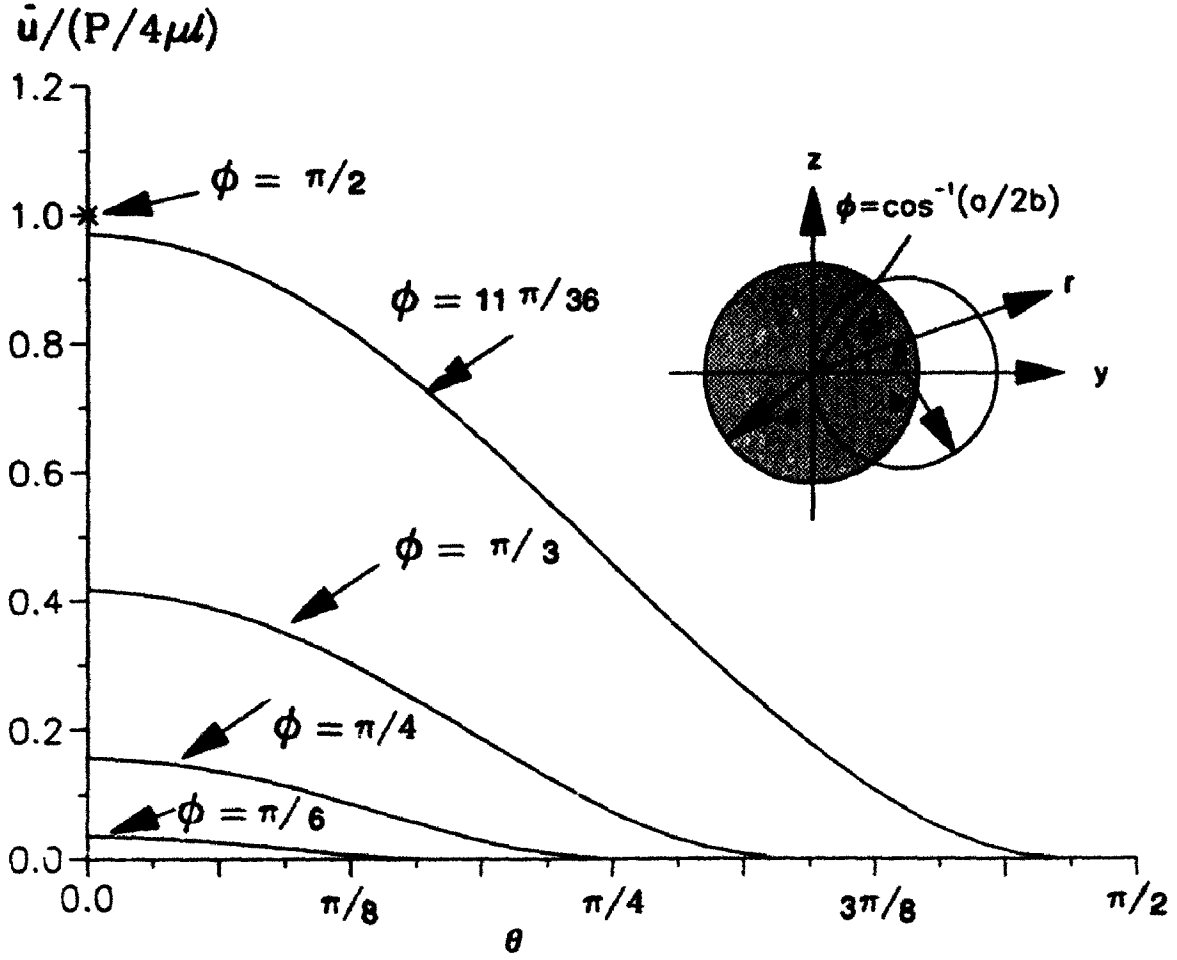

Fig. 3.14: Velocity profiles along the line of maximum velocity in tubes of crescent-shaped cross sections.

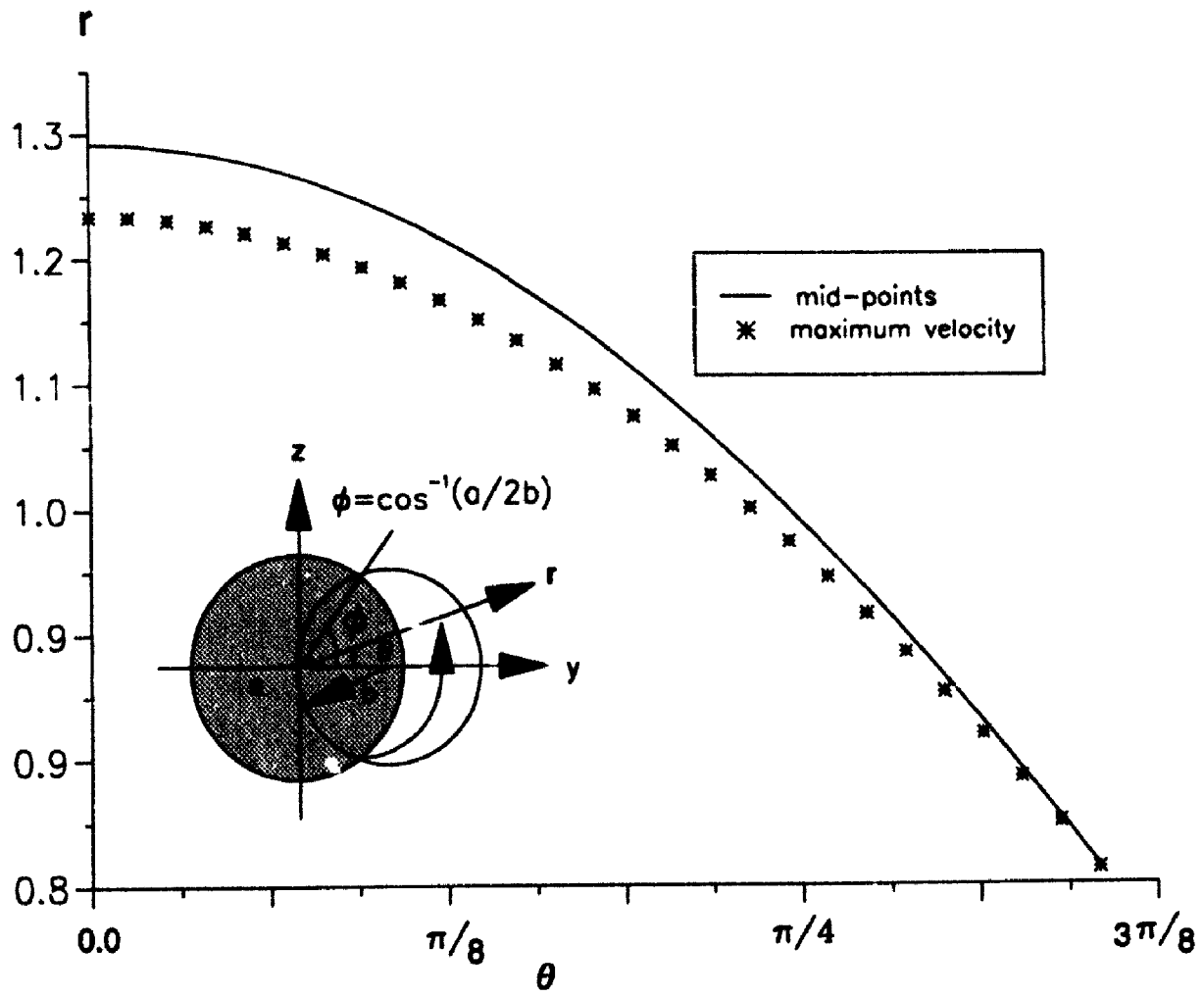

Fig. 3.15: Line of maximum velocity compared with the mid-line in a tube of crescent-shaped cross section with $\phi=7\pi/16$

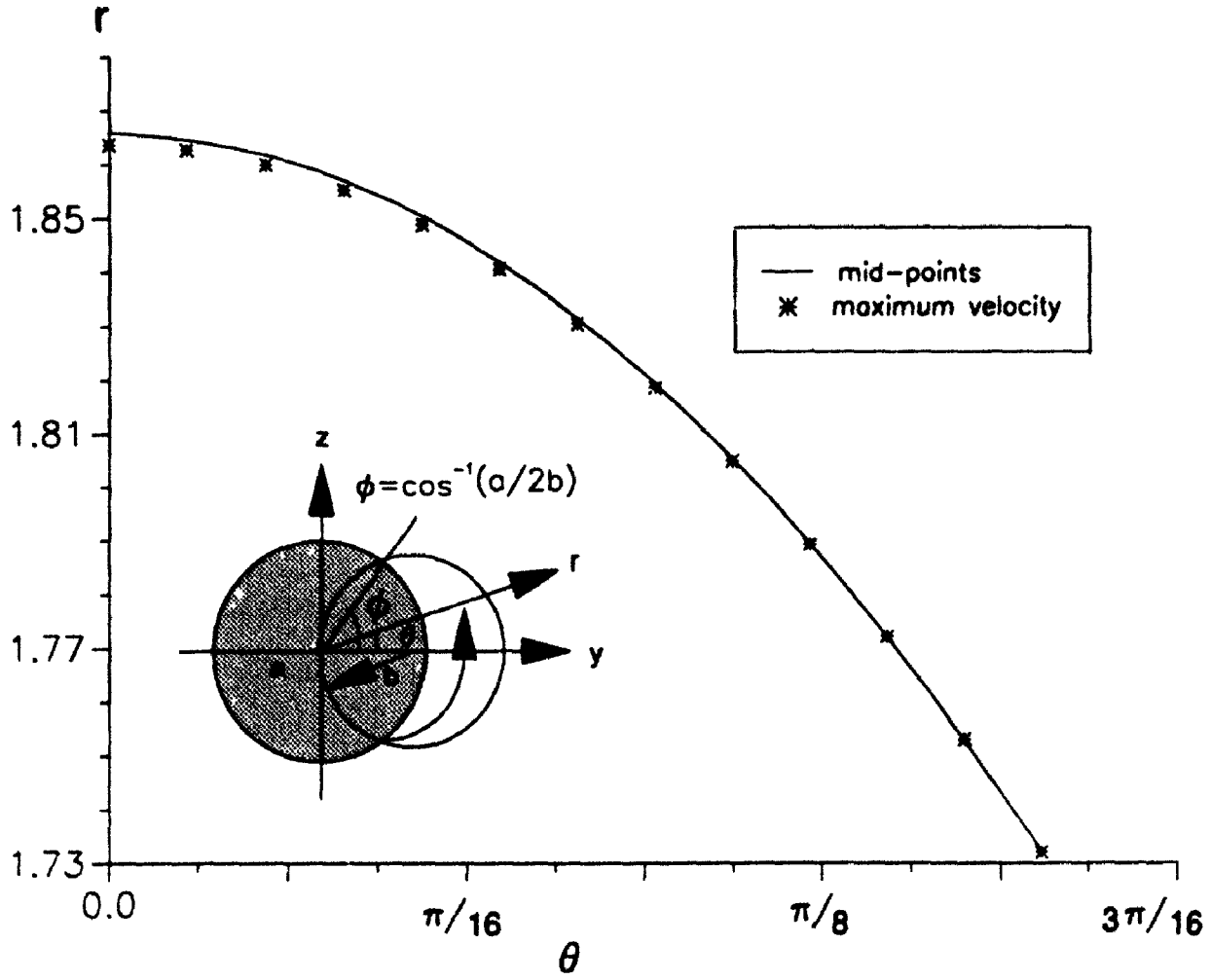

Fig. 3.16: Line of maximum velocity compared with the mid-line in a tube of crescent-shaped cross section with $\phi=\pi/6$

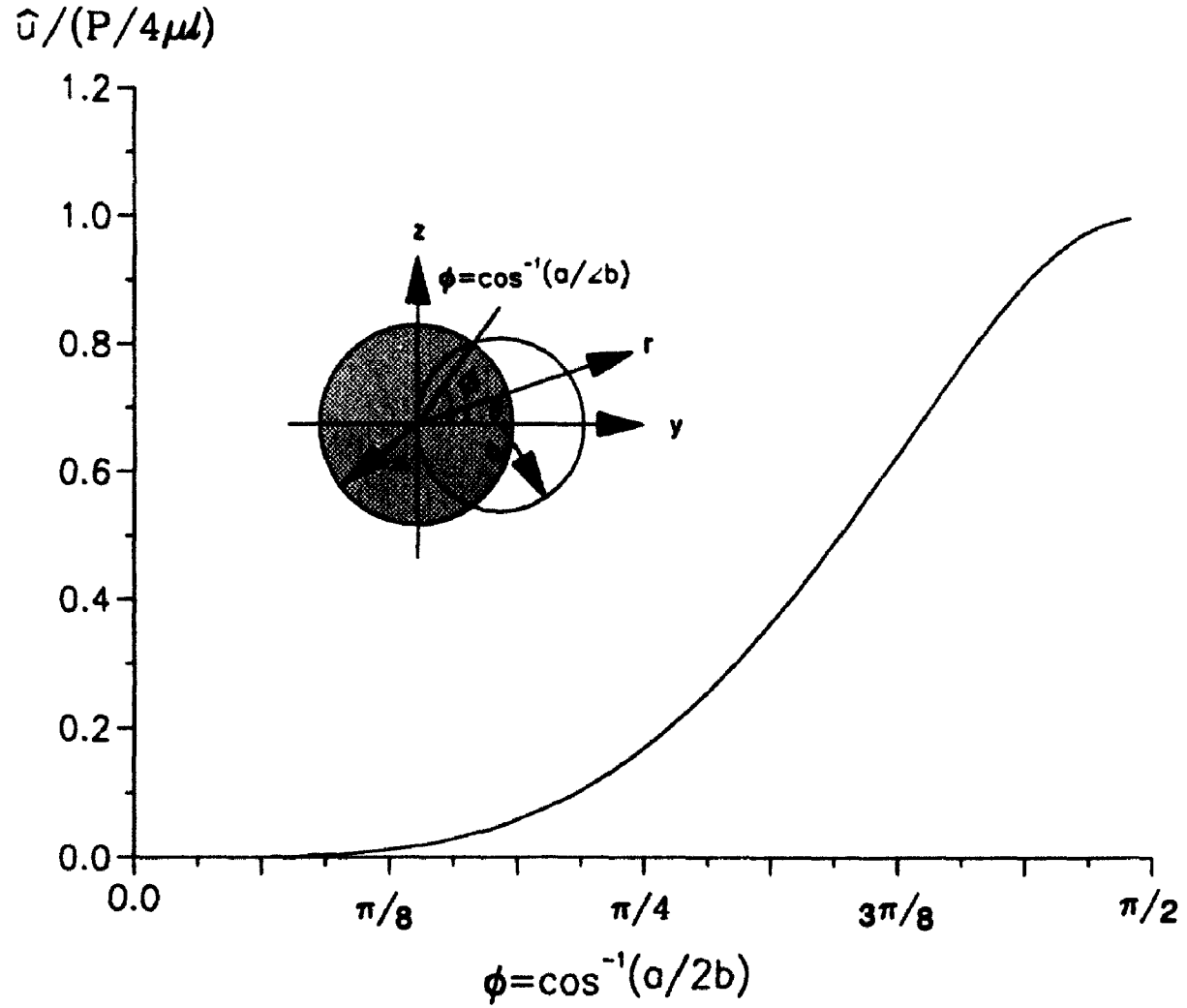

Fig. 3.17: Effects of thickness on maximum velocity in a tube of crescent-shaped cross section.

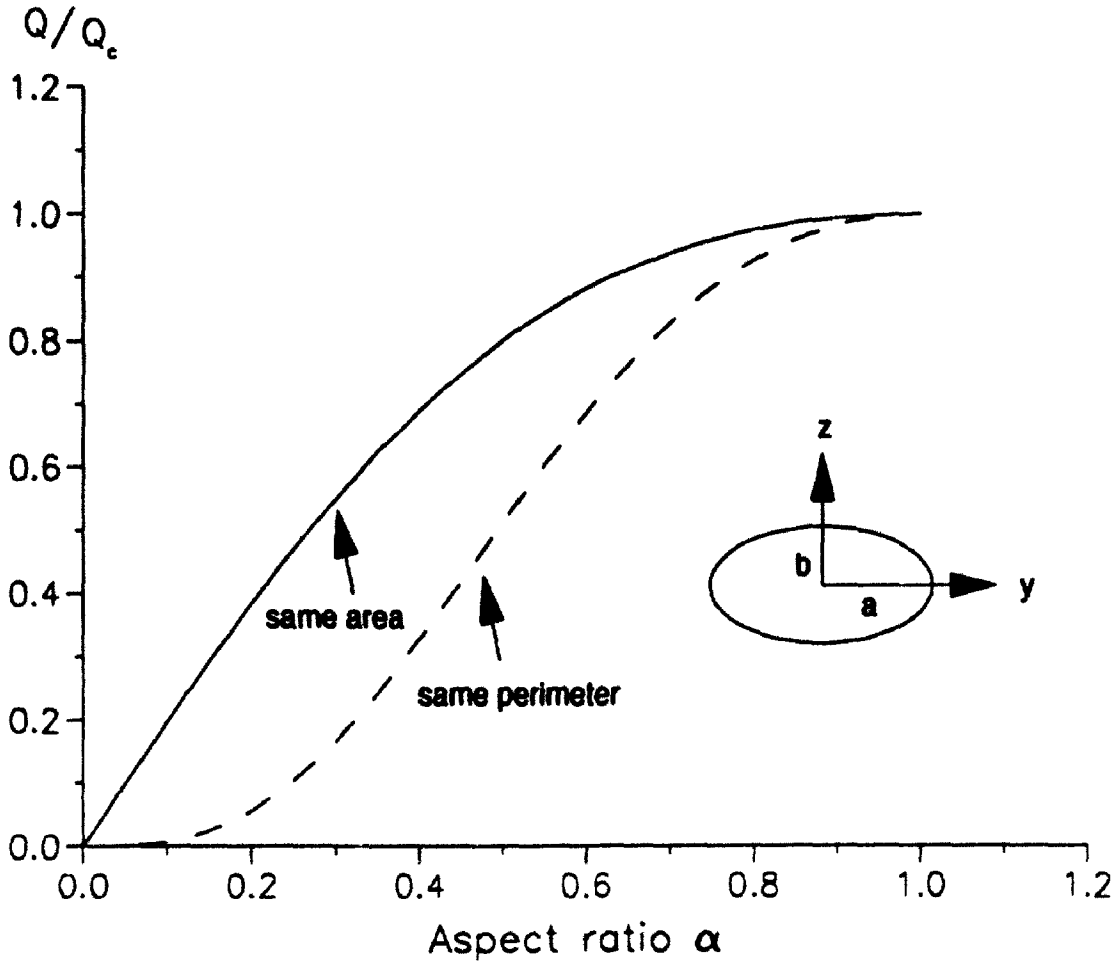

Fig. 3.18: Flow rate in tubes of elliptic cross sections, compared with that in a tube of circular cross section, for different degrees The two tubes have the same cross-sectional area in one case, and the same perimeter in the other.

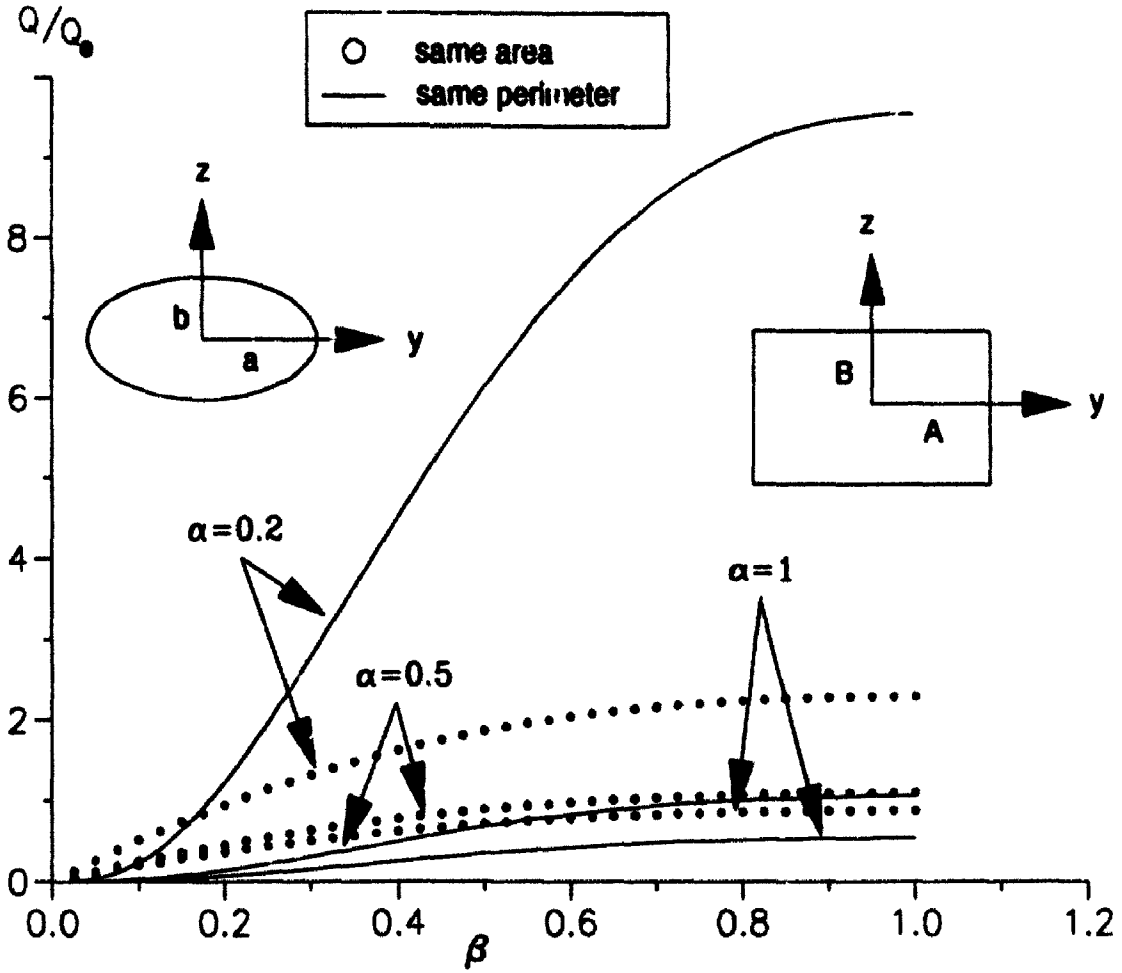

Fig. 3.19: Flow rate in tubes of rectangular and elliptic cross sections of different aspect ratios, compared with that in a tube of circular section. The two tubes have the same cross-sectional area in one case, and the same perimeter in the other.

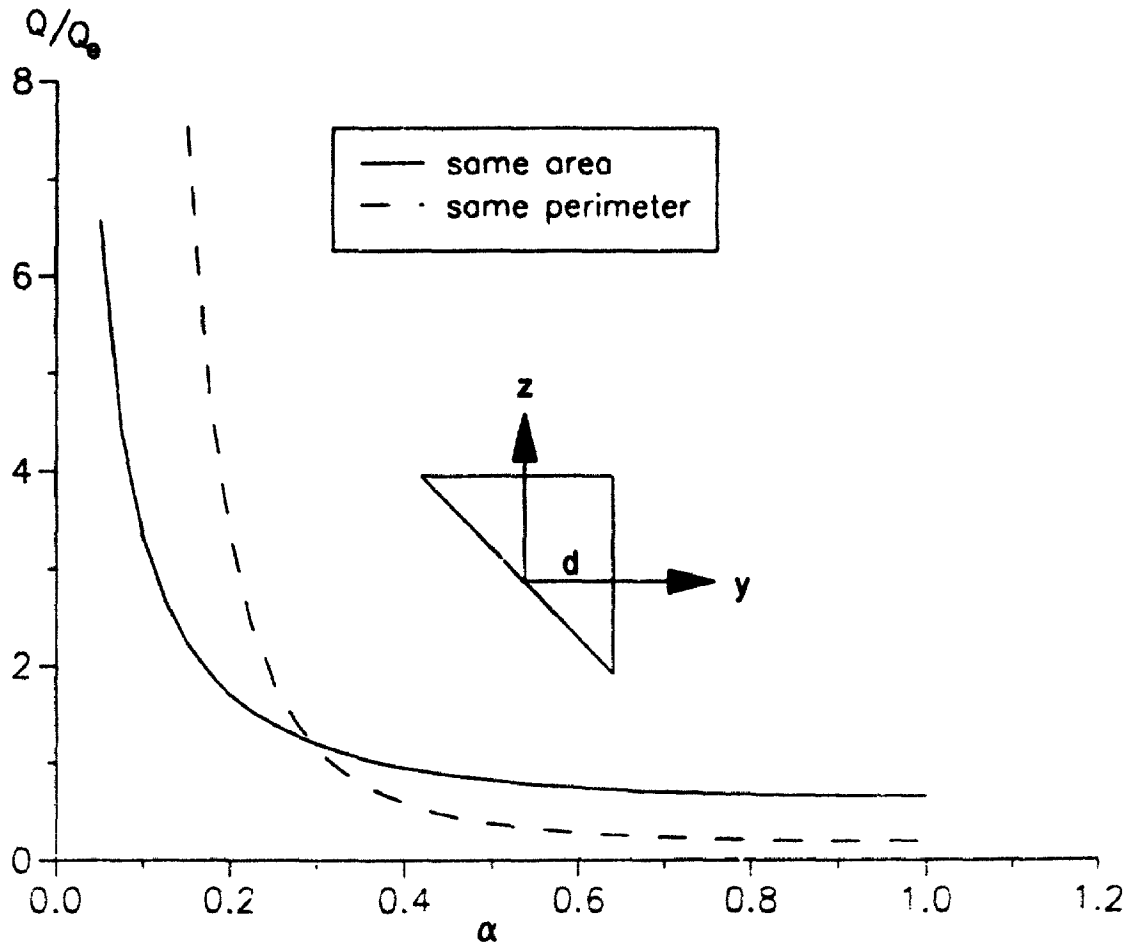

Fig. 3.20: Flow rate in a tube of right angle isosceles triangular cross section, compared with a tube of elliptic cross section of various aspect ratios. The two tubes have the same area in one case, and the same perimeter in the other.

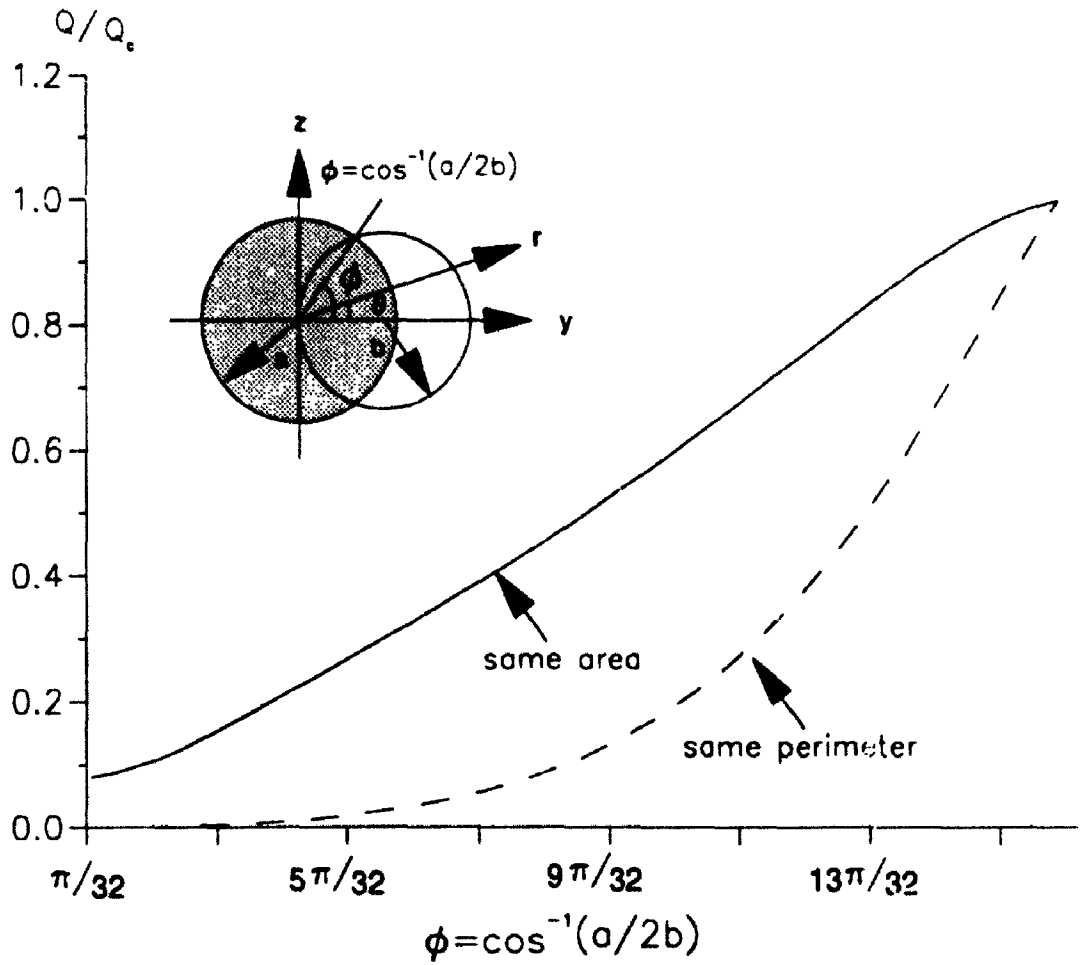

Fig. 3.21: Flow rate in tubes of crescent-shaped cross sections, compared with that in a tube of circular cross section. The two tubes have the same cross-sectional area in one case, and the same perimeter in the other.

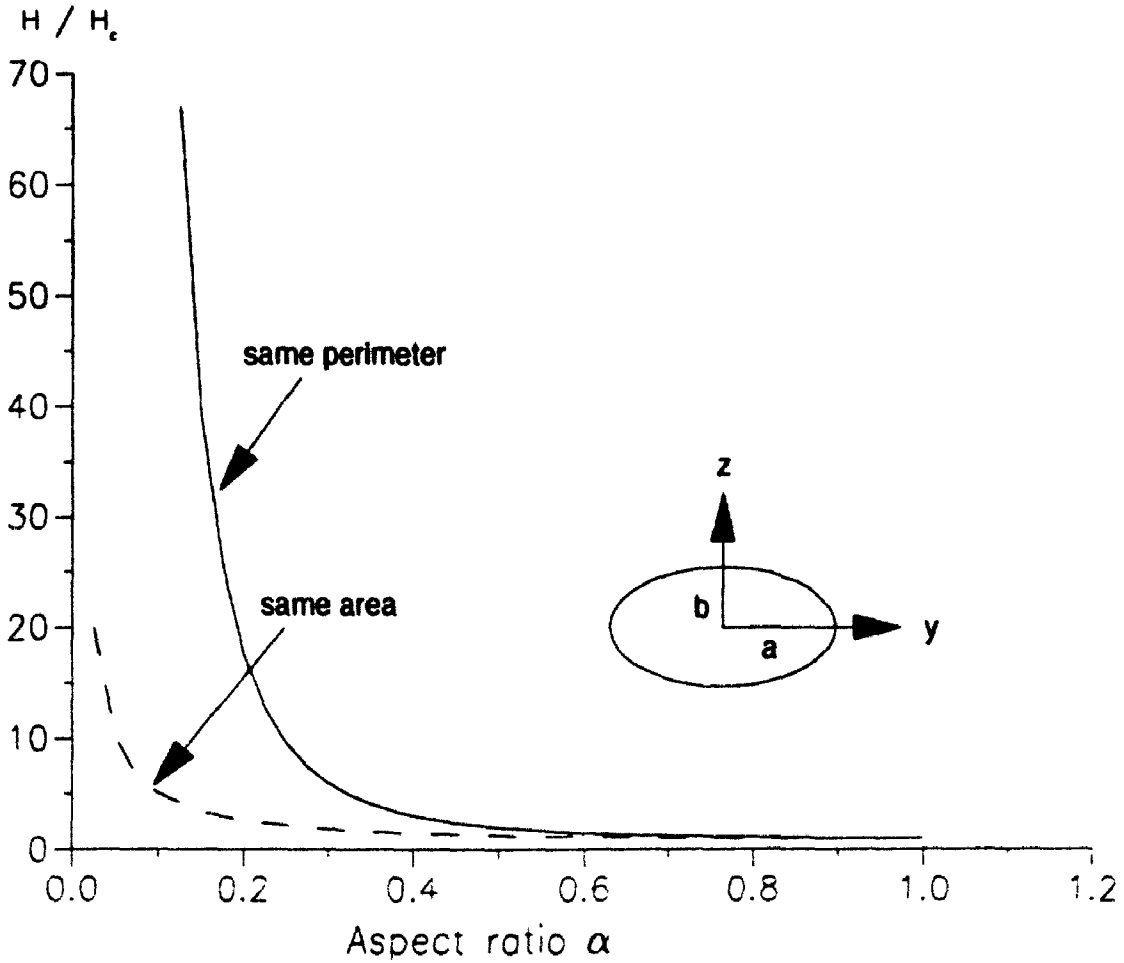

Fig. 3.22: Power in tubes of elliptic cross sections, compared with that in a tube of circular cross section, for different degrees of ellipticity. The two tubes have the same cross-sectional area in one case, and the same perimeter in the other.

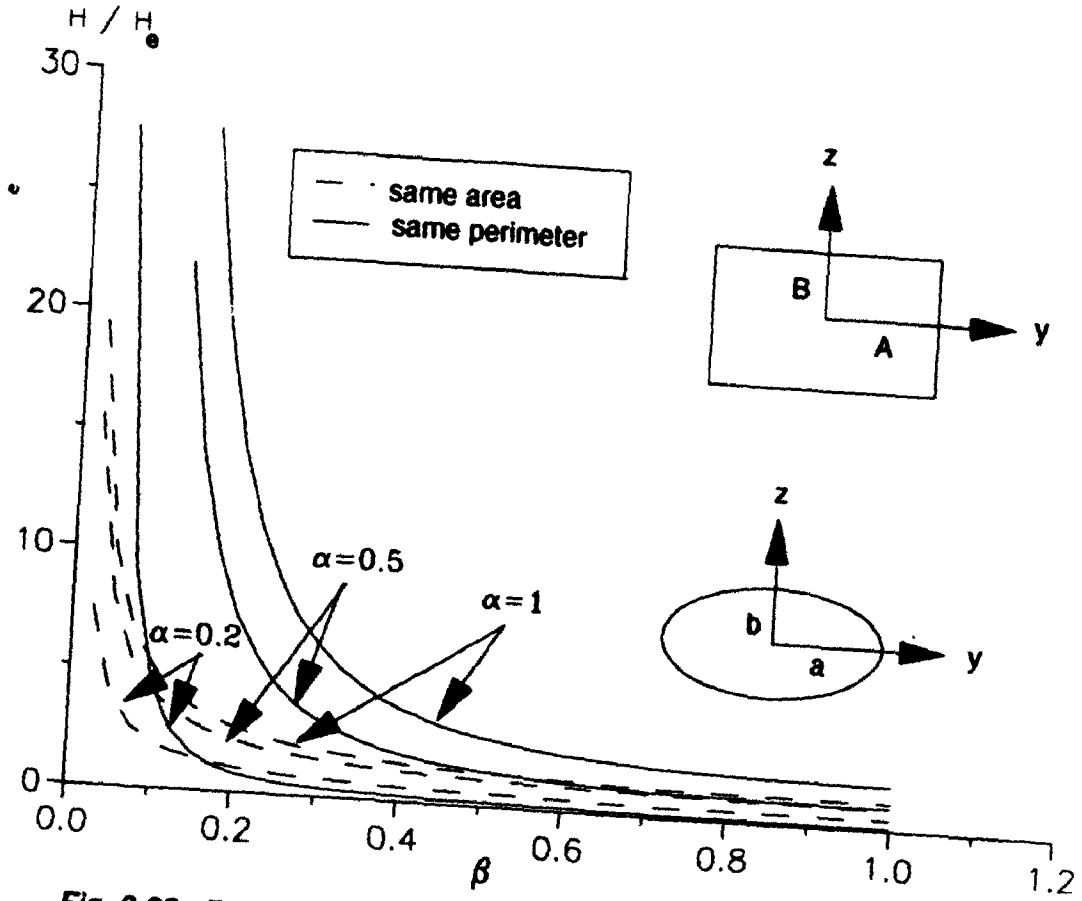

Fig. 3.23: Power in tubes of rectangular cross sections, compared with that in tubes of elliptic cross section of different aspect ratios. The two tubes have the same cross-sectional area in one case, and the same perimeter in the other.

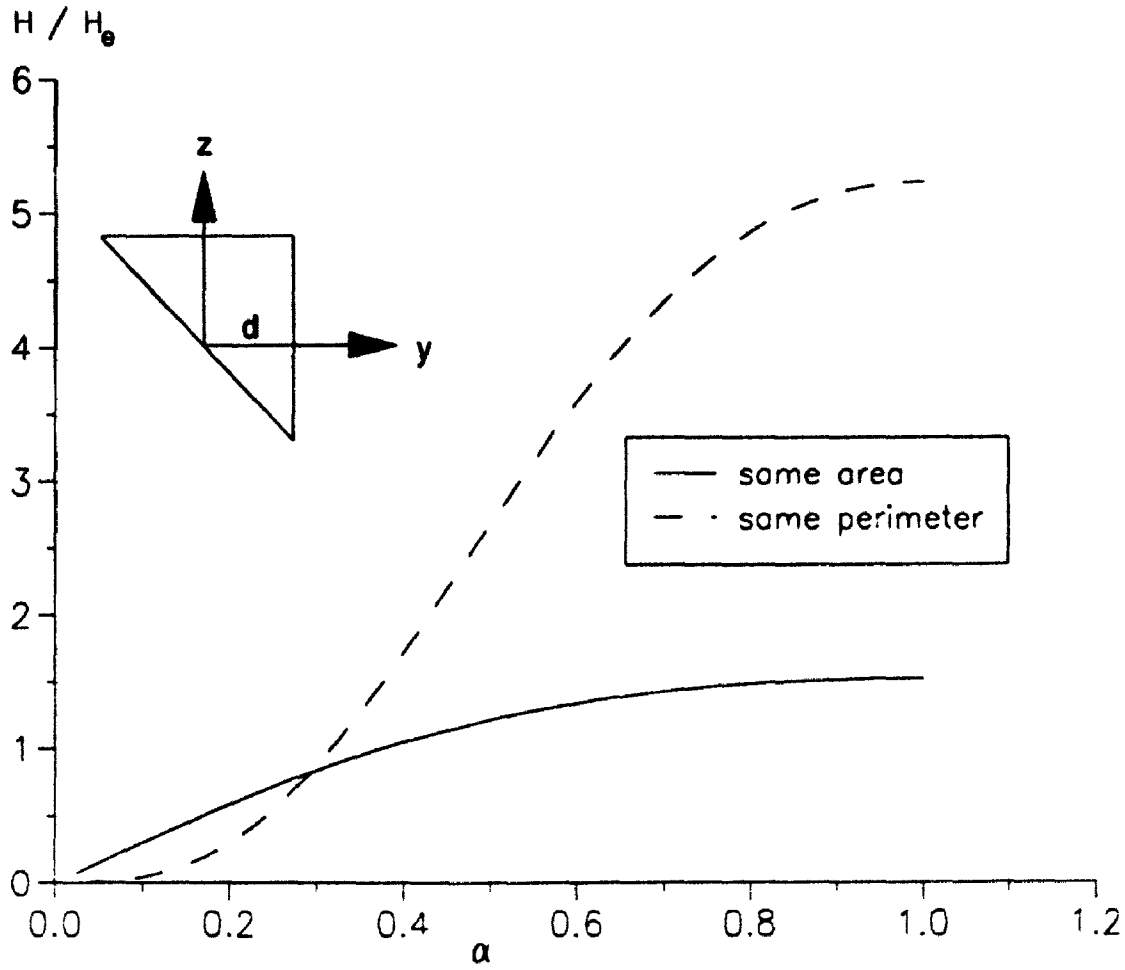

Fig. 3.24: Power in a tube of right angle triangular cross section, compared with that in tubes of elliptic cross sections of different aspect ratios. The two tubes have the same area in one case, and the same perimeter in the other.

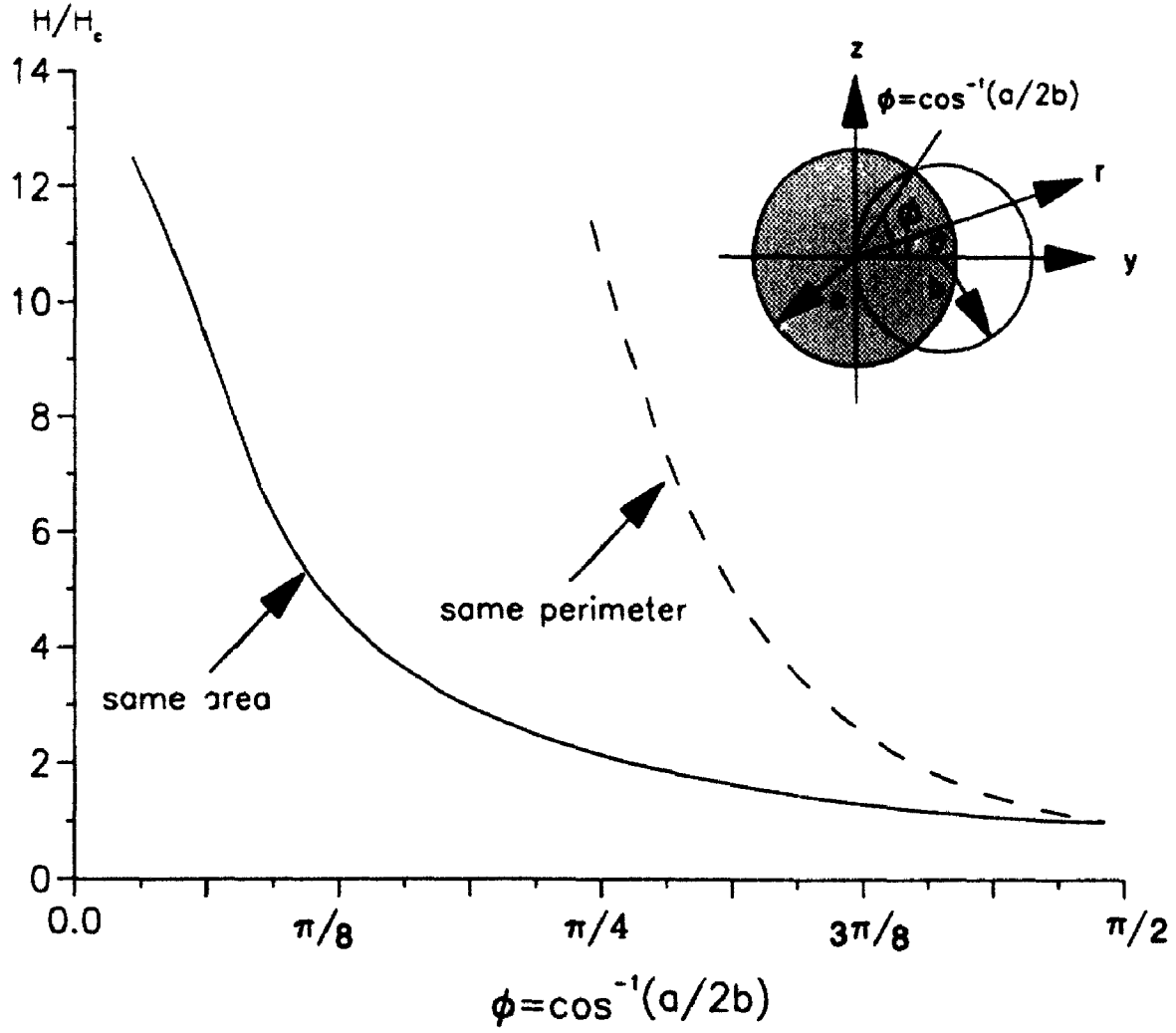

Fig. 3.25: Power in tubes of crescent-shaped cross sections, compared with that in a tube of circular cross section. The two tubes have the same area in one case, and the same perimeter in the other.

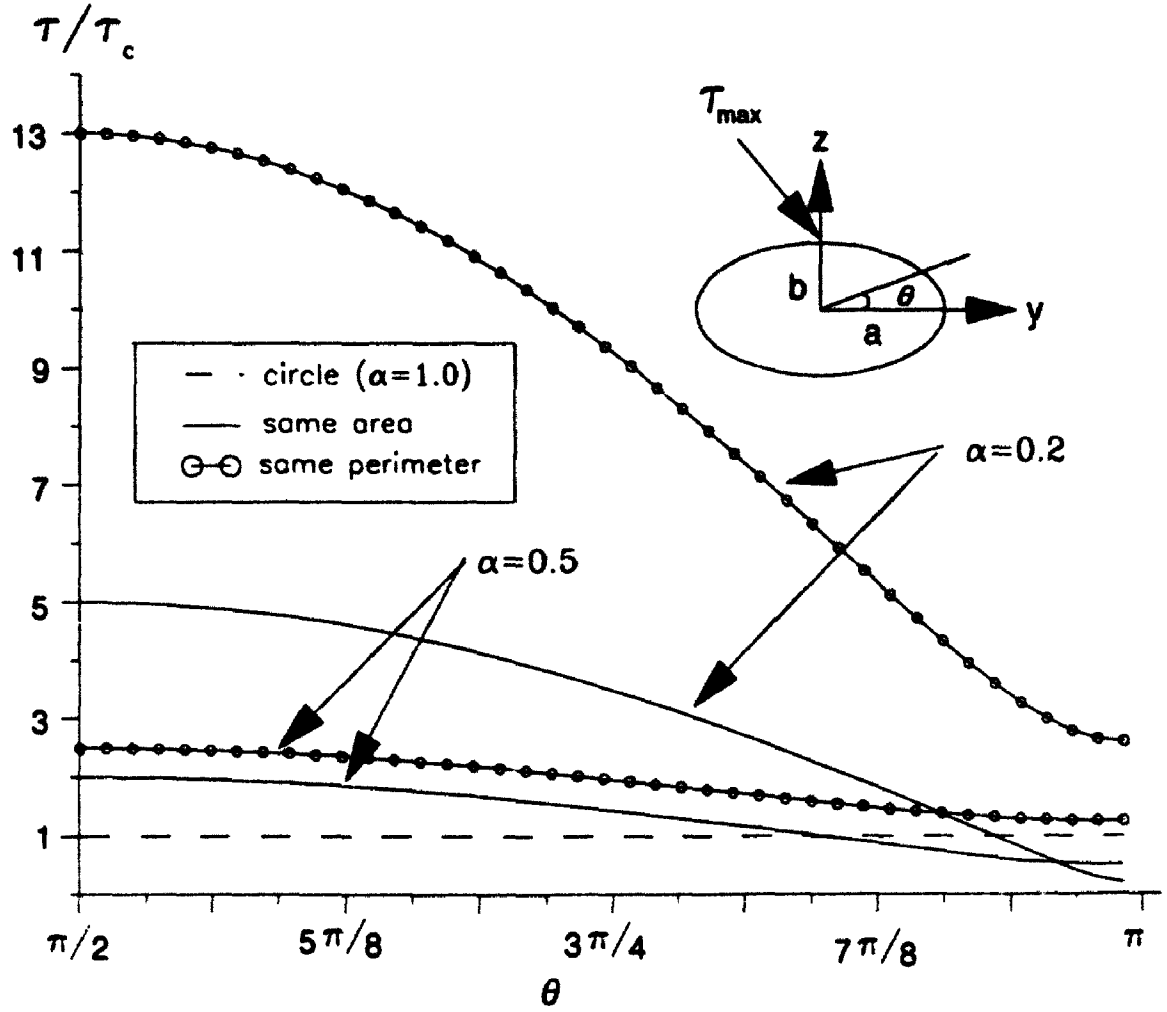

Fig. 3.26: Shearing stress in tubes of elliptic cross sections, compared with that in a tube of circular cross section. The two tubes have the same area in one case, and the same perimeter in the other.

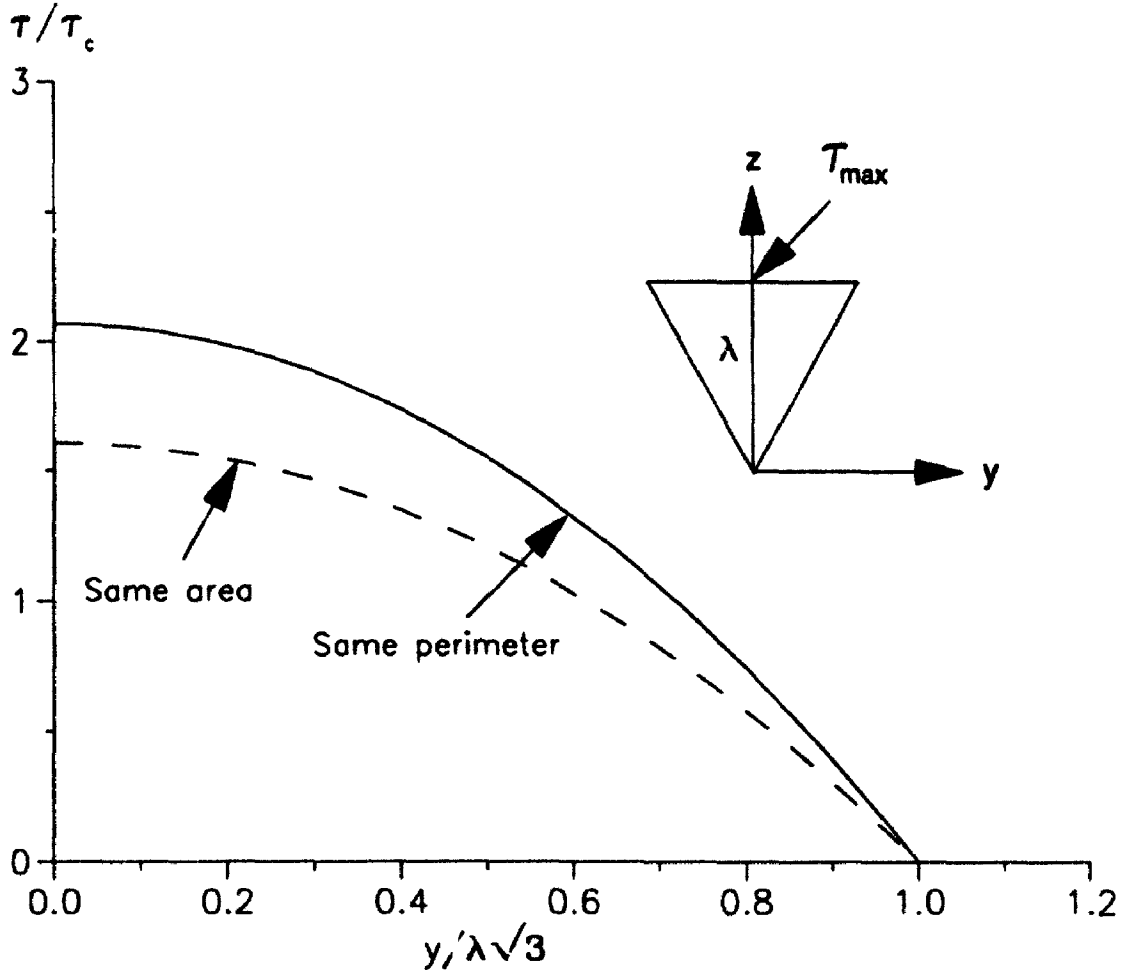

Fig. 3.27: Shearing stress along a side in a tube of equilateral triangular cross section, compared with that in a tube of cross section. The two tubes have the same area in one case, and the same perimeter in the other.

CHAPTER 4: FINITE ELEMENT METHOD FOR FULLY DEVELOPED FLOW IN TUBES OF NON-CIRCULAR CROSS SECTIONS

4.1 Introduction

In the previous chapter analytical solutions for fully developed flow in tubes of some non-circular cross section were obtained. For cross sections of more complicated or irregular shapes only numerical solutions are possible. A finite element method is proposed here to obtain numerical solution for the fully developed flow in tubes of arbitrary cross sections.

The computation of the flow field in tubes of arbitrary cross sections involves computational boundaries that do not coincide with coordinate lines in the physical space. The ability to handle non-uniform and curved boundaries of the computational domain is a particular feature of the finite element method, which is the reason for which we use this method.

The general objective of the finite element method is the same as that of other numerical methods, namely to reduce a set of continuous equations to a set of discrete algebraic equations. The procedure begins with the discretization of the domain (Sketch 4a), i.e., with the division of the continuous region of interest into a finite number of elements which may be of arbitrary shape and size. The only restriction is that the elements

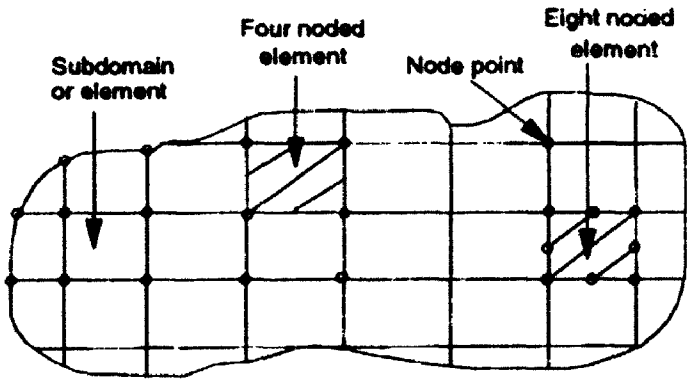

Sketch 4a: Finite element discretization of the domain.

may not overlap and that they cover the complete computational domain. An element type is characterized by its geometric shape and the local trial functions used to express its local behaviour. Each element is associated with a number of discrete points or *nodes* located on the element boundaries. The total number of unknowns at the nodes, function values and their derivatives, are called the *degrees of freedom* of the numerical problem. In two-dimensional problems the domain can be divided into triangles or rectangles, which may have straight or curved sides. In three-dimensional problem the domain can be divided into tetrahedral, cuboidal elements, or elements with curved surfaces.

Within each element, the dependent variables are approximated by linear combinations of known basis functions (also known as *interpolation*, *shape* or *trial functions*). Using a *variational principle*, or a *weighted residual method*, the governing differential equations are transformed into finite element equations. The equations are then integrated over each element and the contributions from each element are collected

together to form a global system of algebraic equations. The resultant equations are solved, after the introduction of appropriate boundary conditions. The nodal values of the variables are determined from solution of this system of equations.

Results are obtained for tubes of rectangular and elliptic cross sections with several aspect ratios, tubes of crescent-shaped cross sections and a tube whose cross section is an oval of Cassini. Results are compared with the corresponding analytical results, where available. Results for elliptic and rectangular cross sections are also compared with those obtained by using a commercial software package (FIDAP, Fluid Dynamics Analysis Package, Fluid Dynamics International). FIDAP is a general purpose finite element program for simulating viscous incompressible flow, including the effects of heat transfer, in two-dimensional, axi-symmetric, and three-dimensional geometries. As a result this package is cumbersome and time consuming.

4.2 Finite Element Formulation

Applying the finite element scheme to Eqn. 2.3.7, the velocity u within each element is approximated by

$$u = \sum_{i=1}^{I} \phi_i(y,z) u_i \tag{4.2.1}$$

where $\phi_i(y,z)$ are two-dimensional *interpolation or shape functions* and u_i are the unknown nodal values.

Substitution of Eqn. 4.2.1 into (2.3.7) leads to

$$\sum_{i=1}^{I} u_i \left[\frac{\partial^2 \phi_i}{\partial y^2} + \frac{\partial^2 \phi_i}{\partial z^2} \right] + K = R(y,z) \tag{4.2.2}$$

where $R(y,z)$ is the residual (error) function resulting from the approximations in (4.2.1). This residual should be as small as possible over the region considered. The integral of the residual, weighted with known weighting functions, is therefore required to vanish over this region. In the *Galerkin weighted residual method* the weighting functions are equal to the interpolation functions, i.e. the weighting functions are chosen to be the functions ϕ_j. Thus employing Galerkin weighted residual approach, Eqn. 4.2.2 becomes

$$\int\int_{\Omega_j} \left[\sum_{i=1}^{I} u_i \left(\frac{\partial^2 \phi_i}{\partial y^2} + \frac{\partial^2 \phi_i}{\partial z^2} \right) \phi_j \right] d\Omega + K \int\int_{\Omega_j} \phi_j(y,z) d\Omega = \int\int_{\Omega_j} R(y,z) \phi_j d\Omega \tag{4.2.3}$$

where Ω_j is the subdomain of all elements containing node j and the summation over i covers all the nodes of Ω_j.

In the Galerkin formulation it is required that

$$\int\int_{\Omega_j} R(y,z) \phi_j(y,z) d\Omega = 0, \quad j = 1,2,\ldots,I$$

This leads, after substitution for R, to the equations

$$\int\int_{\Omega_j}\left[\sum_{i=1}^{I} u_i\left(\frac{\partial^2\phi_i}{\partial y^2}+\frac{\partial^2\phi_i}{\partial z^2}\right)\phi_j\right]d\Omega + K\int\int_{\omega_j}\phi_j d\Omega = 0 \qquad (4.2.4)$$

In these equations it is seen that the integrand in the first integral contains second-order partial derivatives. Using Green's theorem and the fact that on the boundary segment ϕ_j vanishes for $j = 1,2,.....,I$, the system (4.2.4) can be replaced by the equivalent system of equations

$$-\sum_{i=1}^{I} u_i\int\int_{\Omega_j}\left[\frac{\partial\phi_i}{\partial y}\frac{\partial\phi_j}{\partial y}+\frac{\partial\phi_i}{\partial z}\frac{\partial\phi_j}{\partial z}\right]d\Omega = K\int\int_{\omega_j}\phi_j d\Omega \qquad (4.2.5)$$

This system may be represented in matrix form as:

$$\mathbf{CU} = \mathbf{G} \qquad (4.2.6)$$

where C is the global system matrix (known as the *stiffness matrix*), U is the global vector of unknown nodal values u_i and G is a global vector which contains the effects of boundary conditions.

4.2.1 Curved Elements and Numerical Integration

Curved Isoparametric Elements:

Problems involving curved boundaries cannot be modeled satisfactorily by using straight-sided elements. Curved elements known as "isoparametric elements" have been developed for this purpose. The technique consists of mapping or transforming simple

geometrical shapes in some local coordinate system (ξ, η) into curved shapes in the global cartesian coordinate system (y, z). The shape of the curved isoparametric elements is defined by the same interpolation functions as were used to define the field variables in (4.2.1) (Zienkiewicz 1977).

For this purpose we express u as

$$u(\xi, \eta) = \sum_{i=1}^{I} \phi_i(\xi, \eta) u_i \tag{4.2.7}$$

A mapping from the global coordinate system (x, y) to a local coordinates system (ξ, η) is then defined in the following way

$$y = \sum_{i=1}^{I} \phi_i(\xi, \eta) y_i \quad \text{and} \quad z = \sum_{i=1}^{I} \phi_i(\xi, \eta) z_i \tag{4.2.8}$$

where (y_i, z_i) are the coordinates of the ith corner node in physical space and $\phi_i(\xi, \eta)$ are the same interpolation functions used to define u.

In matrix form the relations between the derivatives in the two systems is given by

$$\begin{Bmatrix} \frac{\partial \phi_i}{\partial \xi} \\ \frac{\partial \phi_i}{\partial \eta} \end{Bmatrix} = \begin{bmatrix} \frac{\partial y}{\partial \xi}, \frac{\partial z}{\partial \xi} \\ \frac{\partial y}{\partial \eta}, \frac{\partial z}{\partial \eta} \end{bmatrix} \begin{Bmatrix} \frac{\partial \phi_i}{\partial y} \\ \frac{\partial \phi_i}{\partial z} \end{Bmatrix} = [J] \begin{Bmatrix} \frac{\partial \phi_i}{\partial y} \\ \frac{\partial \phi_i}{\partial z} \end{Bmatrix} \tag{4.2.9}$$

where J is the Jacobian matrix, or conversely

$$\begin{Bmatrix} \frac{\partial \phi_i}{\partial y} \\ \frac{\partial \phi_i}{\partial z} \end{Bmatrix} = [J]^{-1} \begin{Bmatrix} \frac{\partial \phi_i}{\partial \xi} \\ \frac{\partial \phi_i}{\partial \eta} \end{Bmatrix}$$

$$= \frac{1}{|J|} \begin{bmatrix} \frac{\partial z}{\partial \eta}, & -\frac{\partial z}{\partial \xi} \\ -\frac{\partial y}{\partial \eta}, & \frac{\partial y}{\partial \xi} \end{bmatrix} \begin{Bmatrix} \frac{\partial \phi_i}{\partial \xi} \\ \frac{\partial \phi_i}{\partial \eta} \end{Bmatrix} \qquad (4.2.10)$$

where the determinant of J is given by

$$|J| = \frac{\partial y}{\partial \xi}\frac{\partial z}{\partial \eta} - \frac{\partial y}{\partial \eta}\frac{\partial z}{\partial \xi} \qquad (4.2.11)$$

The terms on the right hand side of (4.2.11) are evaluated in terms of the interpolation function defining the coordinate transformation, using Eqn. 4.2.8

$$J = \begin{bmatrix} \sum_{i=1}^{I} \frac{\partial \phi_i}{\partial \xi} y_i, & \sum_{i=1}^{I} \frac{\partial \phi_i}{\partial \xi} z_i \\ \sum_{i=1}^{I} \frac{\partial \phi_i}{\partial \eta} y_i, & \sum_{i=1}^{I} \frac{\partial \phi_i}{\partial \eta} z_i \end{bmatrix}$$

Interpolation Functions:

The interpolation functions for the eight-noded rectangular element of Sketch 4b can be written

for corner nodes as:

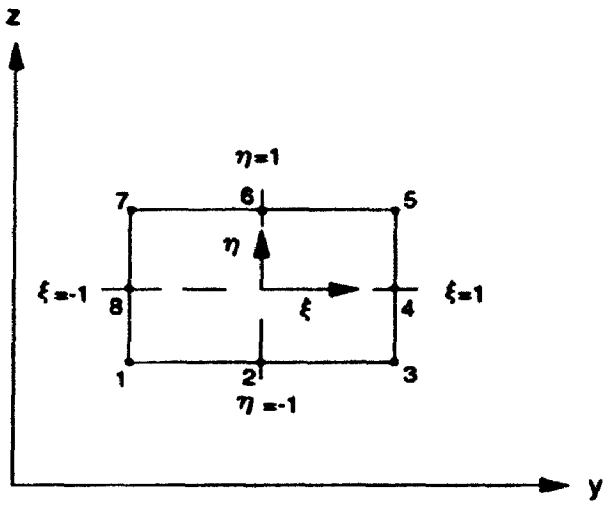

Sketch 4b: Eight noded rectangular element

$$\phi_i = \frac{1}{4}(1+\xi_i\xi)(1+\eta_i\eta)(\xi_i\xi+\eta_i\eta-1)$$

and for mid-side nodes as:

$$\phi_i = \frac{1}{2}(1-\xi^2)(1+\eta_i\eta), \qquad \xi_i = 0$$

$$\phi_i = \frac{1}{2}(1+\xi_i\xi)(1-\eta^2), \qquad \eta_i = 0 \qquad (4.2.12)$$

Numerical Integration:

Writing

$$dydz = |J|\,d\xi d\eta$$

and assuming that the inverse of the Jacobian can be found, we have now reduced the evaluation of the element properties (Eqn. 4.2.5) to that of finding integrals of the form

$$I = \int_{1}^{-1} \int_{1}^{-1} f(\xi, \eta) d\xi d\eta \tag{4.2.13}$$

While the limits of integration are now simple, the transformed integrand f is not a simple function that permits closed-form integration. For this reason, it is necessary to resort to numerical integration. The integration needs to be sufficiently accurate to ensure convergence.

To compute numerically the integral of $f(\xi, \eta)$ (in Eqn. 4.2.13) we use *Gauss-Legendre quadrature* (Stroud and Secrest, 1966). In a rectangular region the most obvious procedure to follow is to first evaluate the inner integral, keeping η constant, i.e.,

$$\int_{-1}^{1} f(\xi, \eta) d\xi = \sum_{j=1}^{n} H_j f(\xi_j, \eta) = \psi(\eta).$$

Then, evaluating the outer integral in a similar manner, we have

$$I = \int_{-1}^{1} \psi(\eta) d\eta$$

$$= \sum_{i=1}^{n} H_i \psi(\eta_i)$$

$$= \sum_{i=1}^{n} H_i \sum_{j=1}^{n} H_j f(\xi_j, \eta_i)$$

$$= \sum_{i=1}^{n} \sum_{j=1}^{n} H_i H_j f(\xi_j, \eta_i) \qquad (4.2.8)$$

where n is the total number of integration points, H_i and H_j are the weighting factors and (ξ_j, η_i) are the coordinate positions.

This method of integral evaluation is usually known as *Gauss- Legendre quadrature* or simply *Gauss quadrature*.

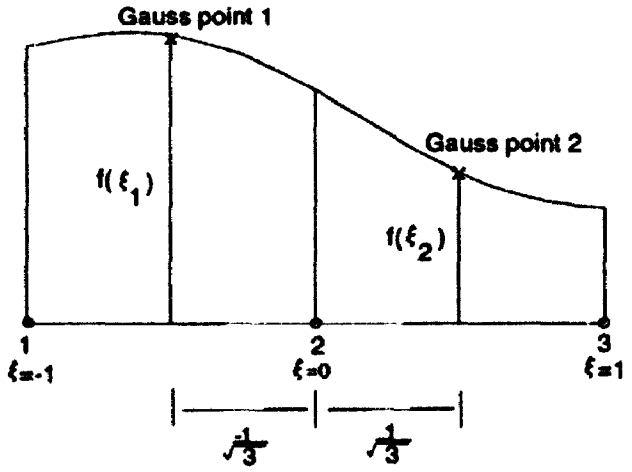

Sketch 4c: Unidimensional two point Gaussian integration.

Sketch 4c illustrates the unidimensional two-point Gaussian integration. Table 4.1 shows the positions and weighting coefficients for Gaussian integration.

n	i	ξ_i	H_i
1	1	0	2
2	1	$1/\sqrt{3}$	1
2	2	$-1/\sqrt{3}$	1

Table 4.1: Positions and weighting coefficients for Gaussian integration.

4.3 Application to Rectangular Cross Sections

For tubes of rectangular cross sections it is computationally advantageous to non-dimensionalize Eqn. 2.3.7 as follows

$$y^* = \frac{y}{A}, \qquad z^* = \frac{z}{B}, \qquad u^* = u\left(-\frac{K}{B^2}\right)$$

where star denotes dimensionless quantities, A, B are the major and minor dimensions of the cross section, and K is the pressure gradient.

Thus in non-dimensional form the governing equation becomes (dropping the stars)

$$\beta^2\frac{\partial^2 u}{\partial y^2} + \frac{\partial^2 u}{\partial z^2} + 1 = 0 \qquad (4.3.1)$$

with boundary conditions

$$u = 0 \qquad at \quad y = \pm 1, \quad z = \pm 1 \tag{4.3.2}$$

We follow the procedure for finite element formulation described in the previous section. Substituting Eqn. 4.2.1 into 4.3.1, using Galerkin formulation, and after some algebraic manipulation we obtain the following system of equations

$$\mathbf{CU} = \mathbf{G} \tag{4.3.3}$$

where a general element of **C** is given by

$$c_{j,i} = -\int_{-1}^{1}\int_{-1}^{1}\left[\beta^2 \frac{\partial \phi_i}{\partial y}\frac{\partial \phi_j}{\partial y} + \frac{\partial \phi_i}{\partial z}\frac{\partial \phi_j}{\partial z}\right] dy\,dz \tag{4.3.4}$$

and a general element in G is given by

$$g_j = \int_{-1}^{1}\int_{-1}^{1} \phi_j\, dy\, dz \tag{4.3.5}$$

The integrals in Eqn. 4.3.5 must be evaluated over each element, individually, using element based coordinate system (ξ, η). Only four contiguous rectangular elements surrounding node j make nonzero contributions to the global integrals in Eqns. 4.3.4 and 4.3.5.

Following Fletcher (1991), Eqn. 4.3.3 takes the following form for a uniform grid

$$[\beta^2 M_z \otimes L_{yy} + M_y \otimes L_{zz}]u_{k,l} = -1 \tag{4.3.6}$$

where $\otimes$ is the tensor or outer product, M_y, M_z are directional operators (sometimes referred to as "mass" operators (Fletcher 1991) and L_{yy}, L_{zz} are directional difference operators. The significance of Eqn. 4.3.6 is that it permits a term-by-term finite element discretization in a manner equivalent to that of the finite difference method. Thus the term $\partial^2 u/\partial y^2$ in Eqn. 4.3.1 is discretized as $[M_z \otimes L_{yy}]u$ and the term $\partial^2 u/\partial z^2$ is discretized as $[M_y \otimes L_{zz}]u$.

The directional difference operators L_{yy} and L_{zz} are defined as

$$L_{yy} = \left(\frac{1}{\Delta y^2}, -\frac{2}{\Delta y^2}, \frac{1}{\Delta y^2} \right)$$
$$L_{zz} = \left(\frac{1}{\Delta z^2}, -\frac{2}{\Delta z^2}, \frac{1}{\Delta z^2} \right)^T \tag{4.3.7}$$

and the directional mass operators M_y and M_z are defined as

$$M_y = M_z^T = \left(\frac{1}{6}, \frac{2}{3}, \frac{1}{6} \right) \tag{4.3.8}$$

On the global grid, the operators in Eqn. 4.3.6 have the following form

$$L_{yy}u_{k,l}=\frac{u_{k-1,l}-2u_{k,l}+u_{k+1,l}}{\Delta y^2}$$

$$M_z u_{k,l}=\frac{1}{6}u_{k,l-1}+\frac{2}{3}u_{k,l}+\frac{1}{6}u_{k,l+1}$$

$$[M_z\otimes L_{yy}]u_{k,l}=\frac{1}{6}\left\{\frac{u_{k-1,l+1}-2u_{k,l-1}+u_{k+1,l-1}}{\Delta y^2}\right\}+\frac{2}{3}\left\{\frac{u_{k-1,l}-2u_{k,l}+u_{k+1,l}}{\Delta y^2}\right\}$$
$$+\frac{1}{6}\left\{\frac{u_{k-1,l}-2u_{k,l}+u_{k+1,l-1}}{\Delta y^2}\right\} \qquad (4.3.9)$$

$$[M_y\otimes L_{zz}]u_{k,l}=\frac{1}{6}\left\{\frac{u_{k-1,l-1},-2u_{k,l-1}+u_{k+1,l}}{\Delta z^2}\right\}+\frac{2}{3}\left\{\frac{u_{k-1,l}-2u_{k,l}+u_{k+1,l}}{\Delta z^2}\right\}$$
$$+\frac{1}{6}\left\{\frac{u_{k-1,l+1}-2u_{k,l+1}+u_{k+1,l+1}}{\Delta z^2}\right\} \qquad (4.3.10)$$

The system of equations formed by applying Eqn. 4.3.6 at each internal node is solved by using a successive-over-relaxation (SOR) iterative method. Iterative methods for solving linear algebraic equations are particularly suitable when the elements of the matrix consist mainly of zeros, because these methods take advantage of the zero elements. The algorithm is written as

$$u^{*}_{k,l}=0.75[1+\frac{A_1}{6}(u^{n}_{k-1,l+1}+u^{n}_{k+1,l+1}+u^{n+1}_{k-1,l-1}+u^{n+1}_{k+1,l-1})$$
$$+A_2(u^{n}_{k,l+1}+u^{n+1}_{k,l-1})+A_3(u^{n+1}_{k-1,l}+u^{n}_{k+1,l})]/A_1 \qquad (4.3.11)$$

where

$$A_1 = \frac{\beta^2}{\Delta y^2} + \frac{1}{\Delta z^2}$$

$$A_2 = \frac{1}{3}\left(-\frac{\beta^2}{\Delta y^2} + \frac{2}{\Delta z^2}\right)$$

$$A_3 = \frac{1}{3}\left(\frac{2\beta^2}{\Delta y^2} - \frac{1}{\Delta z^2}\right)$$

This equation provides an estimate and the following equation an improvement

$$u_{k,l}^{n+1} = u_{k,l}^{n} + \omega(u_{k,l}^{*} - u_{k,l}^{n}) \qquad (4.3.12)$$

where ω is a relaxation parameter. The above finite element formulation is implemented by a FORTRAN program to calculate velocity distribution and flow rate for a tube of rectangular cross section. The relaxation parameter is taken as 1.2.

4.4 Application to Cross Sections with Curved Boundaries

For a tube of an arbitrary cross section, the governing equation (Eqn. 2.3.7) is in the form

$$\frac{\partial^2 u}{\partial y^2} + \frac{\partial^2 u}{\partial z^2} + 1 = 0 \qquad (4.4.1)$$

subject to the boundary condition

$$u = 0 \quad \text{at the tube wall.}$$

where u has been non-dimensionalized in terms of $-K$.

The application of Galerkin finite element method to Eqn. 4.4.1 in a curved domain produces the following system of equations

$$\mathbf{CU} = \mathbf{G} \tag{4.4.2}$$

where a general element of **C** is given by

$$c_{j,i} = -\int\int_{\Omega}\left(\frac{\partial\phi_i}{\partial y}\frac{\partial\phi_j}{\partial y}+\frac{\partial\phi_i}{\partial z}\frac{\partial\phi_j}{\partial z}\right)dy\,dz \tag{4.4.3}$$

where j is the node at which the weight function is centered and i is the contributing node.

A general element of **G** is given by

$$g_j = \int\int_{\Omega}\phi_i\,dy\,dz \tag{4.4.4}$$

We have used curved isoparametric elements for the evaluation of (4.4.2) in physical space. The advantage of the isoparametric formulation is that it is easier to carry out the integration (numerically) in the transformed space where the elements are uniform. We have used triangular elements, an example is shown in Sketch 4d.

We consider u as a function of y and z

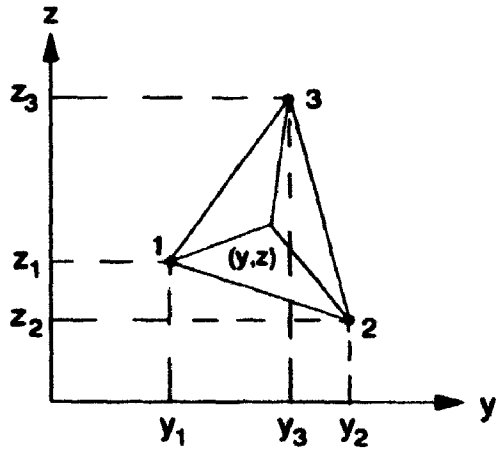

Sketch 4d: Triangular Element

$$u = \alpha_1 + \alpha_2 y + \alpha_3 z \tag{4.4.5}$$

where the coefficients α_1, α_2 and α_3 are to be determined from the relations

$$u_1 = \alpha_1 + \alpha_2 y_1 + \alpha_3 z_1 \qquad \text{at node 1}$$

$$u_2 = \alpha_1 + \alpha_2 y_2 + \alpha_3 z_2 \qquad \text{at node 2}$$

$$u_3 = \alpha_1 + \alpha_2 y_3 + \alpha_3 z_3 \qquad \text{at node 3}$$

In matrix form

$$\begin{Bmatrix} u_1 \\ u_2 \\ u_3 \end{Bmatrix} = \begin{bmatrix} 1 & y_1 & z_1 \\ 1 & y_2 & z_2 \\ 1 & y_3 & z_3 \end{bmatrix} \begin{Bmatrix} \alpha_1 \\ \alpha_2 \\ \alpha_3 \end{Bmatrix} \tag{4.4.6}$$

The inverse of Eqn.4.4.6 gives

$$\begin{Bmatrix}\alpha_1\\ \alpha_2\\ \alpha_3\end{Bmatrix}=\frac{1}{2A_r}\begin{bmatrix}k_{11} & k_{12} & k_{13}\\ k_{21} & k_{22} & k_{23}\\ k_{31} & k_{32} & k_{33}\end{bmatrix}\begin{Bmatrix}u_1\\ u_2\\ u_3\end{Bmatrix} \tag{4.4.7}$$

where
$$k_{11}=(y_2z_3-y_3z_2)/2A_r,\qquad k_{12}=(y_3z_1-y_1z_3)/2A_r$$
$$k_{13}=(y_1z_2-y_2z_1)/2A_r$$
$$k_{21}=(z_2-z_3)/2A_r,\qquad k_{31}=(y_3-y_2)/2A_r$$
$$k_{22}=(z_3-z_1)/2A_r,\qquad k_{32}=(y_1-y_3)/2A_r \tag{4.4.8}$$
$$k_{23}=(z_1-z_2)/2A_r,\qquad k_{33}=(y_2-y_1)/2A_r$$

and A_r is the area of the triangular element given by

$$A_r=(y_2z_3+y_1z_2+y_3z_1)-(y_1z_3+y_3z_2+y_2z_1) \tag{4.4.9}$$

Eqn. 4.4.5 can be written as

$$u(y,z)=\frac{1}{2A_r}(k_{11}+k_{21}y+k_{31}z)u_1+\frac{1}{2A_r}(k_{12}+k_{22}y+k_{32}z)u_2$$
$$+\frac{1}{2A_r}(k_{13}+k_{23}y+k_{33}z)u_3 \tag{4.4.10}$$

which can be expressed as

$$u=\sum_{i=1}^{3}\phi_i u_i \tag{4.4.11}$$

where

$$\phi_1 = \frac{1}{2A_r}(k_{11} + k_{21}y + k_{31}z)$$

$$\phi_2 = \frac{1}{2A_r}(k_{12} + k_{22}y + k_{32}z)$$

$$\phi_3 = \frac{1}{2A_r}(k_{13} + k_{23}y + k_{33}z)$$

Triangular Coordinates

Let $P(y,z)$ be a point in the triangle 123 (Sketch 4d) and A_1, A_2 and A_3 be three sub-triangles of areas A_1, A_2 and A_3 such that

$$A_r = A_1 + A_2 + A_3 \tag{4.4.12}$$

The triangular coordinates are then defined as

$$\zeta_1 = \frac{A_1}{A_r}, \quad \zeta_2 = \frac{A_2}{A_r}, \quad \zeta_3 = \frac{A_3}{A_r} \tag{4.4.13}$$

From Eqns. 4.4.12 and 4.4.13, we get

$$\zeta_1 + \zeta_2 + \zeta_3 = 1$$

Using Eqns. 4.4.9 and 4.4.13 we get the relationship between the Cartesian and the triangular coordinates:

$$y = \sum_{i=1}^{3} \zeta_i(\xi,\eta)y_i, \quad z = \sum_{i=1}^{3} \zeta_i(\xi,\eta)z_i \tag{4.4.14}$$

The integration of polynomial functions, ζ_i, which are defined in terms of the triangular coordinates, is fairly simple and can be calculated using the expression

$$\int\int \zeta_1^i \zeta_2^j \zeta_3^k dA_r = \frac{i!j!k!}{(i+j+k+2)!} 2A_r \qquad (4.4.15)$$

where A_r is defined in Eqn. 4.4.9.

For example,

$$\int\int 3\zeta_1^2 dA_r = 3\left(\frac{2!0!0!}{4!}\right)2A_r = \frac{A_r}{2}$$

$$\int\int 2\zeta_2^1 \zeta_3^1 dA_r = 2\left(\frac{0!1!1!}{4!}\right)2A_r = \frac{A_r}{6}$$

$$\int\int dA_r = \left(\frac{0!0!0!}{2!}\right)2A_r = A_r$$

In this case we have used six-noded triangular elements. Thus the matrix **C** is a 6×6 symmetric matrix and its coefficients are finally given by

$$c_{11} = k_{21}^2 + k_{31}^2, \qquad c_{12} = -\frac{1}{3}(k_{21}k_{22} + k_{31}k_{32}), \qquad c_{13} = -\frac{1}{3}(k_{21}k_{23} + k_{31}k_{33})$$

$$c_{14} = \frac{4}{3}(k_{21}k_{22} + k_{31}k_{32}), \qquad c_{15} = 0, \qquad c_{16} = \frac{4}{3}(k_{21}k_{23} + k_{31}k_{33})$$

$$c_{22} = k_{22}^2 + k_{32}^2 \qquad c_{23} = -\frac{1}{3}(k_{22}k_{23} + k_{32}k_{33}) \qquad c_{24} = c_{14}$$

$$c_{25} = \frac{4}{3}(k_{22}k_{23} + k_{32}k_{33}), \qquad c_{26} = 0, \qquad c_{33} = k_{23}^2 + k_{33}^2$$

$$c_{34} = 0, \qquad c_{35} = \frac{4}{3}(k_{22}k_{23} + k_{32}k_{33}), \qquad c_{36} = c_{16}$$

$$c_{44} = \frac{8}{3}(k_{21}^2 + k_{21}k_{22} + k_{22}^2 + k_{31}^2 + k_{31}k_{32} + k_{32}^2)$$

$$c_{45} = \frac{4}{3}(k_{21}(k_{22} + 2k_{23}) + k_{22}(k_{22} + k_{23}) + k_{31}(k_{32} + 2k_{33}) + k_{32}(k_{32} + k_{33}))$$

$$c_{46} = \frac{4}{3}(k_{21}(k_{21} + k_{23}) + k_{22}(k_{21} + 2k_{23}) + k_{31}(k_{31} + k_{33}) + k_{32}(k_{31} + 2k_{33}))$$

$$c_{55} = \frac{8}{3}(k_{22}^2 + k_{22}k_{23} + k_{23}^2 + k_{32}^2 + k_{32}k_{33} + k_{33}^2)$$

$$c_{56} = \frac{4}{3}(k_{22}(2k_{21} + k_{23}) + k_{23}(k_{21} + k_{23}) + k_{32}(2k_{31} + k_{33}) + k_{23}(k_{31} + k_{33}))$$

$$c_{66} = \frac{8}{3}(k_{21}^2 + k_{21}k_{23} + k_{23}^2 + k_{31}^2 + k_{31}k_{33} + k_{33}^2) \qquad (4.4.16)$$

The coefficients k_{ij} are given by

$$
\begin{aligned}
k_{12} &= (z_2 - z_3)/2A_r, & k_{31} &= (y_3 - y_2)/2A_r \\
k_{22} &= (z_3 - z_1)/2A_r, & k_{32} &= (y_1 - y_3)/2A_r \\
k_{23} &= (z_1 - z_2)/2A_r, & k_{33} &= (y_2 - y_1)/2A_r
\end{aligned}
\tag{4.4.17}
$$

Applying appropriate boundary conditions and using Gauss elimination technique the required solution is finally obtained.

This procedure can be applied to any cross section with a curved boundary. The boundary is specified by means of data points rather than an analytical curve. The general program structure is the same for all cross sections, the only difference is in the type of the finite element mesh to be used in a particular cross section. Nodal point coordinate locations, element locations, element numbers and associated nodal points are given as an input data set, once the element mesh has been chosen. The velocity is set to zero on all boundary nodes. Only the input data set is different for different cross sections. We applied this scheme for the flow in tubes of elliptic and crescent-shaped cross sections, and one whose cross section is an oval of Cassini.

4.5 General Program Structure

In what follows the general program structure for the solution of fully developed flow in tubes of arbitrary cross sections is described. Our finite element code consists of three functional units which shall be referred as the preprocessor, processor and postprocessor units, following Becker, et al., 1981. The preprocessor unit reads and generates the input data. In the processor unit the element matrices and vectors are

calculated and assembled, boundary conditions are imposed and the global set of equations are solved for nodal-point values. The solution is finally printed in the postprocessor unit. The general structure of the program is shown in Sketch 4e. The basic finite element steps are performed by primary subroutines which rely on auxiliary subroutines to carry out secondary operations. All primary subroutines are called from a main program segment called MAIN. A brief description of each subroutine is given below.

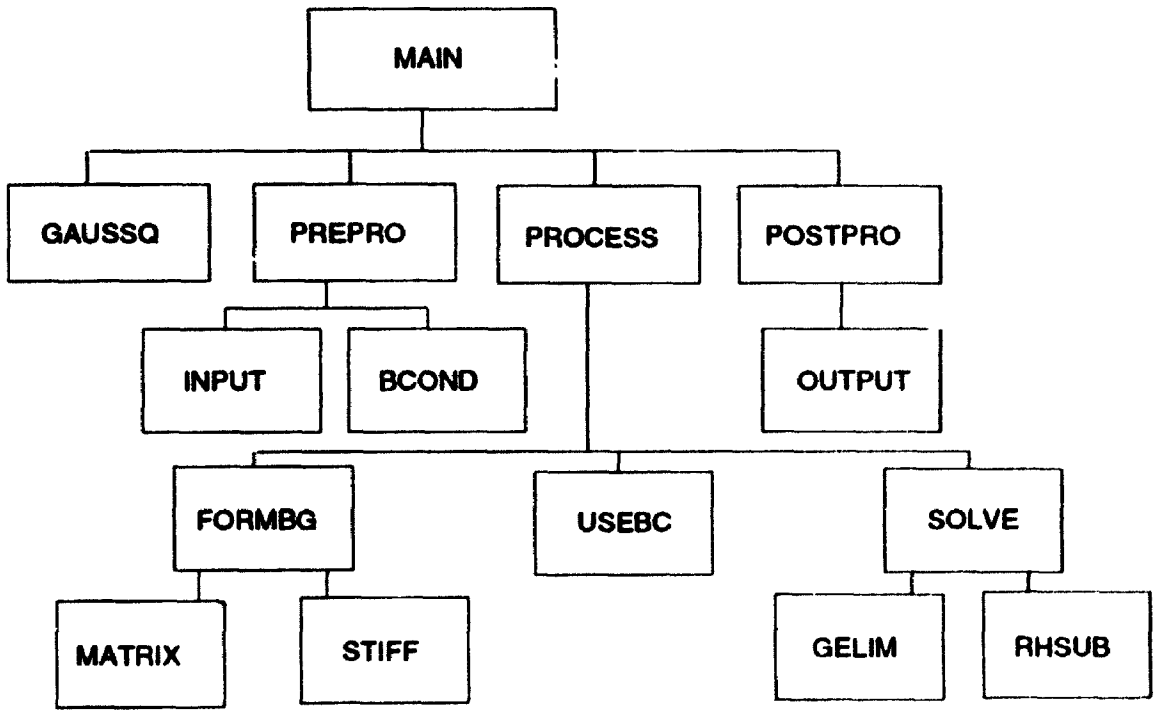

Sketch 4e: General program structure

4.3.1 Subroutines

(1) GAUSSQ

The function of this subroutine is to set up the sampling point positions and weighting factors for the numerical integration of element matrices and vectors. It calculates Gauss quadrature, using two-point integration rules.

(2) PREPRO

This is the preprocessor subroutine. PREPRO calls subroutines to read and generate data.

(a) INPUT

Subroutine INPUT reads and generates input data which includes nodal-point coordinate location, element location, element numbers and associated nodal points and material properties.

(b) BCOND

This subroutine reads data that define the boundary conditions.

(3) PROCESS

This is the processor subroutine. PROCESS calls subroutines which formulate the global matrix, impose the boundary conditions and solve the resulting equations.

(a) FORMBG

This subroutine directs the calculation of the *stiffness matrix* **C** and vector **G** (in Eqn. 4.2.6) by subroutines STIFF and MATRIX.

Subroutine STIFF computes the stiffness matrix and calculates the right hand side vector **G** of Eqn. 4.2.6.

Subroutine MATRIX stores the stiffness matrix into the total matrix.

(b) USEBC

This subroutine modifies the global matrix system required to apply the boundary conditions.

(c) SOLVE

This subroutine directs the solution of the resulting algebraic equations by the routines GELIM and RHSUB.

Subroutine GELIM performs Gaussian elimination on the matrix **C** in Eqn. 4.2.6.

Subroutine RHSUB performs forward substitution on the right-hand-side vector **G** of Eqn. 4.2.6, and then performs back substitution to calculate the values of u.

(4) POSTPRO

This is the postprocessor subroutine. POSTPRO calls subroutines which process the results.

(a) OUTPUT

Subroutine OUTPUT calculates and prints the required results.

4.6 Results and Discussions

Results were obtained for tubes of rectangular and elliptic cross sections with different aspect ratios, for tubes of crescent-shaped cross sections, and a tube whose cross section is an oval of Cassini. Velocities are non-dimensionalized in terms of the maximum velocity in each cross section.

Analytical solutions are available for rectangular, elliptic and crescent-shaped cross sections and thus for these cross sections it was possible to compare the results with exact solutions. In the case of rectangular and elliptic cross sections the results are also compared with corresponding results using the commercial package FIDAP.

4.6.1 Tubes of Rectangular Cross Sections

Finite element results were obtained for rectangular cross sections for which $\beta = B/A$ = 0.2,0.5 and 1.0, where A, B are the major and minor dimensions of the cross section respectively. In Tables 4.2 - 4.4 results are compared with the exact analytical solutions and with those obtained by using FIDAP. The size of the mesh used in the present analysis is the same size as the mesh used to obtain FIDAP solution. For $\beta = 0.2$ and 0.5 a mesh of 30×30 elements was used. For a square cross section a mesh of 20×20 elements was used. FIDAP can only be used on a mainframe computer. It requires a substantial amount

of computer resources (both to store the global system matrix and solution CPU requirement) since it proceeds to solve a three-dimensional problem whether or not the third dimension (x in this case) is involved. The computer requirements increase considerably with a finer mesh (and in the presence of non-linear inertia terms). For example, computer time needed to run a FIDAP program for a tube of rectangular cross section of aspect ratio 0.5 is approximately 0.35 CPU hour. Using our finite element code on a Micro, the same solution is obtained in approximately 3 minutes.

y/A	z/B	Exact $u/\hat{u}$	FIDAP $u/\hat{u}$	Computed $u/\hat{u}$
0.0	0.0	1.0000	1.0000	1.0000
0.0	0.2	0.9600	0.9600	0.9600
0.0	0.4	0.8400	0.8400	0.8401
0.0	0.6	0.6400	0.6401	0.6403
0.0	0.8	0.3600	0.3601	0.3603
0.0	1.0	0.0000	0.0000	0.0000
0.2	0.0	0.9988	0.9987	0.9986
0.4	0.0	0.9915	0.9913	0.9906
0.6	0.0	0.9561	0.9559	0.9541
0.8	0.0	0.7824	0.7824	0.7821
1.0	0.0	0.0000	0.0000	0.0000

Table 4.2: Comparison of numerical and analytical solutions for a tube of rectangular cross section of aspect ratio $\beta = 0.2$.

y/A	z/B	Exact $u/\hat{u}$	FIDAP $u/\hat{u}$	Computed $u/\hat{u}$
0.0	0.0	1.0000	1.0000	1.0000
0.0	0.2	0.9609	0.9608	0.9609
0.0	0.4	0.8430	0.8430	0.8430
0.0	0.6	0.6450	0.6450	0.6450
0.0	0.8	0.3650	0.3649	0.3650
0.0	1.0	0.0000	0.0000	0.0000
0.2	0.0	0.9800	0.9800	0.9800
0.4	0.0	0.9122	0.9122	0.9122
0.6	0.0	0.7692	0.7691	0.7690
0.8	0.0	0.4965	0.4965	0.4958
1.0	0.0	0.0000	0.0000	0.0000

Table 4.3: Comparison of numerical and analytical solutions for a tube of rectangular cross section of aspect ratio $\beta = 0.5$.

y/A	z/B	Exact $u/\hat{u}$	FIDAP $u/\hat{u}$	Computed $u/\hat{u}$
0.00	0.0	1.0000	1.0000	1.0000
0.25	0.0	0.9463	0.9463	0.9463
0.50	0.0	0.7782	0.7782	0.7784
0.75	0.0	0.4741	0.4741	0.4743
1.00	0.0	0.0000	0.0000	0.0000

Table 4.4: Comparison of numerical and analytical solutions for a tube of square cross section.

In Table 4.5 the accuracy of the finite element results is examined for a tube of rectangular cross section with aspect ratio 0.5. An error ϕ is defined by

$$\phi = \Sigma(u_i - u)^2/N^{1/2}$$

and computed at different mesh sizes, where N is the number of elements, u_i is the computed solution of the system of algebraic equations and u is the exact solution.

Mesh size	ϕ	Computed flow rate	Exact flow rate
5×5	0.002588	0.89955	0.9146
10×10	0.000480	0.91027	0.9146
20×20	0.000037	0.91328	0.9146
30×30	0.000014	0.91335	0.9146

Table 4.5: The effect of mesh refinement on finite element solutions for a tube of rectangular cross section of aspect ratio $\beta = 0.5$.

It is clear from this table that the small errors in the velocity (Table 4.5) are compounded when these are integrated to evaluate flow rate, thus producing a somewhat larger error.

4.6.2 Tubes of Elliptic Cross Sections

As a test of proficiency of the finite element scheme, in the case of a cross section with curved boundaries, we apply the scheme here to elliptic cross sections where exact solutions are available (Section 3.4).

Finite element results were obtained for elliptic cross sections for which $\alpha = b/a$=0.1, 0.5, where a, b are the major and minor dimensions of the cross section respectively. For tubes of elliptic cross sections the ratio of $u/\hat{u}$ is given by

$$\frac{u}{\hat{u}} = 1 - \left(\frac{y}{a}\right)^2 - \left(\frac{z}{b}\right)^2$$

It is clear from this equation that the non-dimensional velocity is independent of the aspect ratio and the velocity on the non-dimensional y-axis is the same as the velocity on the non-dimensional z-axis.

In Tables 4.6 and 4.7 results are compared with the exact analytical solutions and with those obtained by using FIDAP. The element mesh size used in both cases are the same (30×30), but the computational time is different. To run FIDAP program for elliptic cross section of aspect ratio 0.5, total computer time needed is approximately 1.55 CPU hour. Using our finite element routine on a Micro, the same solution is obtained is approximately 15 minutes.

y/a	z/b	Exact $u/\hat{u}$	FIDAP $u/\hat{u}$	Computed $u/\hat{u}$
0.0	0.0	1.0000	1.0000	1.0000
0.0	0.3	0.9100	0.9099	0.9095
0.0	0.6	0.6400	0.6399	0.6392
0.0	0.8	0.3600	0.3599	0.3588

Table 4.6: Comparison of numerical and analytical solution for a tube of elliptic cross section of aspect ratio $\alpha = 0.1$.

y/a	z/b	Exact $u/\hat{u}$	FIDAP $u/\hat{u}$	Computed $u/\hat{u}$
0.0	0.0	1.0000	1.0000	1.0000
0.0	0.1	0.9900	0.9900	0.9897
0.0	0.2	0.9600	0.9600	0.9595
0.0	0.3	0.9100	0.9100	0.9093
0.0	0.4	0.8400	0.8399	0.8390

Table 4.7: Comparison of numerical and analytical solution for a tube of elliptic cross section of aspect ratio $\alpha = 0.5$.

4.6.3 Tubes of Crescent-Shaped Cross Sections

Finite element results were obtained for crescent-shaped cross sections for which $\phi = \cos^{-1}(a/2b) = \pi/3$ and $\pi/2$. In Tables 4.8 and 4.9, the results are compared with the exact analytical solutions.

r	Exact $u/\hat{u}$	Computed $u/\hat{u}$
1.0	0.0000	0.0000
1.2	0.7008	0.7004
1.4	0.9829	0.9823
1.6	0.9317	0.9310
1.8	0.5946	0.5939
2.0	0.0000	0.0000

Table4.8: Comparison of numerical and analytical solutions for a tube of crescent-shaped cross section with $\phi = \pi/3$.

r	Exact $u/\hat{u}$	Computed $u/\hat{u}$
0.0	0.0000	0.0000
0.2	0.3600	0.3597
0.4	0.6400	0.6396
0.6	0.8400	0.8395
0.8	0.9600	0.9593
1.0	1.0000	0.9991

Table 4.9: Comparison of numerical and analytical solutions for a tube of crescent-shaped cross section with $\phi = \pi/2$.

4.6.4 Tube having Oval of Cassini Cross Section

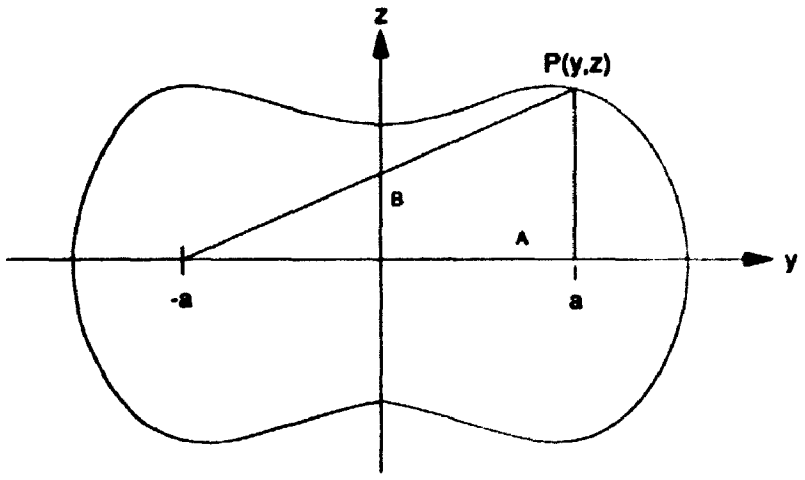

Sketch 4f: Oval of Cassini

An oval of Cassini is a curve described by the coordinates of a point P whose distances from two fixed points (distance $2a$ apart) have a constant product ($=b^2$). The equation of this curve in *polar coordinates* is given by

$$r^4 + a^4 - 2a^2 r^2 \cos 2\theta = b^4$$

An example is shown in Sketch 4e. For the calculations we have taken $A = 2.0$ and $B = 0.7$. The aspect ratio (B/A) of this cross section is 0.35.

Finite element results obtained for this cross section are shown in Fig. 4.1. Non-dimensional velocities $u/\hat{u}$ are obtained along the minor and the major axis. It is seen that the velocity profile is only slightly flattened along the minor axes.

Of more interest, we have calculated the flow rate in this tube numerically and compared it with that in a tube of circular cross section. If the perimeters of the two tubes are equal and if the flow in both tubes is under the same pressure gradient, then the ratio of flow rates is given by

$$\frac{Q_{oc}}{Q_c} = 0.2202$$

which shows that the flow rate is reduced considerably as a result of the shape of the cross section.

We have calculated flow rates in tubes of rectangular and elliptic cross sections of aspect ratio 0.35 (same as the oval of Cassini) and compared them with that in a tube of

circular cross section. The tubes of non-circular cross sections are assumed to have the same perimeter and the same pressure gradient as the tube of circular cross section. The ratio of flow rate of rectangular and circular cross section is given by

$$\frac{Q_r}{Q_c} = 0.2080$$

and the ratio of flow rate of elliptic and circular cross section is

$$\frac{Q_e}{Q_c} = 0.2425$$

Flow rate in all three cases is reduced dramatically.

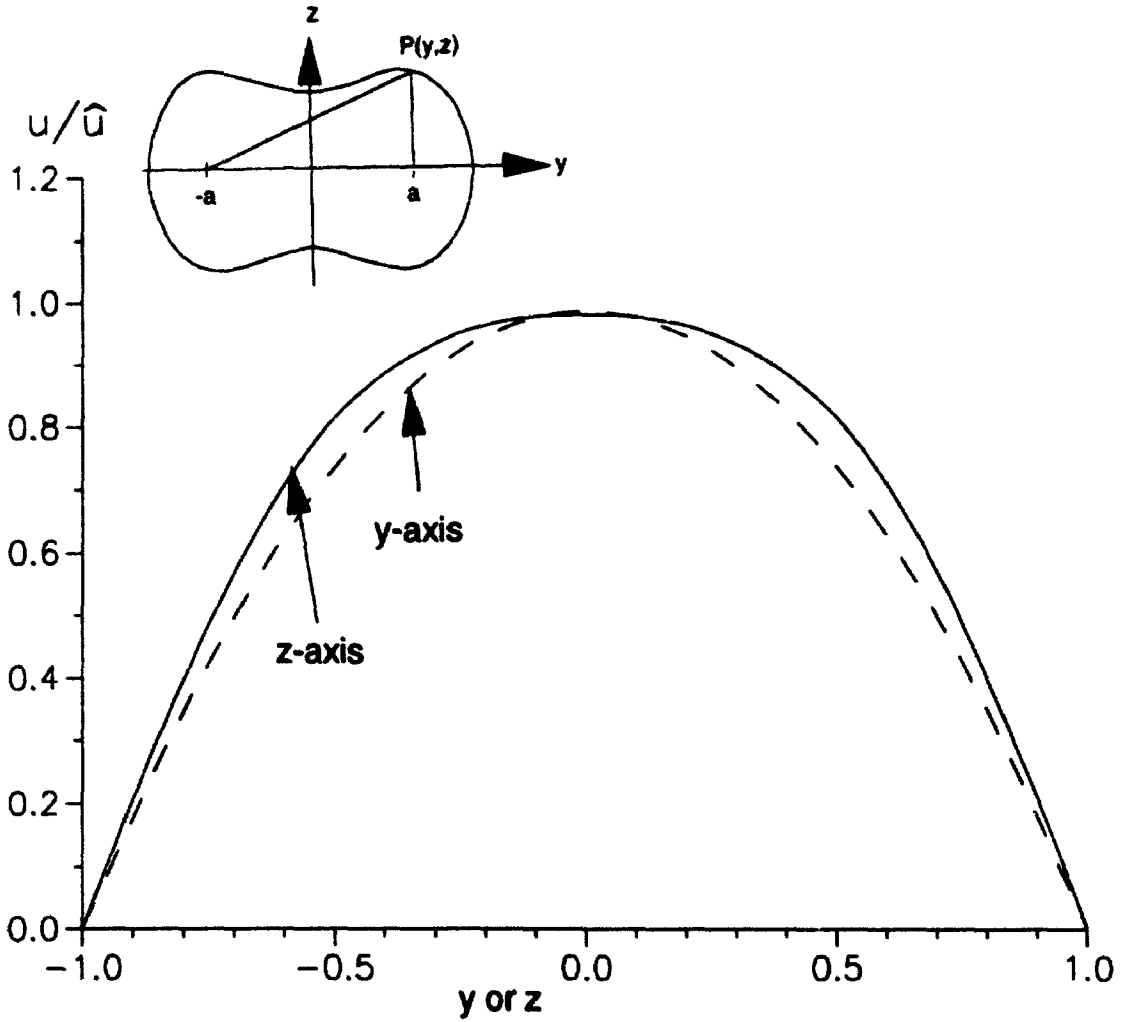

Fig. 4.1: Velocity profiles along the axes in a tube whose cross section is an oval of Cassini.

CHAPTER 5: FINITE ELEMENT METHOD FOR DEVELOPING FLOW IN TUBES OF NON-CIRCULAR CROSS SECTIONS

5.1 Introduction

For developing flow, due to the presence of the nonlinear inertia terms in the governing equations, it is not possible to obtain exact solutions even in the simplest case of a circular cross section. Approximate methods must invariably be used in this case, consisting usually of some simplification of the Navier-Stokes equations, followed by a numerical solution of the simplified equations. Existing studies of entry flow have so far been confined primarily to the case of a tube of circular cross section or to that of two-dimensional flow between parallel plates. For other cross sections, where the axial velocity component in a transverse cross section of the flow field is a function of *two* variables instead of one, there have been only a few isolated reports of theoretical or experimental work in the literature. Some of the theoretical results have been reviewed by Shah and London (1978).

The present chapter is devoted to the problem of developing flow in tubes of non-circular cross sections. The specific aim of the chapter is to develop a relatively simple but accurate finite element method for producing accurate numerical solutions of the problem. Results are compared with existing theoretical and experimental results where available. Results are obtained for a variety of cross sections, which include rectangular and elliptic cross sections of different aspect ratios, crescent-shaped cross

sections, and a cross section bounded by an oval of Cassini. This chapter also presents a review of various methods which have been used for producing solutions of this problem in the past, thus providing an opportunity to evaluate the effectiveness of these methods and the accuracy of their results. Existing results are also compiled and reduced to a standard format in this chapter, so as to allow comparison with each other and later with our own results.

5.2 Review of Previous Work

5.2.1 Theoretical Work

Broadly speaking, four general methods have been used in the past to solve the entry flow problem, usually involving some form of Prandtl's boundary layer approximations, though in some cases the full Navier-Stokes equations have been used. In what follows this previous work is described briefly, in the context of these methods.

Matching Method

Here the flow field is divided into two zones, one near and one far from the entrance. In the zone near the tube entrance boundary layer analysis is used. The analysis does not yield similarity-type velocity profiles, however, and an approximate solution is obtained in terms of a perturbation of the Blasius boundary layer solution. In the zone far from the tube entrance, series solutions are obtained as perturbations of the fully developed velocity profile, the analysis proceeding in an upstream direction. These solutions are then matched with the boundary layer solutions in an intermediate region in order to

obtain a complete solution of the entry flow problem. This technique was first suggested by Boussinesq (1891), was used by Schlichting (1934) for the flow between parallel plates, and later by Atkinson & Goldstein (in Goldstein 1938) for the flow in a tube of circular cross section. Collins & Schowalter (1962), and Roidt & Cess (1962) improved Schlichting's solutions by utilizing additional terms in both the boundary layer series and perturbation series. Gillis & Shimshoni (1966) calculated Atkinson & Goldstein's solution in greater detail, obtaining solutions of the first seven generalized Blasius equations.

Van Dyke (1970) indicated that Schlichting's series solution for small as well as large distance from the entrance actually applies only to conditions far downstream, and another expansion valid near the entrance was proposed to match with Schlichting's series. Wilson (1971) re-examined Van Dyke's entry flow problem and analyzed the boundary layer structure in greater detail for various entrance condition, and Kapila et al. (1973) further extended the work of Van Dyke (1970) and Wilson (1971) by using second-order boundary layer analysis. Van Dyke (1970) discussed the physical aspects of early boundary layer type investigations of the entry flow problem, while Wilson (1971) discussed the mathematical aspects of the problem.

Integral Method

Here the integral form of continuity and momentum equations are used in a flow model consisting of two regions: a developing boundary layer near the wall of the tube and a central inviscid core. The velocity profile in the boundary layer is represented by a polynomial function of the boundary layer thickness δ, as in the standard

Karman-Pohlhausen integral method. In addition to the integral equations, a third equation is required to complete the solution for the three unknowns δ, u and p. This is usually taken either as Bernoulli's equation applied to the centerline core of fluid, or a mechanical energy integral equation applied to the entire cross section of the flow, or a differential form of the momentum equation evaluated at the wall of the tube. The effect of viscous dissipation is taken into account by using the mechanical energy integral equation or the momentum equation. This method was first used by Schiller (1922) for the flow in a tube of circular cross section and for the flow between parallel plates. Schiller assumed a parabolic velocity profile within the boundary layer and applied Bernoulli's equation to the central inviscid core to determine the pressure as function of axial position, thus neglecting the viscous dissipation in the boundary layer. Siegel (1953) and Shapiro et al. (1954) modified this method for the flow in a tube of circular cross section by employing cubic and quartic velocity profiles within the boundary layer. Natio (1975) extended Schillar's solution to the flow between parallel plates, using quartic velocity profiles in the boundary layer.

Campbell & Slattery (1963) extended Schiller's method to take into account viscous dissipation in the entire cross section of the tube. Here the pressure was determined by an application of the energy integral equation over the cross section. Gupta (1965) used Schiller's method and applied the momentum integral equation over the entire cross section of the flow between parallel plates. Later Gupta (1977) used the same method for the flow in a tube of circular cross section. Williamson (1969) also applied Campbell

& Slattery's (1963) approach to the flow between parallel plates but with modified assumptions concerning the velocity profile in the boundary layer, which resulted in a more rapid flow development.

Govinda Rao et al. (1966) also used a momentum integral equation but included the energy loss due to viscous dissipation within the fluid, and applied the method to a tube of circular cross section. Gubin & Levin (1968) used a logarithmic velocity profile in the boundary layer to obtain a solution for the flow in a tube of circular cross section. Fargie & Martin (1971) combined the integral approach of Campbell & Slattery (1963) with a differential form of the momentum equation in a way that led to elimination of the pressure gradient term and produced a relatively simple closed-form expression for the solution.

Chen (1973) applied the momentum integral method to the full Navier-Stokes equations for a solution of the flow in a tube of circular cross section and between parallel plates. The solution takes into account the effects of axial diffusion of momentum and of pressure variation within a cross section, which are neglected when boundary layer approximations are used.

Methods based on Linearization

Here the nonlinear inertia terms in the Navier-Stokes or the boundary layer equation are linearized in various ways to obtain an approximate solution. Thus in this method the flow field is not based on a boundary layer model. Rather, solutions are obtained which are continuous over the entire cross section, as well as in the axial direction from

the entrance to the fully developed region. This technique was used by Langhaar (1942) for a tube of circular cross section, in a method which consists of replacing the inertia terms by $(v\beta^2 u)$ and thus solving an equation of the form

$$\frac{\partial^2 u}{\partial y^2}+\frac{\partial^2 u}{\partial z^2}=\alpha+\beta^2 u \qquad (5.2.1)$$

where α and β are functions of axial coordinate x only. The resulting family of velocity profiles were obtained in terms of Bessel functions, and the solution was found to agree well with other results either near the entrance of the pipe or far downstream, but not in the region in between. Langhaar's approach was used by Han for the flow in a tube of rectangular cross section (1960) and between parallel plates (1961), where a linearized form of the boundary layer equation in conjunction with an integral form of the continuity equation was used, and by Han & Cooper (1962) for the flow in a tube of equilateral triangular cross section. Miller & Han (1971) computed the pressure drop in the entrance region for the flow in tubes of rectangular and equilateral triangular cross sections, using the energy integral equation in conjunction with the simpler velocity profiles of Han & Cooper (1962).

Lundgren et al. (1964) used both the momentum and energy equations and obtained a simple expression for the pressure drop due to flow development which requires a knowledge of only the fully developed velocity profile. McComas (1967) combined these entry pressure drop results with a simple force-momentum balance for the inviscid core to predict the entrance length (but not the details of flow development) in tubes of arbitrary

cross sections.

Targ (1951) linearized the momentum equation by replacing the inertia terms by $\tilde{u}\partial u/\partial x$, where $\tilde{u}$ is the mean axial velocity. In addition, the pressure gradient $(\partial p/\partial x)/\rho$ was replaced by $(2\nu/a)(\partial u/\partial r)_{r=a}$, thereby solving an equation of the form

$$\tilde{u}\frac{\partial u}{\partial x}=\frac{2\nu}{a}\left(\frac{\partial u}{\partial r}\right)_{r=a}+\nu\left[\frac{1}{r}\frac{\partial}{\partial r}\left(r\frac{\partial u}{\partial r}\right)\right]. \tag{5.2.2}$$

In this way the contribution of the momentum change due to pressure gradient was neglected. As a result, the velocity profile develops more slowly near the entrance while at large distance downstream the development is more rapid than predicted by other analysis. Results were obtained for the flow in a tube of circular cross section.

The analysis of Sparrow et al. (1964) differs from the linearization technique of Langhaar (1942) by utilizing a *stretched* axial coordinate x, thus writing

$$\varepsilon(x)\tilde{u}\frac{\partial u}{\partial x}=\Lambda(x)+\nu\nabla^2 u \tag{5.2.3}$$

where $\varepsilon(x)$ is a mean velocity weighting factor and $\Lambda(x)$ is a function which includes the pressure gradient $(dp/dx)/\rho$ and the residual inertia terms. In this analysis the dimensionless axial velocity is expressed as the sum of the fully developed velocity and a "difference velocity" which represents an entrance region correction. A mechanical energy equation is used to obtain an additional equation for the pressure gradient, and an asymptotic series was obtained for the flow in a tube of circular cross section and

between parallel plates.

The method of Sparrow et al. (1964) is restricted to cross sections in which the velocity profile depends on only one transverse coordinate, that is for a tube of circular cross section or for the flow between parallel plates. Wiginton & Wendt (1969), Fleming & Sparrow (1969), Wiginton & Dalton (1970) and Aggarwala & Gangal (1975) extended this method to cases where the velocity profile depends on two transverse coordinates. The method of Wiginton & Wendt (1969) was suitable for any cross section which can be mapped onto a rectangle. In the analysis of Fleming & Sparrow (1969) an eigenvalue problem was solved for the difference velocity for a tube of arbitrary cross section. Application of the solution was made to tubes of rectangular cross sections of aspect ratios 0.2 and 0.5 and to tubes of isosceles triangular cross sections of 30 and 60-deg apex angles. Wiginton & Dalton (1970) used a slightly different exponential function in the eigenfunction expansion of the velocity difference and analyzed the entry flow problem in tubes of rectangular cross sections of aspect ratios 0.2, 0.5 and 1.0. Aggarwala & Gangal (1975) solved an integro-differential eigenvalue problem obtained by linearizing the Navier-Stokes equations to obtain a solution for tubes of equilateral and right isosceles triangular cross sections.

Wiginton (1975) used the method of Wiginton & Wendt (1969) to study the entry flow problem in a general non-circular cross section. The problem was set up as an eigenvalue problem and the solution involved the determination of zeros of a series to obtain the eigenvalues. The results were not applied to any specific cross section and therefore no comparison is possible with other results.

A linearization method was also used by Narang & Krishnamoorthy (1976) but using the full Navier-Stokes equations rather than the boundary layer equation. Results were obtained for the flow between parallel plates only, however, and for Reynolds numbers ranging from 2 to 4000.

Numerical Method

In numerical studies of the developing flow problem mostly finite difference schemes have been used. These schemes involve reduction of the continuity and momentum equations to finite difference form, with subsequent numerical solution.

Numerical solutions of entry flow problem based on boundary layer equation were obtained by Bodoia & Osterle (1961) and Naito & Hishida (1972) for the flow between parallel plates. Following Bodoia & Osterle (1961), Hornbeck (1964) used a finite difference marching procedure to analyze the flow development in the entrance region of a tube of circular cross section and obtained velocity profiles somewhat different from those of Langhaar (1942), but agreed reasonably well with regard to entrance length and pressure drop. Christiansen & Lemmon (1965), and Manohar (1969) also used finite difference analysis for a tube of circular cross section. Patankar & Spalding (1972), Curr et al. (1972), and Briley (1974) obtained finite difference solutions for tubes of rectangular cross sections. Carlson & Hornbeck (1973) used a finite difference scheme to analyze the entrance flow in a tube of square cross section based on a model which consists of the axial momentum equation, continuity equation and an assumed relation between the transverse velocities. Garg (1983) used this method for tubes of rectangular cross sections, of aspect ratios 0.2 and 0.5. Miller (1971) used finite difference schemes for tubes of

square and equilateral triangular cross sections at a Reynolds number of 1000, but using the definition of McComas (1967) for the entrance length. This definition predicts lower values of the entrance length as shall be discussed later.

Rubin et al. (1977) studied numerically the flow in a tube of rectangular cross section. The entry region is treated by a boundary layer/potential core analysis, followed by a second-order boundary layer solution, with and without mass transfer. Numerical solutions were obtained for a tube of square cross section, and the results extended from the entrance to the fully developed region.

Numerical solutions of the full Navier-Stokes equations were reported by Vrentas et al. (1966) and Friedmann et al. (1968) for a tube of circular cross section and by Wang & Longwell (1964), Gillis & Brandt (1964), Morihara & Cheng (1973) for the flow between parallel plates. Schmidt & Zeldin (1968, 1969) and McDonald et al. (1972) also used the full Navier-Stokes equations in a numerical study of the flow in a tube of circular cross section and between parallel plates.

5.2.2 Experimental Work

In contrast to analytical work there has been very little experimental work on developing flow in tubes of non-circular cross sections, likely because of experimental difficulties. For the flow in a tube of circular cross section, velocity measurements were obtained by Pfenninger (1952), Leite (1956), Nikuradse (in Prandtl & Tietjens 1957), and Reshotko (1958).

Measurements of velocity and axial pressure drop for tubes of rectangular cross sections with aspect ratios 0.2 and 0.5 were performed by Sparrow et al. (1967). Goldstein & Kreid (1967) measured the developing velocity profiles in a tube of square cross section by using Laser-Doppler flowmeter. Beavers et al. (1970) presented experimental data on pressure drop for the flow in tubes of rectangular cross sections with aspect ratios ranging from 1/59 to 1.0. Muchnik et al. (1973) measured the velocity development in tubes of rectangular cross sections with aspect ratios 0.5, 0.25 and 0.1.

5.3 Summary of Existing Results

In engineering applications the entry length L and the pressure drop K are usually the most important quantities, and in what follows we compare the values of these quantities in tubes of non-circular cross sections, where available, with the corresponding values for a tube of circular cross section.

For the flow in a tube of circular cross section there are many results, by different authors, for the entry length and for the pressure drop along the entry region. We shall use the analytical results of Collins & Schowalter's (1962) for circular cross section in what follows because they are in good agreement with the classical experimental results of Nikuradse (in Prandtl & Tietjens 1957).

To compare the actual pressure drop along the entry region is not meaningful because the distance over which it occurs is different, either for different cross sections

or as obtained by different investigators. We consider instead the ratio of pressure drop over the corresponding entry length, which can be regarded as a mean or quasi pressure gradient.

The entrance length is defined as the distance downstream from entrance at which the center-line velocity attains 99% of its fully developed value, although other definitions can be found in the literature. We shall use the above definition in what follows and denote it by L, then define a dimensionless entrance length by

$$L^+ = \frac{L}{(D_h R_e)} \tag{5.3.1}$$

where D_h is the hydraulic or equivalent diameter and R_e is the Reynolds number based on mean velocity and hydraulic diameter, as defined before. Collins & Schowalter's (1962) results for a tube of circular cross section give

$$L_c^+ = 0.061$$

The pressure drop along the entrance region, in non-dimensional form, can be defined by

$$K = \frac{P_0 - P(L^+)}{\rho \bar{u}^2/2} \tag{5.3.2}$$

where $P(L^+)$ is the pressure at L^+ and P_0 is the pressure at the tube entrance. Based on Collins & Schowalter's (1962) results, for a tube of circular cross section,

$$K_c = 1.33$$

We define the *mean* or *quasi pressure gradient* along the entry region by

$$k = \frac{K}{L^+} \tag{5.3.3}$$

Again, the results of Collins & Schowalter (1962) for a tube of circular cross section give

$$k_c = 21.8032$$

The dimensionless entrance length L^+ for rectangular cross sections of aspect ratios $\beta = minor\,axis/major\,axis = 0.2, 0.5$ and 1.0 (square) as determined by different authors, and normalized in terms of the entrance length in a tube of circular cross section, are shown in Table 5.1. The corresponding results for the pressure drop K are shown in Table 5.2. It is seen that, with the exception of McComas' (1967) result, entrance length is shorter for a tube of circular cross section. The values of McComas(1967), we believe, is too low for reasons to be discussed later. The values for Fleming & Sparrow (1969) are based on a graphical interpretation of their results. The entrance lengths of Han (1960) are somewhat low and the pressure drops are high because of the approximations made in the calculations, which led to more rapid flow development. The pressure drops of Beavers et al. (1970) are based on experimental results.

Based on these results we have calculated the quasi pressure gradient for tubes of rectangular cross sections with aspect ratios 0.2, 0.5 and 1.0 in Table 5.3. The results of Fleming & Sparrow (1969) and those of Wiginton & Dalton (1970) indicate that the value of this gradient is higher in a tube of circular than in a tube of rectangular cross section, while Han's (1960) results indicate the reverse.

$\beta =$	1.0	0.5	0.2
Han (1960)	1.2328	1.0819	
McComas (1967)	0.5311	0.4180	
Fleming & Sparrow (1969)		1.5574	1.3114
Wiginton & Dalton (1970)	1.4754	1.3934	1.3114

Table 5.1: Values of non-dimensional entrance length L^+ in tubes of rectangular cross sections, normalized in terms of the entrance length in a tube of circular cross section.

β =	1.0	0.5	0.2
Han (1960)	1.5188	1.3533	
Lundgren et al. (1964)	1.1669	1.0398	
Fleming & Sparrow (1969)		1.0977	0.7218
Beavers et al. (1970)	0.9849	0.8872	0.6616
Wiginton & Dalton (1970)	1.2255	1.0827	0.7594
Miller & Han (1971)	1.0774	0.9631	0.7000

Table 5.2: Values of pressure drop K in tubes of rectangular cross sections, normalized in terms of the pressure drop in a tube of circular cross section.

β =	1.0	0.5	0.2
Han (1960)	1.2320	1.2508	
Fleming & Sparrow (1969)		0.7048	0.5504
Wiginton & Dalton (1970)	0.8306	0.7770	0.5790

Table 5.3: Values of quasi pressure gradient k in tubes of rectangular cross sections, normalized in terms of the quasi pressure gradient in a tube of circular cross section.

Table 5.4 summarizes the values of entrance length, pressure drop and quasi pressure gradient for a tube of equilateral triangular cross section, again normalized in terms of the corresponding values in a tube of circular cross section. The values are based on the results of Han & Cooper (1962), McComas (1967) and Flemming & Sparrow (1969). With the exception of entrance length of McComas' (1967), the table indicates that these values are higher in a tube of triangular cross section than they are in a tube of circular cross section.

	Han & Cooper (1962)	McComas (1967)	Fleming & Sparrow (1969)
L^+	1.0000	0.6524	1.1639
K	1.3534	1.3669	1.2556
k	1.3534	2.0951	1.0788

Table 5.4: Values of entrance length, pressure drop and quasi pressure gradient in a tube of equilateral triangular cross section, normalized in terms of the corresponding values in a tube of circular cross section.

The entrance length, pressure drop and quasi pressure gradient for tubes of elliptic cross sections with $\alpha = minor\,axis/major\,axis$ = 0.8, 0.6 and 0.2, normalized in terms of the corresponding values in a tube of circular cross section are shown in

Table 5.5. The values are based on McComas (1967) which are the only reported results for elliptic cross sections. Again, the values for L^+ are too low, and hence those of k are too high, we believe, for the following reasons.

$\alpha =$	0.8	0.6	0.2
L^+	0.3590	0.3557	0.3491
K	1.002	1.002	1.002
k	2.9717	2.8180	2.8710

Table 5.5: Values of entrance length, pressure drop and quasi pressure gradient in tubes of elliptic cross sections, normalized in terms of the corresponding values in a tube of circular cross section.

There may be two reasons for which McComas' (1967) results predict entrance lengths that are generally smaller than those found by the others. One reason may be the neglect of viscous dissipation in the approximate method used, which may be insignificant when the boundary layer is thin but becomes increasingly important further downstream. The expected error resulting from this is consistent with a smaller predicted entrance length. Another reason is that the definition of entrance length is different in McComas (1967), where it is given by

$$L^+ = \frac{(\hat{u}/\bar{u})^2 - 1 - K_\infty}{fR_e}$$

where K_∞ is defined by

$$K_\infty = \frac{2}{A}\int\int\left[\left(\frac{u}{\bar{u}}\right)^3 - \left(\frac{u}{\bar{u}}\right)^2\right]dA$$

and u is the fully developed velocity, $\hat{u}, \bar{u}$ are the maximum and average velocity, and f is the fully developed friction factor (McComas 1967). This definition is clearly different in physical interpretation from that commonly used, and hence the general discrepancy in the corresponding values.

It is clear from the above summary that existing results on developing flow in tubes of non-circular cross sections are neither complete nor uniformly agreed upon. The purpose of the present chapter was therefore to extend the finite element method used in the previous chapter to produce a systematic numerical study of developing flow in tubes of non-circular cross sections.

5.4 Finite Element Formulation for Developing Flow

Applying the finite element scheme to the non-dimensional Navier-Stokes equations (Eqns. 2.2.5-6), the velocities and the pressure within each element are approximated by

$$u = \sum_{i=1}^{8} u_i \phi_i, \quad v = \sum_{i=1}^{8} v_i \phi_i, \quad w = \sum_{i=1}^{8} w_i \phi_i$$

and

$$p = \sum_{i=1}^{4} p_i \psi_i \tag{5.4.1}$$

where ϕ_i, ψ_i are the interpolation or shape functions and u_i, v_i, w_i, p_i are unknown nodal-values of dependent variables. It will be noted that eight-noded elements are used for velocities and only four-noded elements for pressure.

Substitution of Eqn. 5.4.1 into Eqn. 2.2.5a leads to

$$\sum_{i=1}^{8} \phi_i u_i \sum_{j=1}^{8} \frac{\partial \phi_j}{\partial x} u_j + \sum_{i=1}^{8} \phi_i v_i \sum_{j=1}^{8} \frac{\partial \phi_j}{\partial y} u_j + \sum_{i=1}^{8} \phi_i w_i \sum_{j=1}^{8} \frac{\partial \phi_j}{\partial z} u_j$$

$$+ \sum_{l=1}^{4} \frac{\partial \phi_l}{\partial x} p_l - \frac{1}{R_e} \left(\sum_{j=1}^{8} \frac{\partial^2 \phi_j}{\partial y^2} u_j + \sum_{j=1}^{8} \frac{\partial^2 \phi_j}{\partial z^2} u_j \right) = R \tag{5.4.2}$$

where R is the residual (error) function resulting from the use of approximations (5.4.1). Thus employing Galerkin weighted residual approach over n_e elements, Eqn. 5.4.2 becomes

$$\sum_{k=1}^{n_e} \int_{V_e} \phi_k \left[\left(\sum_{i=1}^{8} \phi_i u_i \sum_{j=1}^{n_e} \frac{\partial \phi_j}{\partial x} u_j + \sum_{i=1}^{8} \phi_i v_i \sum_{j=1}^{n_e} \frac{\partial \phi_j}{\partial y} u_j + \sum_{i=1}^{8} \phi_i w_i \sum_{j=1}^{n_e} \frac{\partial \phi_j}{\partial z} u_j \right) \right.$$

$$\left. + \sum_{l=1}^{4} \frac{\partial \psi_l}{\partial x} p_l - \frac{1}{R_e} \left(\sum_{j=1}^{8} \frac{\partial^2 \phi_j}{\partial y^2} u_j + \sum_{j=1}^{8} \frac{\partial^2 \phi_j}{\partial z^2} u_j \right) \right] dV_e = 0 \tag{5.4.3}$$

Here the outer summation refers to each element in the domain and the inner summation over the appropriate number of nodes in an element. Using Gauss theorem the second-order term can again be reduced to

$$\int_{V_e} \phi_k \left(\sum_{j=1}^{8} \frac{\partial^2 \phi_j}{\partial y^2} u_j + \sum_{j=1}^{8} \frac{\partial^2 \phi_j}{\partial z^2} u_j \right) dV_e$$

$$= \int_{A_e} \phi_k \sum_{j=1}^{8} \frac{\partial \phi_j}{\partial n} u_j dA_e - \int_{V_e} \left(\frac{\partial \phi_k}{\partial y} \sum_{j=1}^{8} \frac{\partial \phi_j}{\partial y} u_j + \frac{\partial \phi_k}{\partial z} \sum_{j=1}^{8} \frac{\partial \phi_j}{\partial z} u_j \right) dV_e \qquad (5.4.4)$$

where A_e denotes the element surface. With this the momentum equation in the x-direction becomes

$$\sum_{k=1}^{n_e} \int_{V_e} \left[\phi_k \phi_i \left(u_i \frac{\partial \phi_j}{\partial x} + v_i \frac{\partial \phi_j}{\partial y} + w_i \frac{\partial \phi_j}{\partial z} \right) u_j + \phi_k \frac{\partial \psi_l}{\partial x} p_l \right.$$

$$\left. + \frac{1}{R_e} \left(\frac{\partial \phi_k}{\partial y} \frac{\partial \phi_j}{\partial y} + \frac{\partial \phi_k}{\partial z} \frac{\partial \phi_j}{\partial z} \right) u_j \right] dV_e - \frac{1}{R_e} \int_{A_e} \phi_k \frac{\partial \phi_j}{\partial n} u_j dA_e = 0 \qquad (5.4.5a)$$

and similarly the momentum equations in the y and z directions are

$$\sum_{k=1}^{n_e} \int_{V_e} \left[\left(\phi_k \phi_i \left(u_i \frac{\partial \phi_j}{\partial x} + v_i \frac{\partial \phi_j}{\partial y} + w_i \frac{\partial \phi_j}{\partial z} \right) v_j + \phi_k \frac{\partial \psi_l}{\partial y} p_l \right. \right.$$

$$\left. \left. + \frac{1}{R_e} \left(\frac{\partial \phi_k}{\partial y} \frac{\partial \phi_j}{\partial y} + \frac{\partial \phi_k}{\partial z} \frac{\partial \phi_j}{\partial z} \right) v_j \right] dV_e - \frac{1}{R_e} \int_{A_e} \phi_k \frac{\partial \phi_j}{\partial n} v_j dA_e = 0 \qquad (5.4.5b)$$

$$\sum_{k=1}^{n_e}\int_{V_e}[\phi_k\phi_i(u_i\frac{\partial\phi_j}{\partial x}+v_i\frac{\partial\phi_j}{\partial y}+w_i\frac{\partial\phi_j}{\partial z})w_j+\phi_k\frac{\partial\psi_l}{\partial z}p_l$$

$$+\frac{1}{R_e}(\frac{\partial\phi_k}{\partial y}\frac{\partial\phi_j}{\partial y}+\frac{\partial\phi_k}{\partial z}\frac{\partial\phi_j}{\partial z})w_j]dV_e-\frac{1}{R_e}\int_{A_e}\phi_k\frac{\partial\phi_i}{\partial n}w_j dA_e=0 \qquad (5.4.5c)$$

The set of governing equations is completed by the continuity equation,

$$\sum_{i=1}^{n_e}\int_{V_e}\psi_k\left(\frac{\partial\phi_j}{\partial x}u_j+\frac{\partial\phi_j}{\partial y}v_j+\frac{\partial\phi_j}{\partial z}w_j\right)dV_e=0 \qquad (5.4.6)$$

in which the weighting function is now taken as ψ_k associated with four-noded elements, as was used for pressure. In this way, the pressure is evaluated through the continuity equation and a lower order polynomial is used in this process (Hood Taylor 1974, Olson 1976).

Combining the momentum and continuity equations into a single matrix equation produces a system of the form

$$\mathbf{AU}=\mathbf{B} \qquad (5.4.7)$$

where **A** is a global system matrix, **U** is the global vector of unknowns (velocities and pressure) and **B** is the global vector which contains the effects of boundary condition.

Each coefficient of matrix A has the form

$$A_{kj} = \sum_{1}^{n_e} \int_{V_e} [a_{kj}] dV_e \tag{5.4.8}$$

where

$$a_{11} = \phi_k \phi_i (u_i \frac{\partial \phi_j}{\partial x} + v_i \frac{\partial \phi_j}{\partial y} + w_i \frac{\partial \phi_j}{\partial z}) + \frac{1}{R_e} (\frac{\partial \phi_k}{\partial y} \frac{\partial \phi_j}{\partial y} + \frac{\partial \phi_k}{\partial z} \frac{\partial \phi_j}{\partial z})$$

$$a_{12} = 0, \quad a_{13} = 0, \quad a_{14} = \phi_k \frac{\partial \psi_l}{\partial x}$$

$$a_{21} = 0, \quad a_{22} = a_{11}, \quad a_{23} = 0, \quad a_{24} = \phi_k \frac{\partial \psi_l}{\partial y}$$

$$a_{31} = 0, \quad a_{32} = 0, \quad a_{33} = a_{11}, \quad a_{34} = \phi_k \frac{\partial \psi_l}{\partial z}$$

$$a_{41} = \psi_k \frac{\partial \phi_j}{\partial x}, \quad a_{42} = \psi_k \frac{\partial \phi_j}{\partial y}, \quad a_{43} = \psi_k \frac{\partial \phi_j}{\partial z}, \quad a_{44} = 0 \tag{5.4.9}$$

The components of B are given by

$$B_k = \sum_{1}^{n_e} \int_{A_e} [b_k] dA_e \tag{5.4.10}$$

where,

$$b_1 = b_2 = b_3 = \frac{1}{R_e} \phi_k \frac{\partial \phi_j}{\partial n} \quad \text{and} \quad b_4 = 0 \tag{5.4.11}$$

5.4.1 Curved Isoparametric Elements

For curved isoparametric elements a mapping from the global coordinate system (x, y, z) to a local coordinate system (ξ, η, ζ) is defined in the following way

$$x = \sum_{i=1}^{8} \phi_i(\xi, \eta, \zeta) x_i, \quad y = \sum_{i=1}^{8} \phi_i(\xi, \eta, \zeta) y_i, \quad z = \sum_{i=1}^{8} \phi_i(\xi, \eta, \zeta) z_i \tag{5.4.12}$$

The relations between the derivatives in the two systems are then given by

$$\begin{Bmatrix} \frac{\partial \phi_i}{\partial \xi} \\ \frac{\partial \phi_i}{\partial \eta} \\ \frac{\partial \phi_i}{\partial \zeta} \end{Bmatrix} = \begin{bmatrix} \frac{\partial x}{\partial \xi}, & \frac{\partial y}{\partial \xi}, & \frac{\partial z}{\partial \xi} \\ \frac{\partial x}{\partial \eta}, & \frac{\partial y}{\partial \eta}, & \frac{\partial z}{\partial \eta} \\ \frac{\partial x}{\partial \zeta}, & \frac{\partial y}{\partial \zeta}, & \frac{\partial z}{\partial \zeta} \end{bmatrix} \begin{Bmatrix} \frac{\partial \phi_i}{\partial x} \\ \frac{\partial \phi_i}{\partial y} \\ \frac{\partial \phi_i}{\partial z} \end{Bmatrix} = \mathbf{J} \begin{Bmatrix} \frac{\partial \phi_i}{\partial x} \\ \frac{\partial \phi_i}{\partial y} \\ \frac{\partial \phi_i}{\partial z} \end{Bmatrix} \tag{5.4.13}$$

where $\mathbf{J}$ is the Jacobian matrix, or conversely

$$\begin{Bmatrix} \frac{\partial \phi_i}{\partial x} \\ \frac{\partial \phi_i}{\partial y} \\ \frac{\partial \phi_i}{\partial z} \end{Bmatrix} = \mathbf{J}^{-1} \begin{Bmatrix} \frac{\partial \phi_i}{\partial \xi} \\ \frac{\partial \phi_i}{\partial \eta} \\ \frac{\partial \phi_i}{\partial \zeta} \end{Bmatrix} \tag{5.4.14}$$

The element of volume becomes, in the usual way

$$dx\,dy\,dz = |\mathbf{J}|\, d\xi\, d\eta\, d\zeta \tag{5.4.15}$$

where $|\mathbf{J}|$ is the determinant of **J**.

Thus the coefficients of the element matrix, defined in Eqn. 5.4.8 can now be evaluated. For example,

$$I_1 = \int_{V_e} c_{11}(x, y, z)dxdydz \tag{5.4.16}$$

Using the above formulation this integral can be reduced to one of the form

$$I_1 = \int_{-1}^{1}\int_{-1}^{1}\int_{-1}^{1} \bar{c}_{11}(\xi, \eta, \zeta)d\xi d\eta d\zeta \tag{5.4.17}$$

and this integral in turn is evaluated by numerical quadrature. We used Gauss quadrature for this purpose, for which the numerical algorithm is given by

$$I_1 = \int_{-1}^{1}\int_{-1}^{1}\int_{-1}^{1} \bar{c}_{11}d\xi d\eta d\zeta = \sum_{i=1}^{n}\sum_{j=1}^{n}\sum_{k=1}^{n} H_i H_j H_k \bar{c}_{11}(\xi_i, \eta_j, \zeta_k) \tag{5.4.18}$$

where H_i, H_j, H_k are the weighting factors, n is the total number of integration points and ξ_i, η_j, ζ_k are coordinate positions. Third-order Gaussian integration was used to evaluate the integrals.

We have used curved isoparametric elements for the flow in tubes of elliptic and crescent-shaped cross sections, and one whose cross section is an oval of Cassini.

5.4.2 Iterative Procedure

The main object of the numerical procedure is a solution of Eqn. 5.4.7. This is done by an iterative process in which a simple convergence sequence and a method of variable updating is used. The main steps are:

(1) The initial values of the primitive variables are taken as

$$u_0^n, v_0^n, w_0^n \quad \text{and} \quad p_0^n.$$

(2) The updated values of the same variables are then obtained as

$$u^{(n+1)}, v^{(n+1)}, w^{(n+1)} \quad \text{and} \quad p^{(n+1)}.$$

by using the initial values and solving the equations (Eqn. 5.4.7) for u, v and w.

(3) The following quantities

$$\frac{u^{(n+1)} - u_0^n}{u^{(n+1)}}, \quad \frac{v^{(n+1)} - v_0^n}{v^{(n+1)}}, \quad \frac{w^{(n+1)} - w_0^n}{w^{(n+1)}} \quad \text{and} \quad \frac{p^{(n+1)} - p_0^n}{p^{(n+1)}}$$

are evaluated at all nodes. A check is then made to ascertain the difference between the initial and updated values. When sufficient agreement is reached within a specified tolerance the solution is complete.

(4) If the difference is not within a specified tolerance then the initial values are updated in the following way

$$u_0^{(n+1)} = 0.5(u^{(n+1)} + u_0^n), \quad v_0^{(n+1)} = 0.5(v^{(n+1)} + v_0^n),$$

$$w_0^{(n+1)} = 0.5(w^{(n+1)} + w_0^n) \quad \text{and} \quad p_0^{(n+1)} = 0.5(p^{(n+1)} + p_0^n)$$

in which the weighting factor is being taken as 0.5.

Steps (1) to (4) are repeated until the tolerance is reached at all points within the domain and at all boundary points.

The formulation of finite element equations and the procedure for solving the system of equations for the developing flow are the same as was described earlier for fully developed flow. The general program structure is as was described in Section 4.5.

5.5 Results and Discussions

In this section we present the results of the present study based on the numerical solution described in the previous section. The raw results consist of velocity profiles in the entrance region of tubes of non-circular cross sections. The presentation and discussion of the results will be divided into four subsections dealing separately with tubes of rectangular cross sections of different aspect ratios, tubes of elliptic cross sections of different aspect ratios, a tube of crescent-shaped cross section, and a tube whose cross section is an oval of Cassini. The results are compared with the results of others where available, as reviewed briefly earlier.

For developing flow, use of the FIDAP package proved to be impractical. Because it is designed to deal with a fairly general problem, including the effects of heat transfer,

in two-dimensional, axi-symmetric, and three-dimensional geometry, the package requires substantial amounts of storage and computing time (Sec. 4.6.1). Because of these limitations it was only possible to use a coarse mesh, which produced less accurate results. Thus FIDAP was not used to produce final results for developing flow.

The evolution of velocity at the centerline of the tube is commonly used as an indicator of flow development, along with velocity profiles at a succession of axial locations. Our results are presented in terms of these details.

From theoretical considerations, it can be shown that for a fixed aspect ratio of a tube of non-circular cross section the centerline velocity can be expressed as (Sparrow et al., 1967)

$$u_{CL} = f(x^+, y^+, z^+)$$

where $x^+ = x/R_e, y^+ = y/(\text{major dimension}), z^+ = z/(\text{minor dimension})$ and u_{CL} is the centerline velocity. This representation removes the explicit dependence of the results on the length of the tube and on the Reynolds number and it is used in presenting the results in this chapter.

5.5.1 Tubes of Rectangular Cross Sections

Solutions were obtained for rectangular cross sections for which $\beta = B/A = 0.2, 0.5, 1.0$, where A, B are the major and minor dimensions of the cross section respectively. These values were chosen since experimental results are available for these aspect ratios.

The experimental results of Sparrow et al. (1967) and Goldstein & Kreid (1967) and the analytical results of Han (1960) were used for comparison. Results from the first two references were not available in numerical form and had to be adapted from graphs.

For rectangular cross sections the centerline velocity is the maximum velocity for the tube. The development of centerline velocity for tubes with β= 0.2, 0.5, 1.0 (square) is shown in Fig. 5.1. The figure indicates that the development is very rapid near the entrance of the tube and proceeds more slowly downstream. The fully developed values of u_{cl} were found (from fully developed calculations in Chapter 3) to be 1.715, 1.9917, 2.0962 for β = 0.2, 0.5, 1.0 respectively. For β = 0.5, present results are also compared with the results of Han (1960) and the experimental results of Sparrow et al. (1967). It is seen that the approximate solution of Han predicts a slightly more rapid flow development, while agreement with experiment is good. For β = 1.0 (square) present results are compared with the experimental results of Goldstein & Kreid (1967) and the agreement is reasonably good, and indicates that (99%) developed flow was achieved in the numerical integration.

The effect of mesh refinement on the centerline velocity for a tube of rectangular cross section is shown in Table 5.6.

Mesh Size	u_{CL}
5×5	1.9559
10×10	1.9666
15×15	1.9697
30×30	1.9710
40×40	1.9711

Table 5.6: The effect of mesh refinement on finite element solutions.

The development of axial velocity profiles along the symmetry planes of the tube is shown in Figs. 5.2, 5.3, for a rectangular tube of $\beta = 0.2$. The solid curves in these figures represent the present numerical results and the data points represent the experimental results of Sparrow et al. (1967). The agreement between the two is reasonably good.

Comparisons of Figs. 5.2 and 5.3, illustrate the slight difference in flow development along the xy-plane (major axis) and xz-plane (minor axis). In the xy-plane (Fig. 5.2) it is seen that with increasing downstream distance a boundary layer develops along the wall, which then spreads into the uniform core flow. Consequently, the velocity in the core increases in order to satisfy mass conservation, and owing to this process the initial

flat velocity profile grows successively more rounded. However, since β is small, there still remains a relatively flat portion even under fully developed conditions. This general trend is also seen in the xz-plane (Fig. 5.3). There are, however, interesting differences in detail. First of all the initial velocity profile there is already somewhat rounded, showing stronger effects of boundary layer growth in this case. Relative to the minor dimension, the boundary layer appears to be thicker than it does relative to the major dimension. With increasing downstream distance, the flat portion of the velocity profile is ultimately engulfed by the growing boundary layers in both planes. The last profile shown in the sequence in each case (Fig. 5.2, 5.3) corresponds to 99% of the fully developed value of u_{CL}.

The development of axial velocity profiles for a tube of rectangular cross section of aspect ratio $\beta = 0.5$ is shown in Figs. 5.4 and 5.5, particularly in order to compare with the experimental results of Sparrow et al. (1967). The overall development of the flow is similar to that discussed earlier for $\beta = 0.2$ but the rate of development and the ratio of maximum to mean velocity are somewhat different in the two cases. The last profile shown in the sequence in each case (Figs, 5.4, 5.5) corresponds to 99% of the fully developed value of u_{CL}.

A sequence of velocity profiles for the flow in tube of square cross section is shown in Fig. 5.6, particularly in order to compare with the experimental measurements of Goldstein & Kreid (1967). The overall development of the flow is similar to that discussed earlier for $\beta = 0.2, 0.5$: that is the initial flat profile becomes more and more rounded with increasing downstream distance. The only difference here is that in the case of a

square cross section the velocity profile is more rounded initially. The rate of development and the ratio of maximum to mean velocity are also somewhat different for a square cross section compared with other cross sections. The agreement between the present results and the experimental measurements of Goldstein Kreid (1967) is fairly good. In this case comparison is also possible for velocity profiles in the diagonal planes of the square, as shown in Fig. 5.7. The velocity gradient in the corner evaluated at the wall, is zero, as expected, and the agreement between the present numerical results and the experimental results of Goldstein & Kreid (1967) is again fairly good.

Table 5.7 summarizes the present and existing results where available for the non-dimensional entrance length in a tube of rectangular cross section with different aspect ratios. The results agree well with those of Wiginton & Dalton (1970). The centerline velocities for tubes of rectangular cross sections of aspect ratios 0.2, 0.5 and 1.0 were found to attain 99% of their fully developed values at $x^+ = 0.08, 0.085$ and 0.09 respectively. The entrance length is shorter for smaller aspect ratio.

β =	0.2	0.5	1.0
Present	0.0800	0.0850	0.0900
Han (1960)	----	0.0660	0.0752
McComas (1967)	----	0.0255	0.0324
Fleming Sparrow (1969)	0.0800	0.0950	----
Wiginton Dalton (1970)	0.0800	0.0850	0.0900

Table 5.7: Values of dimensionless entrance lengths L^+ in tubes of rectangular cross sections with various aspect ratios.

5.5.2 Tubes of Elliptic Cross Sections

Solutions were obtained for tubes of elliptic cross sections for which $\alpha = b/a = 0.2$, 0.5 and 1.0 (circle) where a, b are the major and minor dimensions of the cross section respectively. The development of velocity profiles in the xy-plane (major axis) and xz-plane (minor axis) of a tube of elliptic cross section with $\alpha = 0.5$ is shown in Figs. 5.8 and 5.9. The general development trend is similar to that in a tube of rectangular cross section as described earlier. With increasing downstream distance the flat portion of the velocity profile is ultimately engulfed by the growing boundary layer, though in this case the fully developed profile is more peaked than that in a tube of rectangular cross section. The last profile shown in the sequence (Figs. 5.8, 5.9) corresponds to 99% of the fully developed value of u_{CL}. It should also be noted that in the region near the wall, the results show again that the flow slows down with increasing axial distance, as expected, due to

the retarding effect of the boundary layer. In the region near the centerline the flow accelerates with increasing axial distance in order to compensate for the above reduction in mass flow. This general trend is also seen in the xz-plane (Fig. 5.9). The sequence of profiles in the xy-plane and xz-plane of a tube of elliptic cross section with $\alpha = 0.2$ behaves in a similar way and is not shown. There is only a small difference between the tubes with $\alpha = 0.2$ and 0.5 in terms of the rate of development (Fig. 5.10).

An important difference between the flow in tubes of elliptic and rectangular cross sections is that the ratio of maximum and mean velocity in the elliptic case is *independent of the aspect ratio* of the ellipse. In the rectangular case this velocity ratio varies with aspect ratio. This major difference between rectangular and elliptic cross sections is coupled with a corresponding difference in the details of the flow development in the two cases as shown in Fig. 5.10.

For elliptic cross sections the centerline velocity is the maximum velocity for the tube. The development of the centerline velocity in the entrance region of tubes of elliptic cross sections with aspect ratios $\alpha = 0.2, 0.5, 1.0$ is shown in Fig. 5.10, where the results are compared with the corresponding results for rectangular cross sections of the same aspect ratios (and the same minor and major dimensions). For tubes of elliptic cross sections the fully developed values of u_{CL} were found (from fully developed calculations in Chapter 3) to be 2.0 for all aspect ratios (as can be shown analytically) and the course of development of u_{CL} is very close in the three cases of $\alpha = 0.2, 0.5$ and 1.0. Development is again very rapid near the tube entrance and proceeds more slowly with increasing downstream distance, as in tubes of rectangular cross sections.

Table 5.8 summarizes the present and McComas's (1967) results for the dimensionless entry lengths in tubes of elliptic cross sections with α =0.2 , 0.5 and 1.0 (circle). While the results of McComas (1967) are found to predict lower values for entrance length as discussed earlier, we use them here for comparison since they are the only results available for this cross section. For α = 0.2, 0.5, 1.0 our results indicate that the flow becomes (99%) developed at x^+ = 0.0535 and 0.0550, 0.06 respectively, thus the entrance length in a tube of elliptic cross section is shorter than that in a tube of circular cross section.

α =	0.2	0.5	1.0*
Present	0.0535	0.0550	0.0600
McComas (1967)	0.0212	0.0216	0.0260

Table 5.8: Values of dimensionless entrance lengths L^+ in tubes of elliptic cross sections with various aspect ratios. * The accepted value for a tube of circular cross section is 0.06 (Nikuradse, 1957) or 0.061 (Collins & Schowalter, 1962).

5.5.3 Tube of Crescent-Shaped Cross Section

Solutions were obtained for a tube of crescent-shaped cross section bounded by two circular arcs, in which the first circle is of radius "a" with center at the origin and the second circle is of radius "b" touching the z-axis at the origin (Fig. 5.11). $\phi = \cos^{-1}(a/2b)$

determines the thickness of the cross section, and thus its value acts as a thickness parameter. An important feature of a crescent-shaped cross section is that it has curved boundaries as well as sharp corners. This cross section is useful to study the effects of curved boundaries and sharp corners *in combination*.

The development of velocity at the centerline of a tube with $\phi = \pi/3$ is plotted in Fig. 5.11. The development is very rapid near the entrance of the tube and proceeds more slowly with increasing downstream distance. The fully developed value of u_{CL} was found (from fully developed calculations in Chapter 3) to be 2.12. The centerline velocity was found to attain 99% of its fully developed value at $x^+ = 0.0650$. No other results are available for comparison.

The development of velocity profiles along the symmetry plane of a tube of crescent-shaped cross section with $\phi = \pi/3$ is shown in Fig. 5.12. The overall development of the flow is similar to that in tubes of rectangular and elliptic cross sections, that is, there is a central core where the velocity profile is flat and accelerating, surrounded by developing boundary layers. With increasing downstream distance the profile becomes more and more peaked.

Velocity profiles were also obtained along the mid-line chord of a tube of crescent-shaped cross section, and the development of these profiles is shown in Fig. 5.13. The velocity gradient in the corner evaluated at the wall is zero, as expected, and there is a point of inflection in these profiles. The last profile shown in the sequence in Figs. 5.12, 5.13 corresponds to 99% of the fully developed value of u_{CL}.

5.5.4 Tube having Oval of Cassini Cross Section

Solutions were obtained for a tube whose cross section is an oval of Cassini. An oval of Cassini is a curve described by the coordinates of a point P whose distances from two fixed points (distance $2a$ apart) have a constant product ($= b^2$) (Fig. 5.14).

The velocity development at the centerline of the tube is shown in Fig. 5.14. The development is again very rapid near the tube entrance and proceeds more slowly with increasing downstream distance. The fully developed value of u_{CL} was found (from fully developed calculation in Chapter 3) to be 1.99 for this cross section. The centerline velocity was found to attain 99% of its fully developed value at x^+=0.053. Comparing this value with those in Tables 5.7,5.8 we see that the entrance length of a tube of oval of Cassini cross section is shorter than that in tubes of rectangular and elliptic cross sections of comparable aspect ratio.

The development of axial velocity profiles along the symmetry planes of the tube is shown in Figs. 5.15 and 5.16. Comparisons of these figures illustrate the slight difference in flow development along the xy-plane (major dimension) and the xz-plane (minor dimension). In the xy-plane (Fig. 5.15) it is seen that with the increasing downstream distance a boundary layer develops along the wall, which then spreads in order to satisfy mass conservation, and owing to this process the initial flat velocity profile grows successively more rounded. While this general trend is also seen in the xz-plane (Fig. 5.16), in this case the initial profile is more flat, which is fairly similar to that in a tube of rectangular cross section with aspect ratio 0.2 (Figs. 5.2-3). With increasir g

downstream distance, the flat portion of the velocity profile is ultimately engulfed by the growing boundary layers in both planes. The last profile shown in the sequence in each case (Figs. 5.15, 5.16) corresponds to 99% of the fully developed value of u_{c_l}.

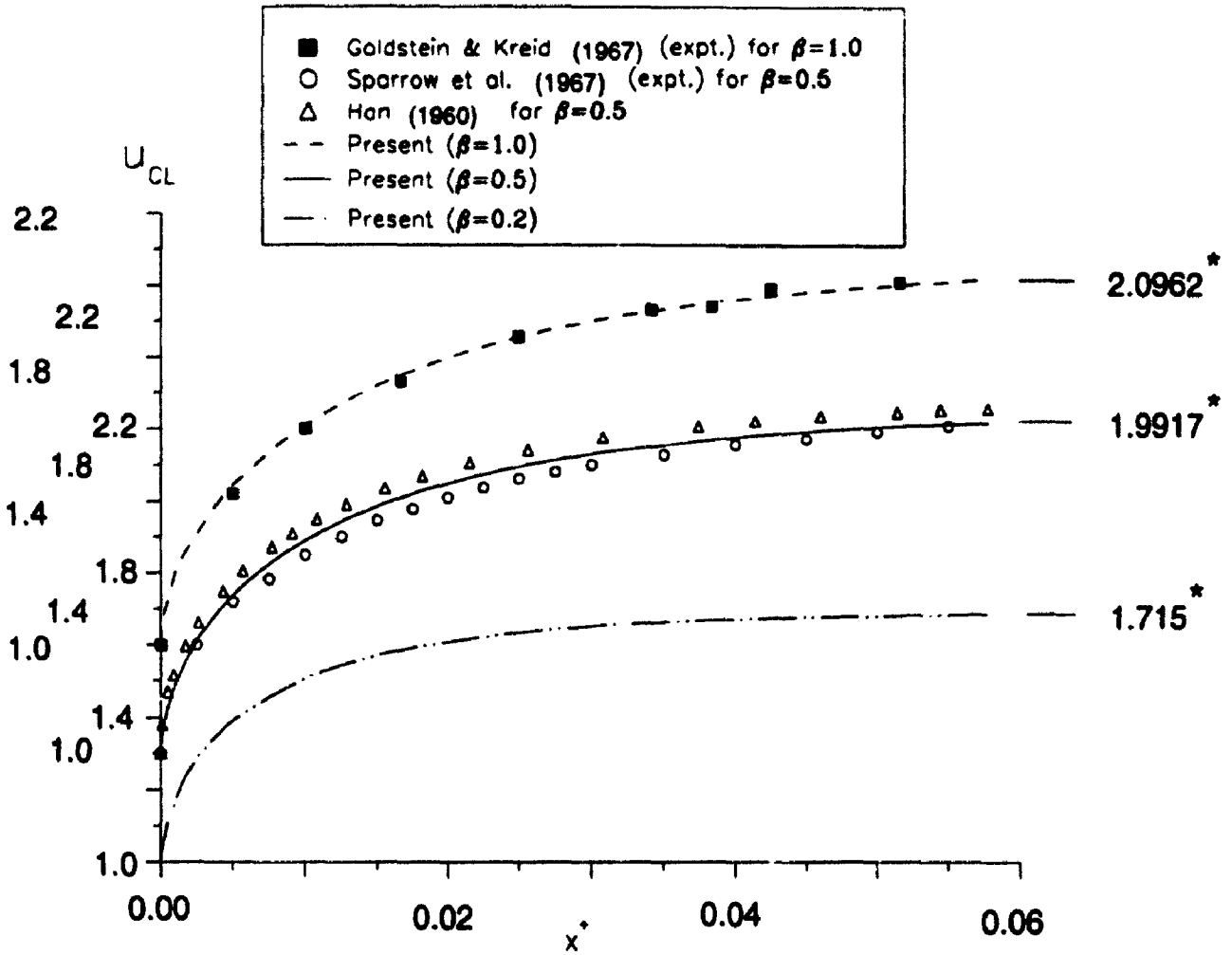

Fig. 5.1: Development of centerline velocity in tubes of rectangular cross sections having different aspect ratios.
(* Fully developed values).

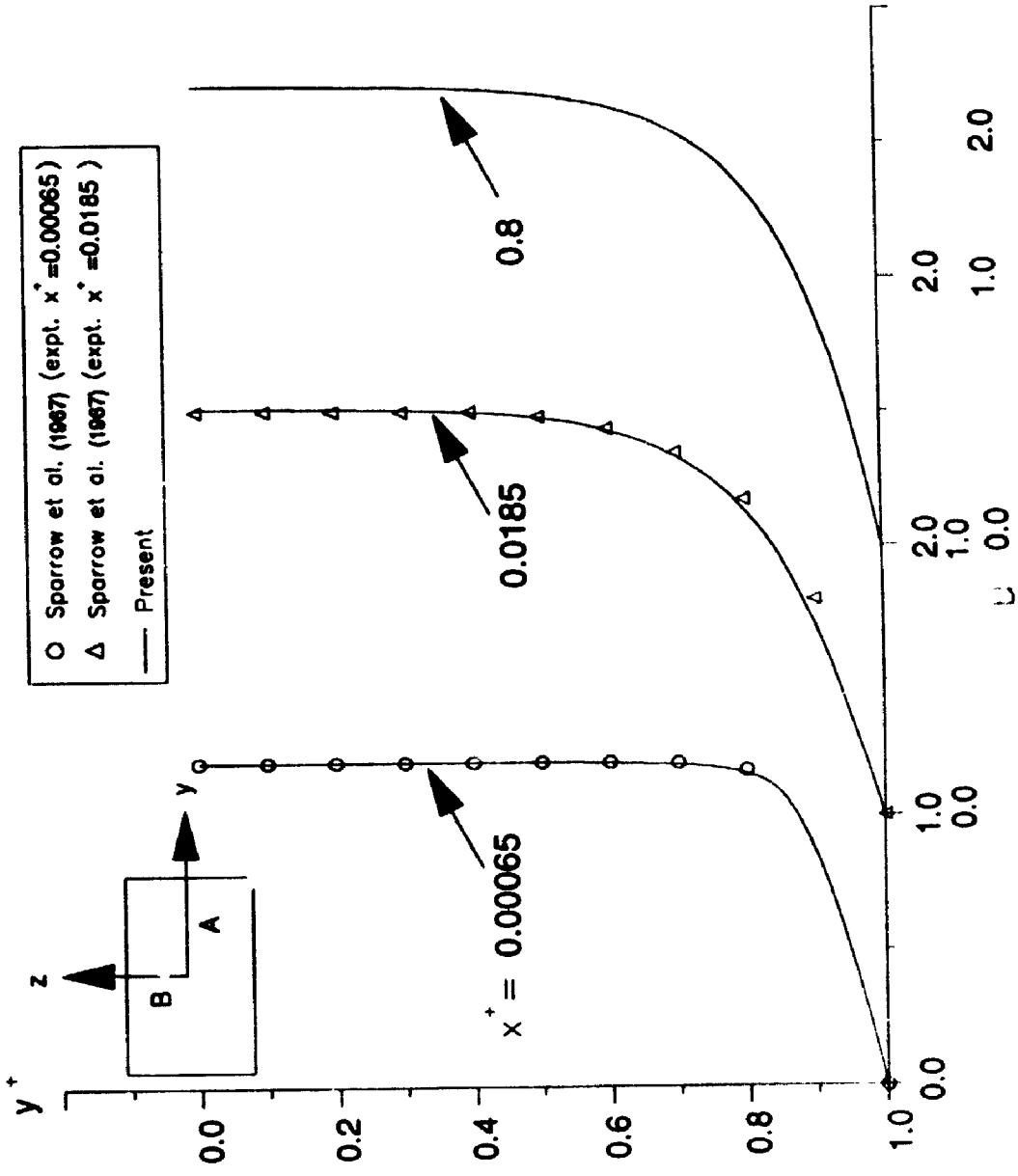

Fig. 5.2: Development of velocity profile along major axis in a tube of rectangular cross section of aspect ratio 0.2.

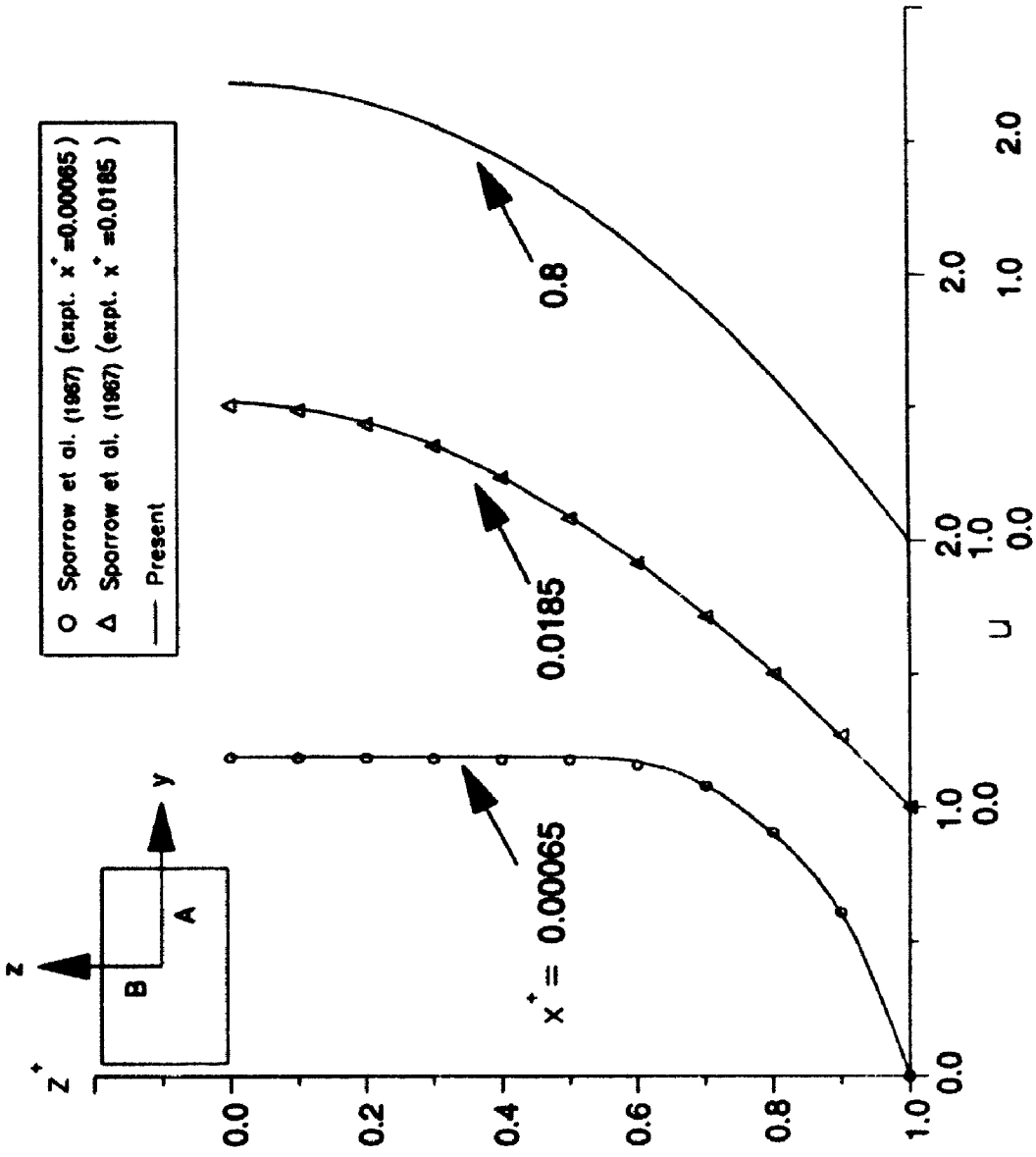

Fig. 5.3: Development of velocity profile along minor axis in a tube of rectangular cross section of aspect ratio 0.2.

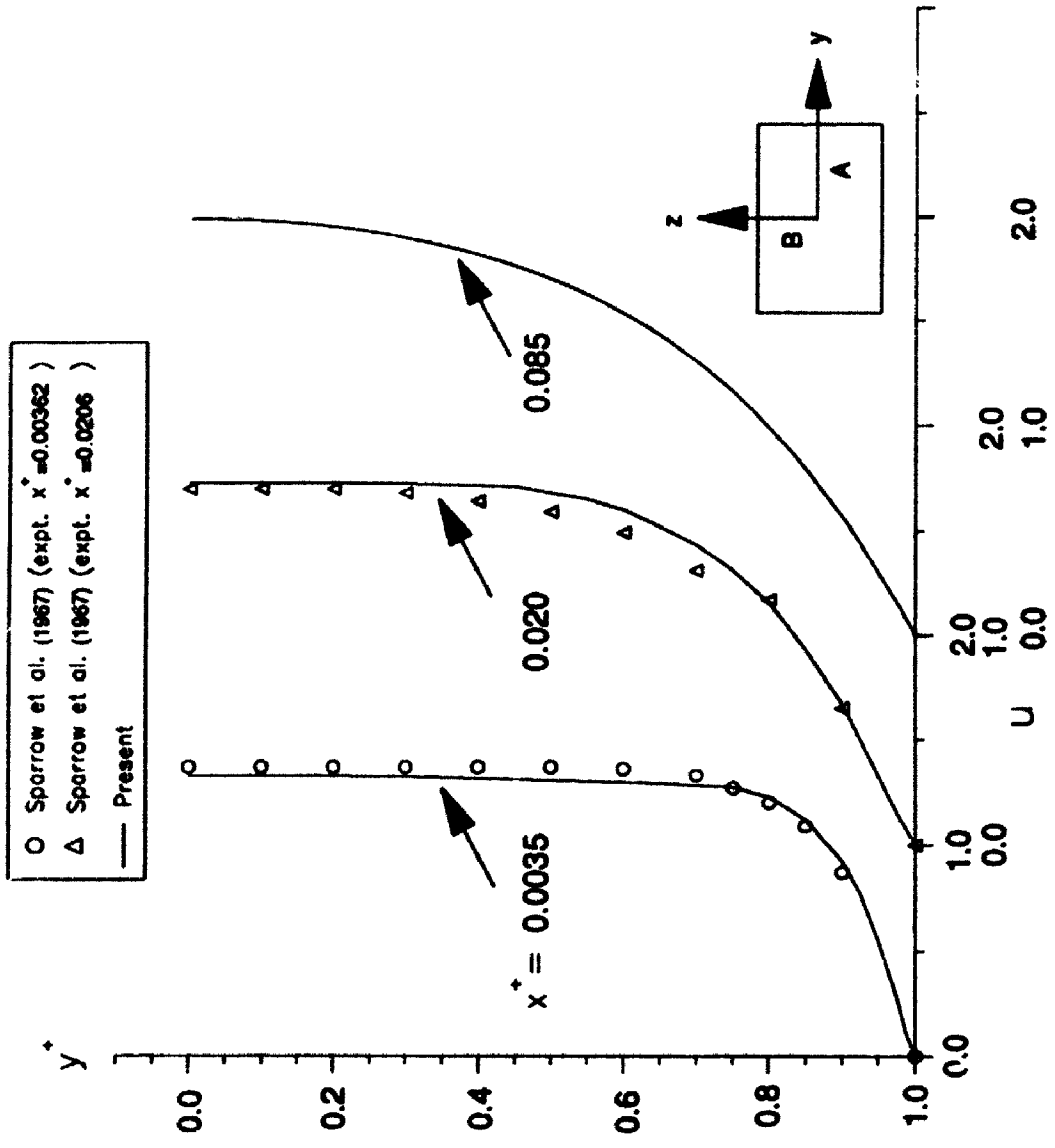

Fig. 5.4: Development of velocity profile along major axis in a tube of rectangular cross section of aspect ratio 0.5.

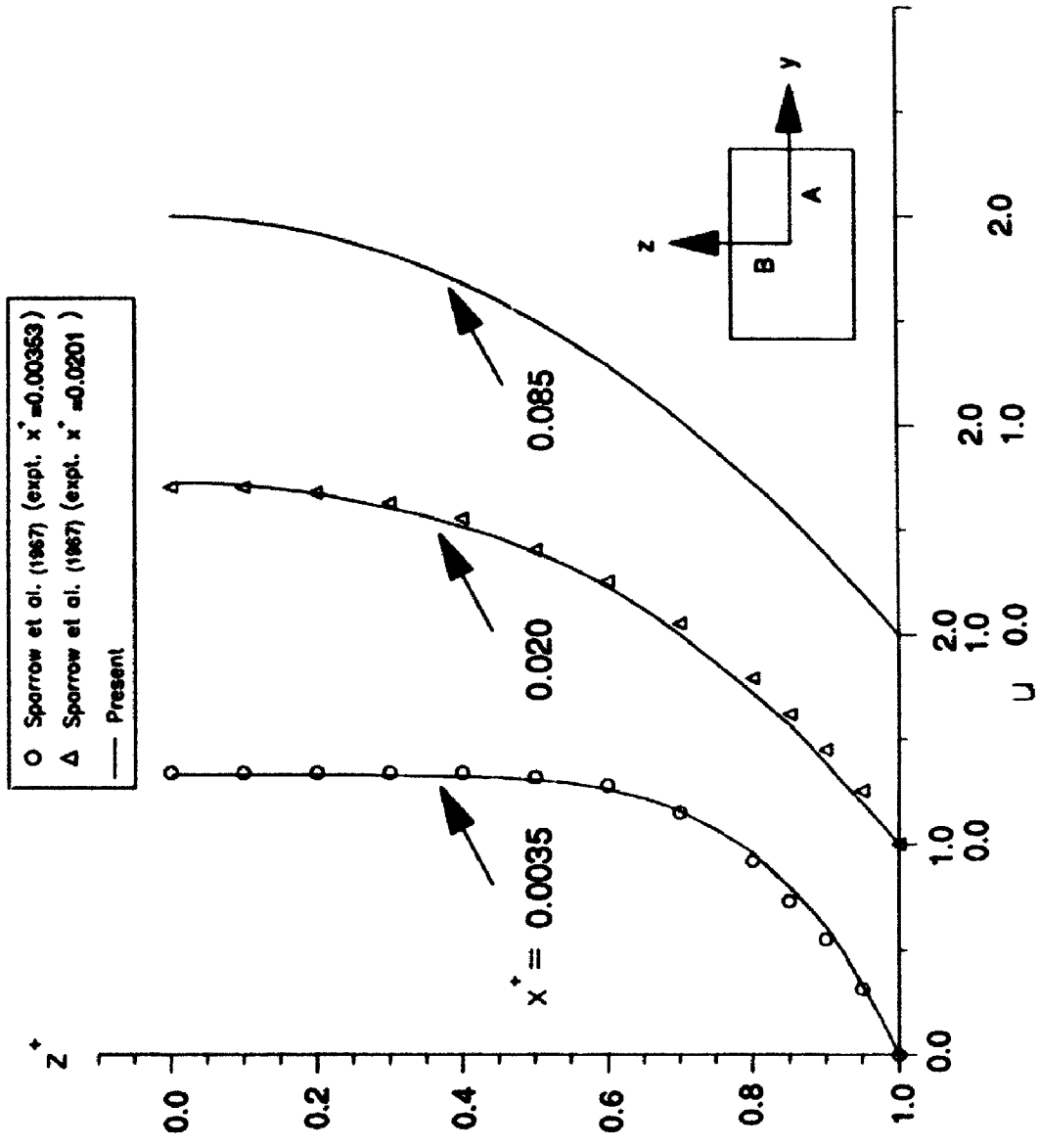

Fig. 5.5: Development of velocity profile along minor axis in a tube of rectangular cross section of aspect ratio 0.5.

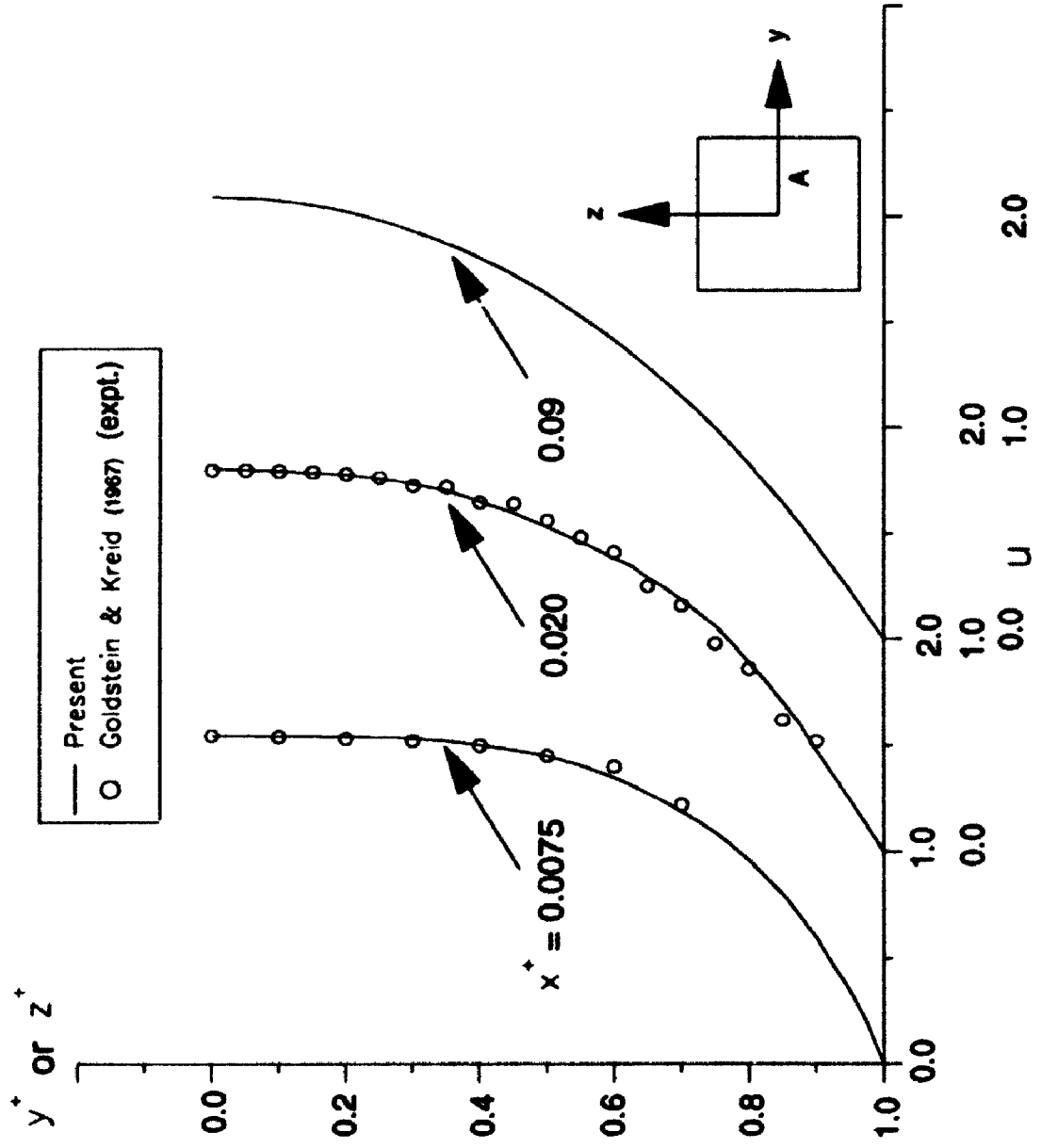

Fig. 5.6: Development of velocity profile in a tube of square cross section.

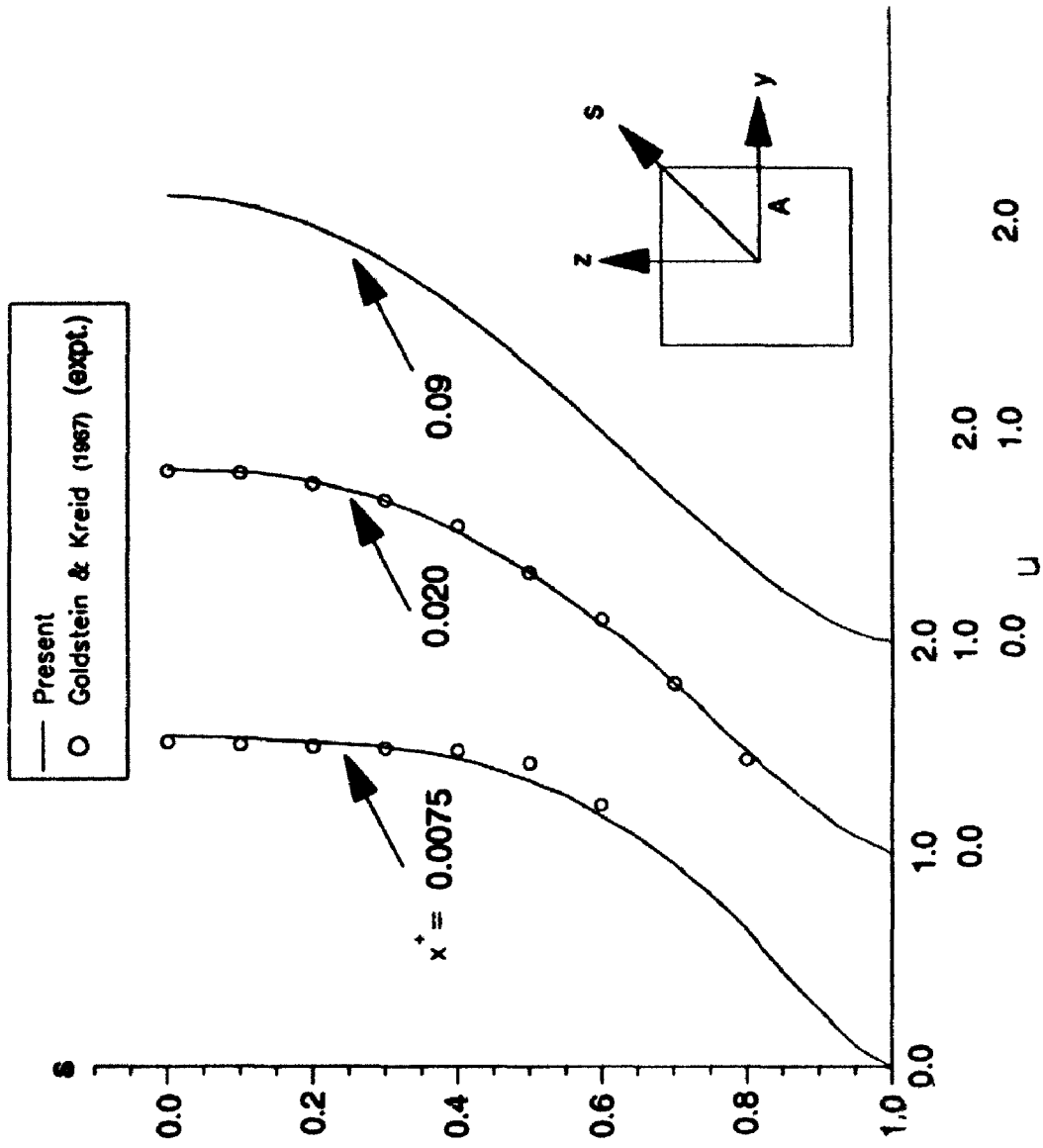

Fig. 5.7: Development of velocity profile along a diagonal in a tube of square cross section.

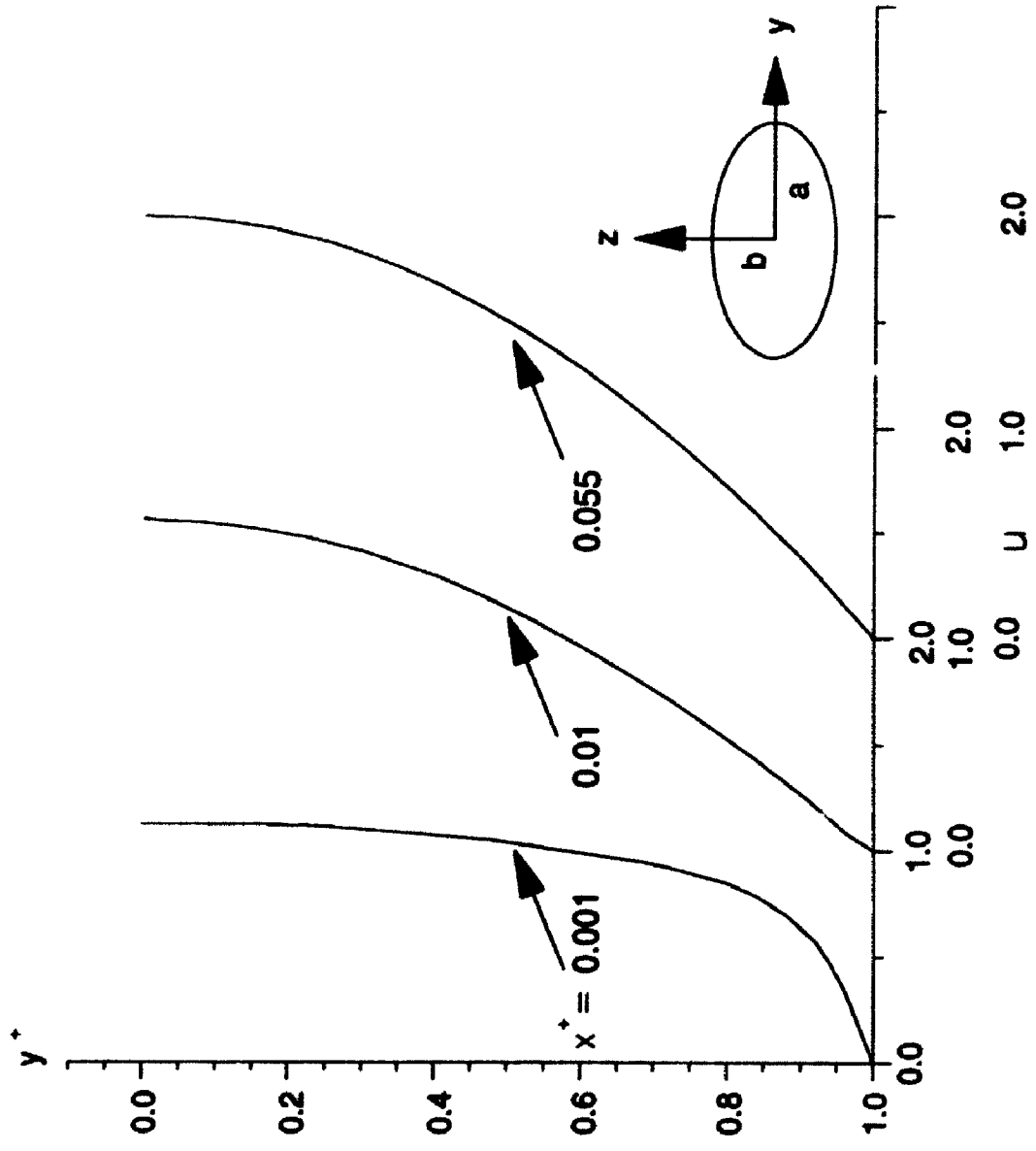

Fig. 5.8: Development of velocity profile along major axis in a tube of elliptic cross section of aspect ratio 0.5.

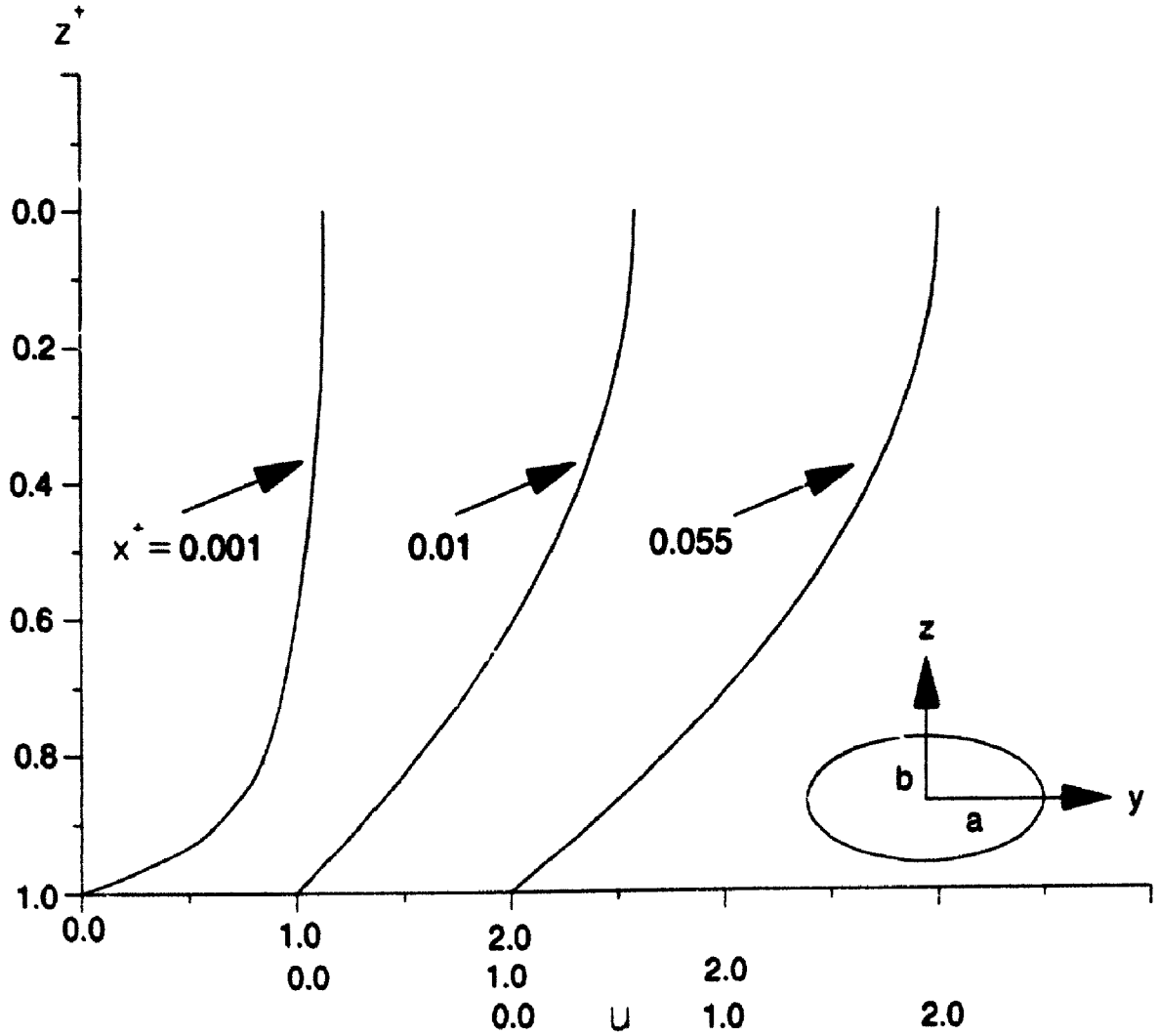

Fig. 5.9: Development of velocity profile along minor axis in a tube of elliptic cross section of aspect ratio 0.5.

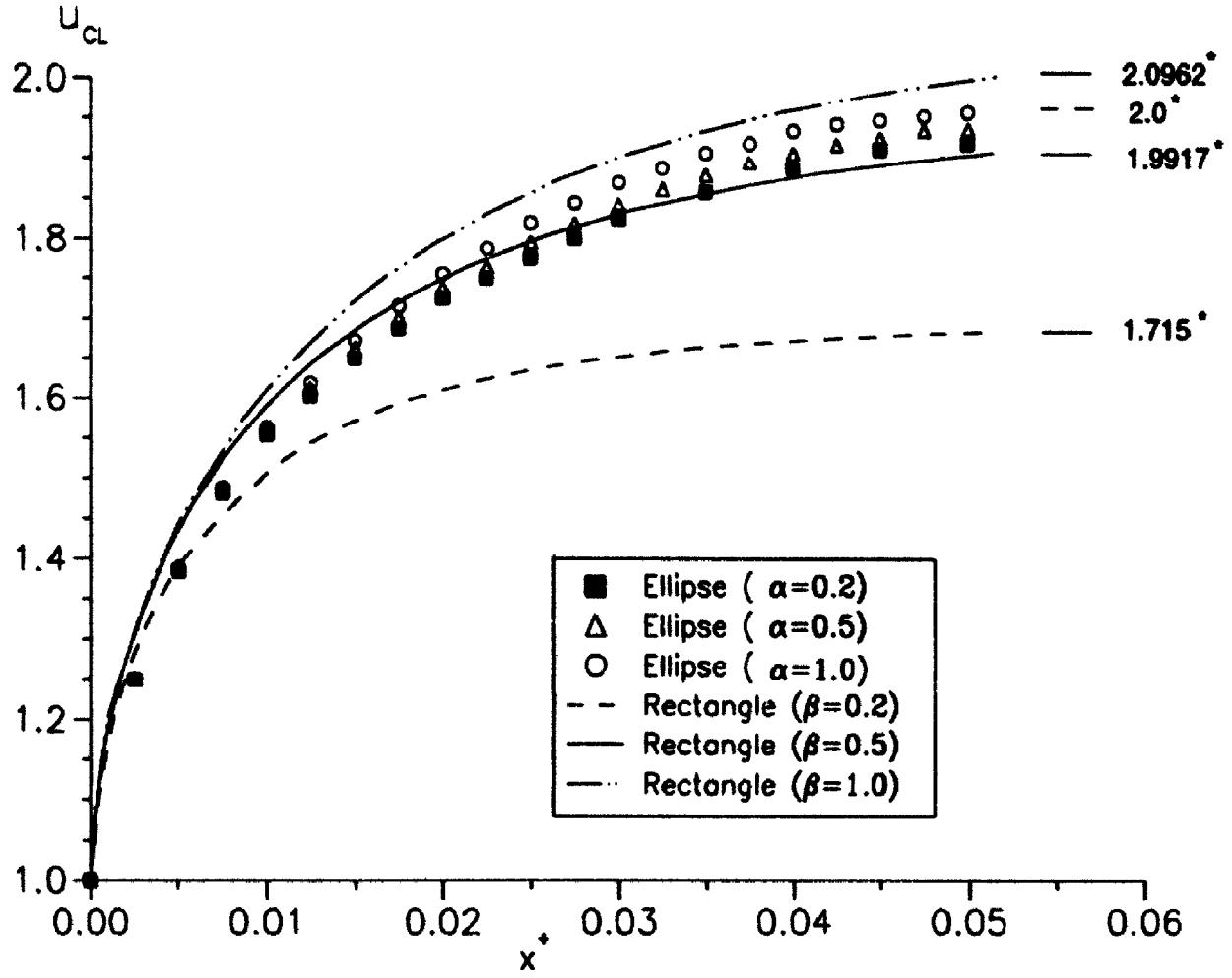

Fig. 5.10: Development of centerline velocity in tubes of elliptic and rectangular cross sections having the same aspect ratios. (* Fully developed values:—— rectangular, — — elliptic).

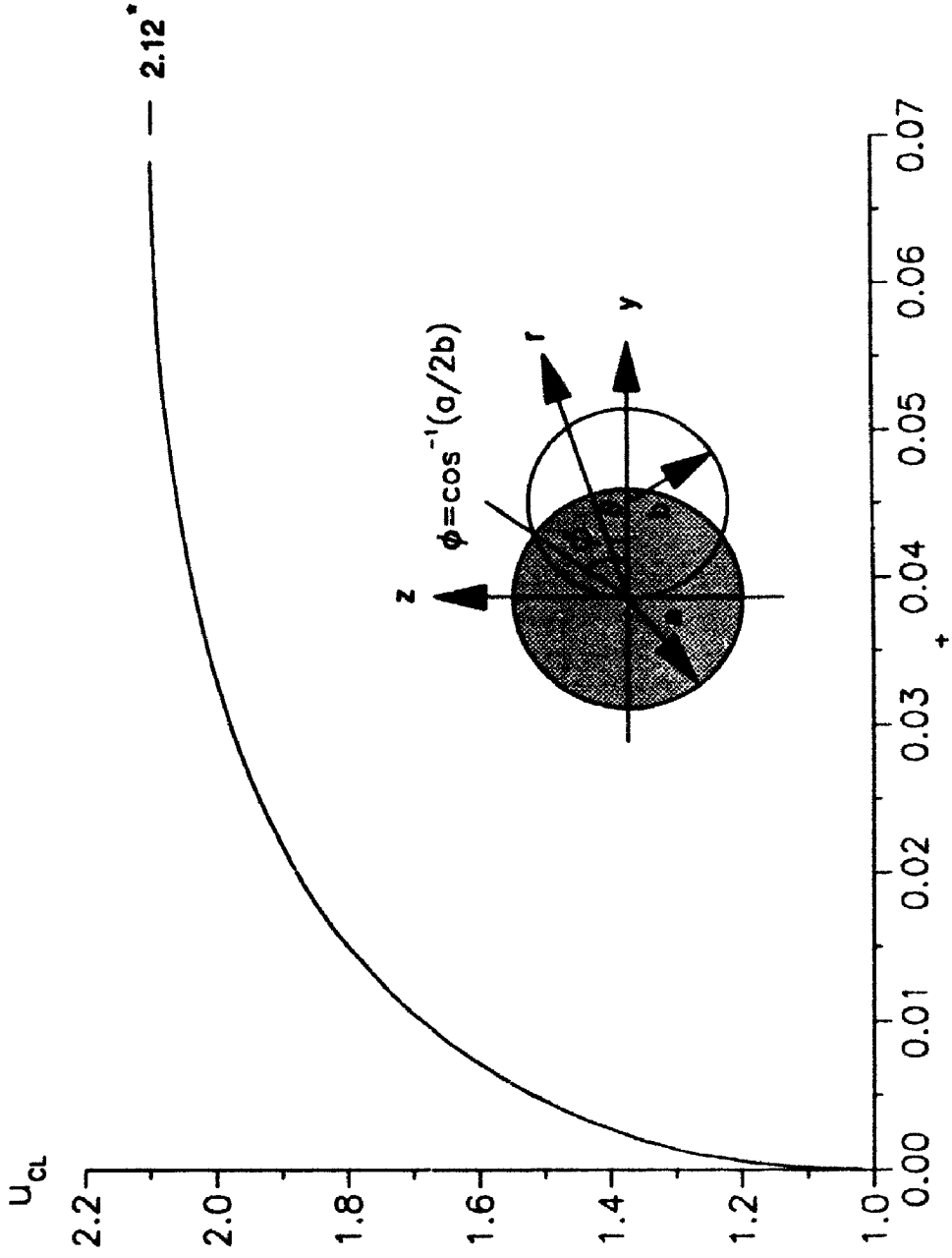

Fig. 5.11: Development of centerline velocity in a tube of crescent-shaped cross section with $\phi=\pi/3$ (* fully developed values).

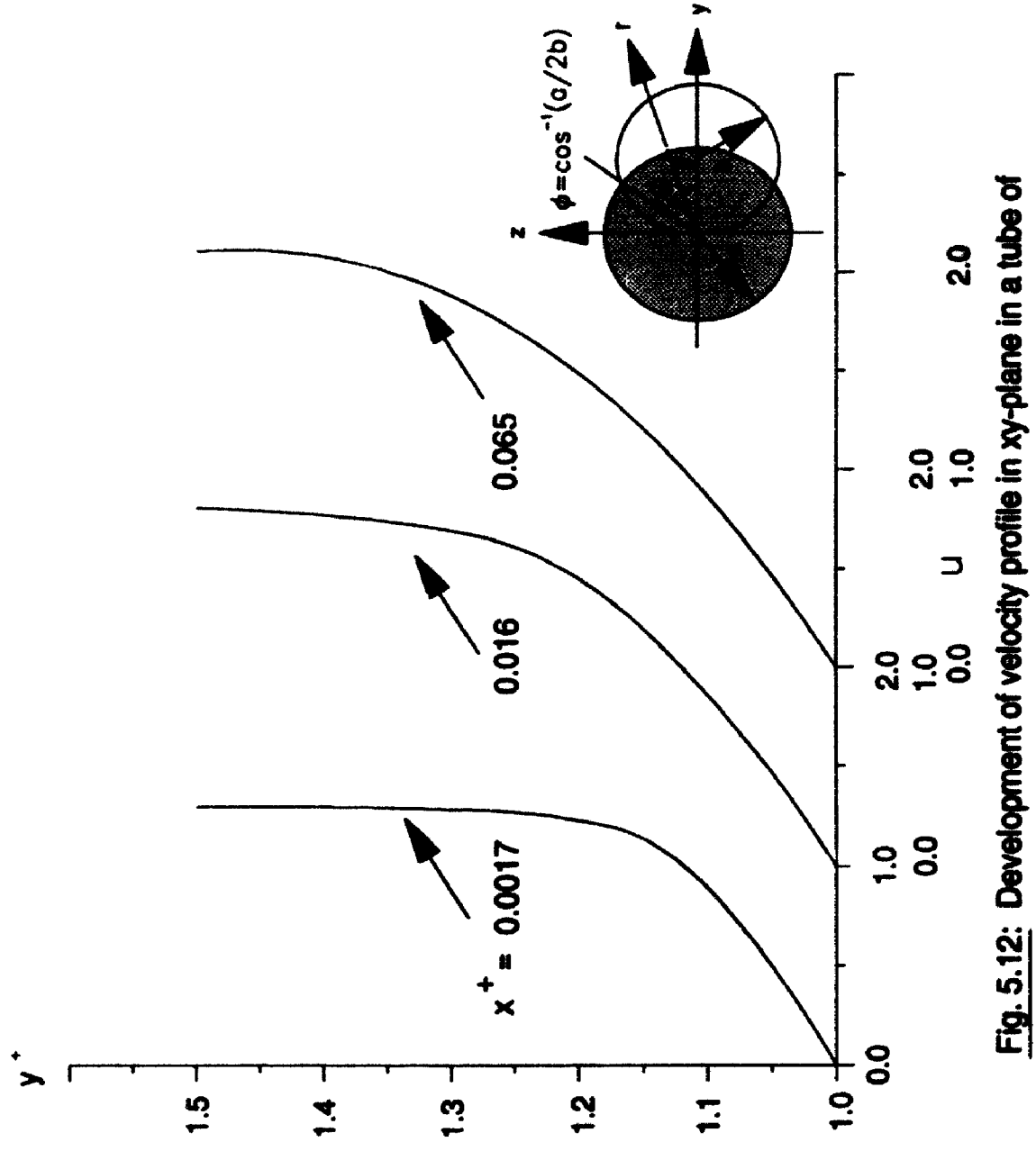

Fig. 5.12: Development of velocity profile in xy-plane in a tube of crescent-shaped cross section with $\phi = \pi/3$

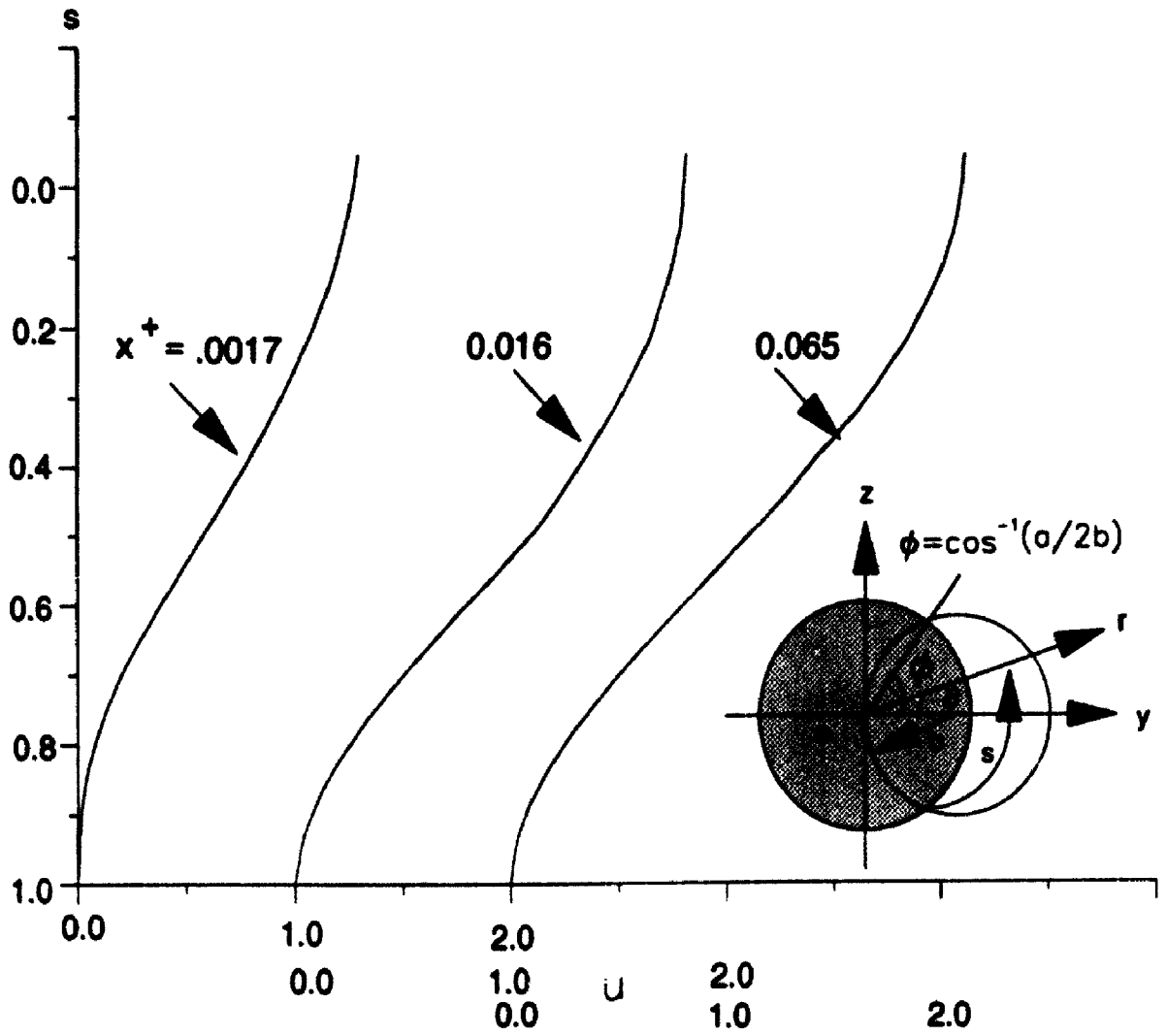

Fig. 5.13: Development of velocity profile along mid-line chord in a tube of crescent-shaped cross section with $\phi=\pi/3$

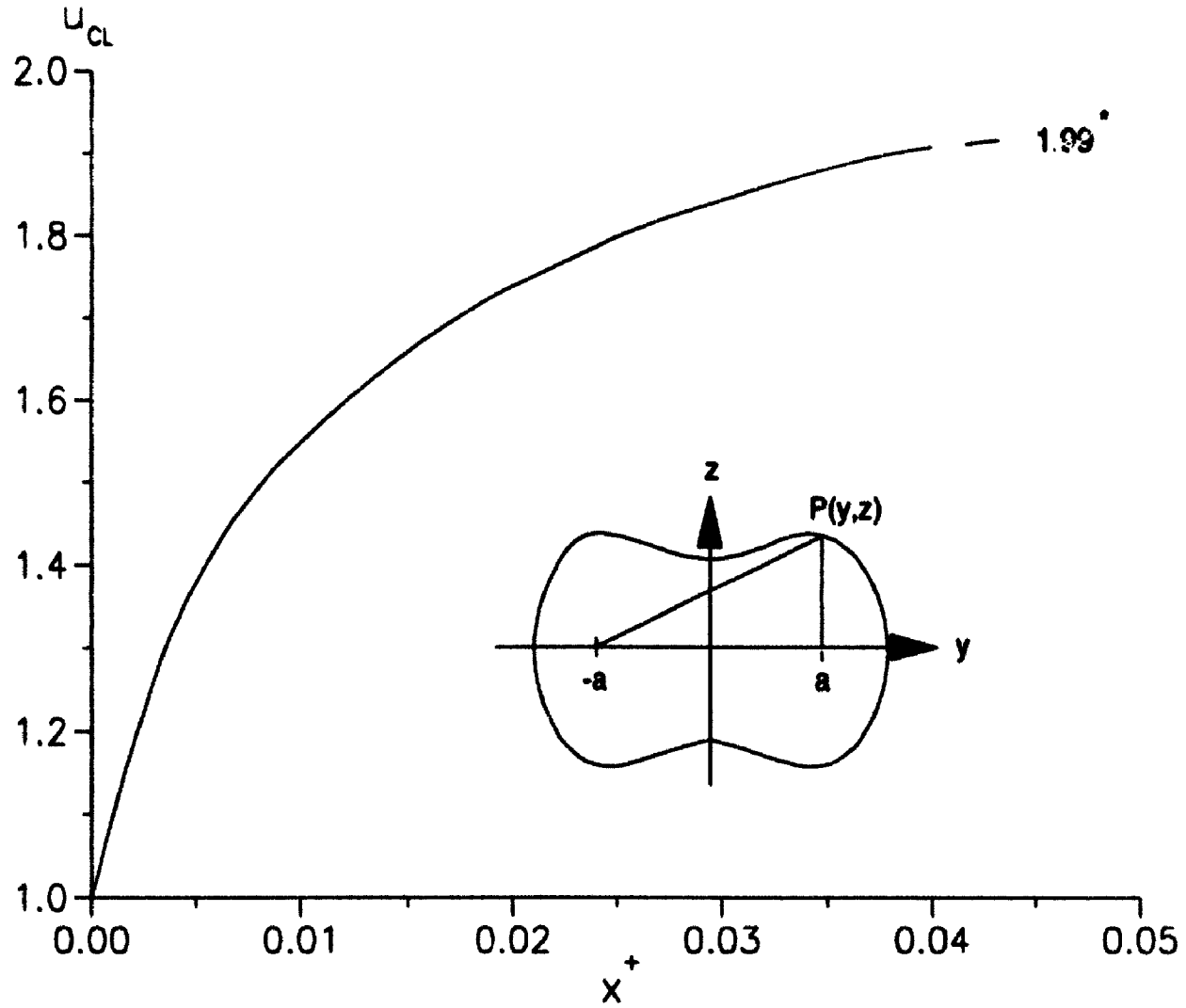

Fig. 5.14: Development of centerline velocity in a tube whose cross section is an oval of Cassini. (* Fully developed values).

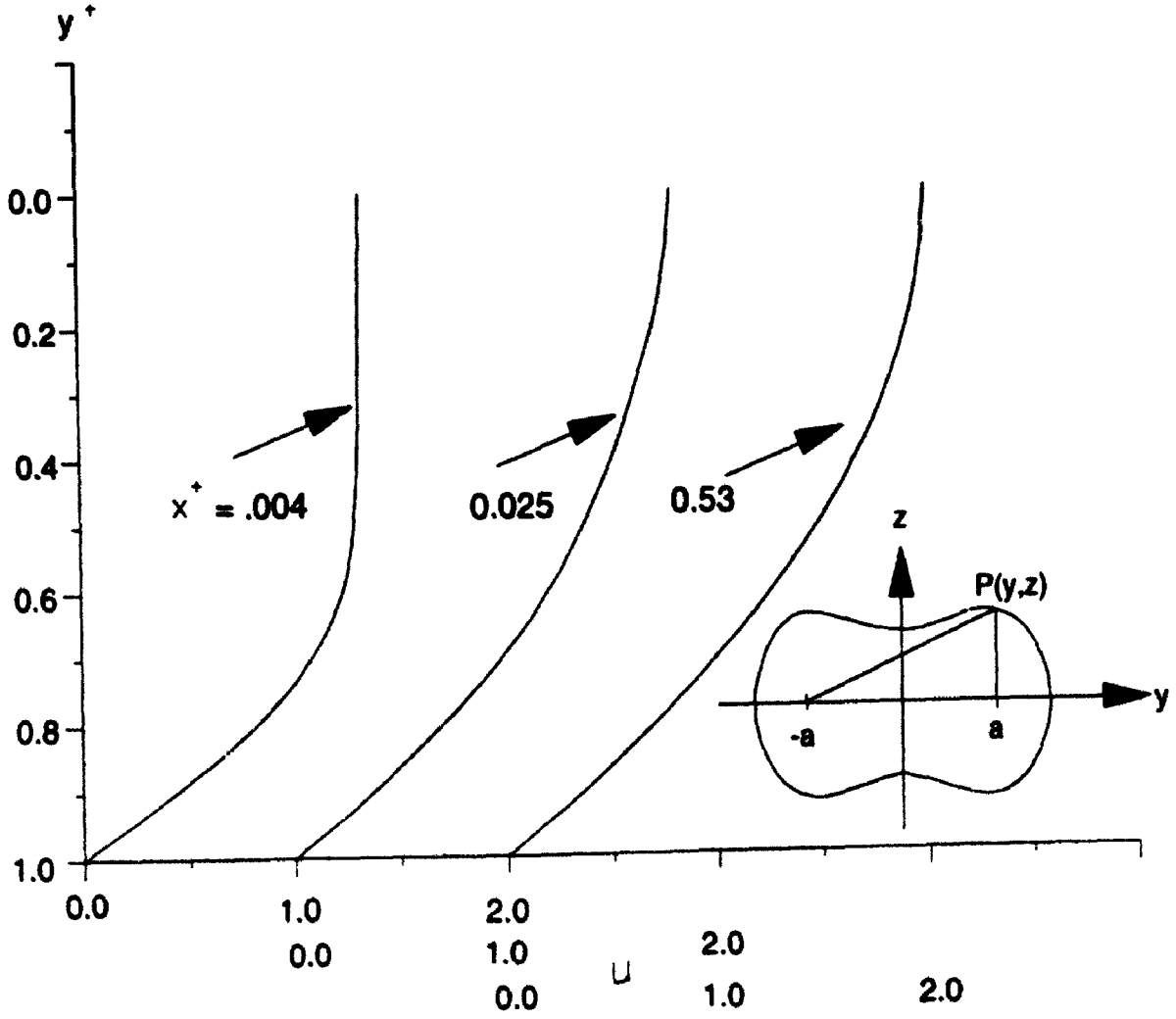

Fig. 5.15: Development of velocity profile along major axis in a tube whose cross section is an oval of Cassini.

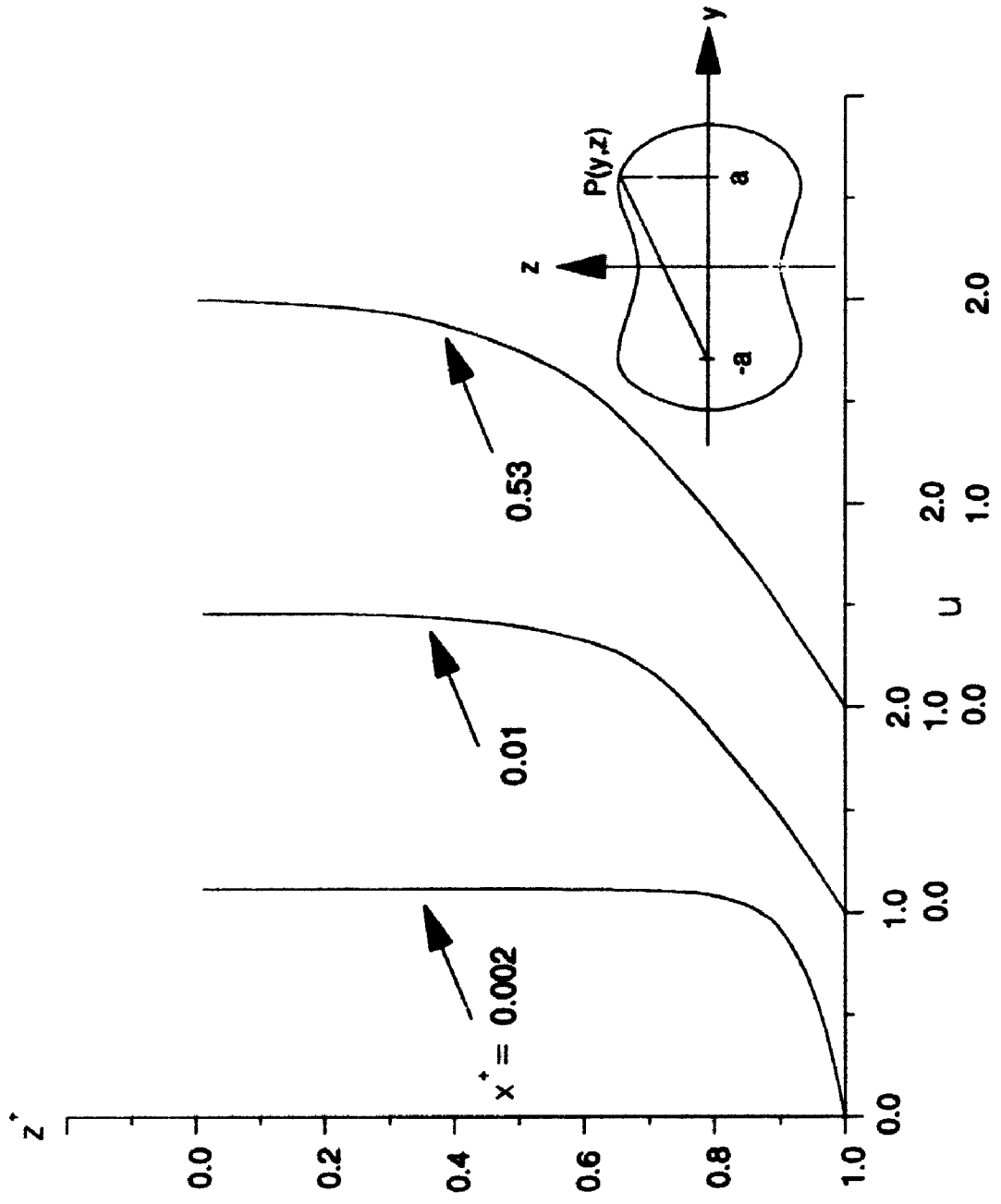

Fig. 5.16: Development of velocity profile along minor axis in a tube whose cross section is an oval of Cassini.

CHAPTER 6: SUMMARY AND CONCLUSION

6.1 The Problem

In this thesis steady, laminar, viscous incompressible flow in tubes of non-circular cross sections is investigated. It is known that when a viscous fluid enters a tube of constant cross section, at a certain distance downstream it will assume a fully developed velocity profile which becomes invariant further downstream. While theoretically this condition is reached only asymptotically, for practical purposes an *entrance length* is usually defined as the distance downstream from entrance at which the centerline velocity attains 99% of its fully developed value. Flow in the developing region is generally referred to as *developing or entry flow* and flow in the invariant region is known as *fully developed flow*. In this thesis we consider both problems, in tubes of non-circular cross sections.

Flow in tubes is important because it has numerous applications in engineering and industry as well as in blood flow. While tubes of circular cross sections are the most common, tubes of non-circular cross sections are also fairly common in engineering applications, particularly in heat exchangers.

For fully developed flow in tubes of non-circular cross sections there has been only isolated solutions for specific cross sections (Dryden et al. 1956, and Berker, 1963) and these have generally dealt with only some aspect of the flow.

For developing flow analysis has so far been confined primarily to the case of a tube of circular cross sections (Goldstein 1938, Schlichting 1968) or that of two-dimensional flow between parallel plates (Van Dyke 1970, Zamir & Camiletti 1982, Camiletti & Zamir 1984). For non-circular cross sections, where the axial velocity component in a transverse cross section of the flow field is a function of *two* variables instead of *one*, the available analytical solutions which involve various degrees of approximation are limited to rectangular and some triangular cross sections (Shah & London 1978).

In all these studies the problem of developing flow and the problem of fully developing flow are treated separately. To the best of our knowledge there has been no systematic study of the problems of developing and fully developed flow in combination and for tubes of non-circular cross sections.

The specific aims of this thesis have been (a) to look at the problems of developing flow and fully developed flow *in combination*, (b) to consider non-circular cross sections in a more *systematic manner* than has been done in the past, and (c) to develop a relatively simple finite element technique for producing accurate numerical solutions of laminar flow in tubes of fairly arbitrary cross sections.

We have studied different classes of cross sections both analytically (fully developed problem only) and numerically (both problems), considered the type of solution possible in each case, and examined the full features of the flow in each case so as to allow comparisons. The cross sections we studied include elliptic and rectangular cross sections of different aspect ratios, equilateral and right angle isosceles triangular

cross sections, crescent-shaped cross sections and a cross section bounded by an oval of Cassini. We believe that this selection of cross sections represent an important range of cases both from the point of view of engineering and industrial applications and of solutions of the governing equations. An important feature of a crescent-shaped cross section is that it has curved boundaries as well as sharp corners. This cross section is thus useful to study the effects of curved boundaries and sharp corners *in combination*.

6.2 Methods of Solution

Fully developed flow is governed by a Poisson type equation (2.3.7) for the mainstream velocity. There is no general solution in tubes of arbitrary cross section, but the problem can be solved for specific cross sections.

For fully developed flow the solutions are unique, implying that the transverse velocity components are identically zero. Also for fully developed flow exact analytical solutions are obtained for some cross sections. The solutions fall into three basic categories depending on the shape of the cross section. In the first category, which includes the circular, elliptic, equilateral triangular and crescent-shaped cross sections, solutions are possible in closed form. In the second, including rectangular and right angle isosceles triangular cross sections, solutions are in the form of infinite series. In the third, including cross sections of more complicated or irregular shapes, only numerical solutions are possible.

For developing flow, due to the presence of nonlinear inertia terms in the governing equations, it is not possible to obtain exact solutions even in the simplest case of a circular

cross section. Approximate methods must invariably be used in this case, consisting usually of some simplification of the Navier-Stokes equations, followed by a numerical solution of the simplified equations. Thus the problem usually involves some form of Prandtl's boundary layer approximations, though in some cases the full Navier-Stokes equations have been used. Previous work on the problem is briefly reviewed in the context of four general methods which have been used: simple matching, integral equations, linearized equations, and numerical methods. This review provides us an opportunity to evaluate the effectiveness of these methods and the accuracy of their results. Existing results are also compiled and reduced to a standard format so as to allow comparison with each other and later with our own results.

In numerical studies of the flow in tubes of non-circular cross sections, mostly finite difference schemes have been used. In the present study a simple finite element scheme is proposed for obtaining exact numerical solutions of the governing equations of developing flow as well as of fully developed flow. The ability to handle non-uniform and curved boundaries of the computational domain is a particular feature of the finite element method, which is the reason for which we use this method. The particular method we use is based on *Galerkin weighted residual method.* The analysis is applied to tubes of elliptic and rectangular cross sections of several aspect ratios, tubes of crescent-shaped cross sections and a tube whose cross section is an oval of Cassini.

6.3 Results and Discussions

For fully developed flow analytical solutions were obtained for some non-circular cross sections which include elliptic and rectangular cross sections of different aspect ratios, equilateral and right angle isosceles triangular cross sections, and crescent-shaped cross sections with different thickness parameters. Results for velocity profile, maximum and mean velocity, flow rate, pumping power, wall shear stress and friction factor were calculated. These physical characteristics of the flow are examined in order to determine how these characteristics are affected by certain geometrical features of the cross section. Thus results for non-circular cross sections are compared with each other, using the case of a circle as a reference. The tubes being compared are assumed to have either (a) the same cross-sectional area or (b) the same cross-sectional perimeter. The flow rate is compared for tubes having the same driving pressure gradient. The pumping power is compared for tubes having the same flow rate.

In general it is found that a tube of circular cross section is more efficient than tubes of non-circular cross sections, in the sense that a circular tube produces a greater volume of flow for a given pressure gradient than does a non-circular tube of the same cross-sectional area or perimeter length. Among tubes of rectangular cross sections with a given cross-sectional area or a given perimeter, a tube of square cross section has maximum flow rate.

It is also found that for non-circular cross sections with sharp corners, the velocity gradient varies around the periphery and approaches zero at the corners; which means that the shear stress goes to zero at the corners. The maximum shearing stress is found

to be at the end of the minor axis for elliptic cross section, at the mid-point of a side of an equilateral triangular and rectangular cross section, at the mid-point of the hypotenuse of a right angle isosceles triangular cross section and at the peak of the convex side of a crescent-shaped cross section.

A tube of circular cross section requires less pumping power to drive the flow for a given flow rate than does a non-circular tube of the same cross-sectional area or the same perimeter. Among tubes of rectangular cross sections with a given cross-sectional area or a given perimeter, a tube of square cross section requires less power to drive the flow.

A unique feature of fully developed flow in a tube of elliptic cross section is that the ratio of maximum to mean velocity is *independent of the aspect ratio.* In other cases this ratio varies with aspect ratio (of rectangular cross sections) or thickness (of crescent-shaped cross sections) and generally lies in the range of 1.5 – 2.18. For elliptic cross sections the ratio is 2.0 for all aspect ratios. Another interesting feature of the flow in a tube of elliptic cross section is that the contours of constant velocity are themselves elliptic and have the same aspect ratio as the cross section. For cross sections with sharp corners, the corners become rounded by the contours of equal velocity. In the case of rectangular cross sections the contour lines become elliptic near the center of the cross section.

An important question in the case of cross sections with sharp corners is that of secondary flow. In the case of *external* flows theoretical and experimental results (Zamir, 1981) show that secondary flow exists at the corner. In the case of *internal* flows which

are being considered here the secondary flow is identically zero in fully developed flow. In developing flow secondary flow is usually neglected in approximate boundary layer type analysis, but in exact numerical solutions as we have here the secondary flow velocities are actually computed and can be easily tabulated. However, an important difference between internal and external flow is that in internal flow secondary flow velocities *decay* as the flow develops.

Finite element results are obtained for tubes of rectangular and elliptic cross sections of aspect ratios 0.2, 0.5 and 1.0, a tube of crescent-shaped cross section with $\phi = \pi/3$, and a tube whose cross section is an oval of Cassini. Since experimental results for developing flow in a tube of rectangular cross section are available only for aspect ratios 0.2, 0.5 and 1.0, these values have been chosen for that reason. For fully developed flow, results are compared with the corresponding analytical results, where available. Results for elliptic and rectangular cross sections are also compared with those obtained by using a commercial software package (FIDAP) (see discussions in Secs. 4.6.1 and 5.5). Agreement is good in all cases. The accuracy of our finite element scheme can be increased considerably by varying element shape and mesh size. The results we obtained were sufficiently accurate for the purpose of the thesis.

For developing flow, results are compared with the corresponding results from previous work, where available, including some results from experimental work. For tubes of crescent-shaped cross section and cross section bounded by an oval of Cassini, no other results are available for comparison.

The evolution of velocity along the centerline of the tube is commonly used as an indicator of flow development, along with velocity profiles at a succession of axial locations. In general the development of centerline velocity for tubes of non-circular cross sections is very rapid near the entrance of the tube and proceeds very slowly downstream. The development of velocity profiles along the symmetry planes of the tubes shows clearly that with increasing downstream distance a boundary layer develops along the wall, which then spreads into the uniform core flow. Consequently, the velocity in the core increases in order to satisfy mass conservation, and owing to this process the initial flat velocity profile grows successively more rounded. The overall development of the flow is fairly similar for all non-circular cross sections but the rate of development and the ratio of maximum to mean velocity are somewhat different in each case. The development of velocity profiles along the symmetry planes of tubes of rectangular cross sections of 0.2 and 0.5 aspect ratios are also compared with the experimental results of Sparrow et al. (1967). The agreement between the experimental results and the present results is reasonably good. The development of velocity profiles in the diagonal plane of a tube of square cross section and along the mid-line chord of a tube of crescent-shaped cross section were also obtained. The velocity gradient in corners, evaluated at the wall is zero, as expected. In the case of a tube of square cross section results are compared with the experimental results of Goldstein & Kried (1967) and the agreement between these results is fairly good.

The development of centerline velocity in tubes of non-circular cross sections is very rapid near the entrance of the tube and proceeds more slowly downstream. For rectangular cross sections present results are compared with the experimental results of

Sparrow et al. (1967) and Goldstein and Kreid (1967) and the analytical results of Han (1960), and the agreement is reasonably good. The centerline velocities for tubes of rectangular cross sections of aspect ratios 0.2, 0.5 and 1.0 (square) were found to attain 99% of their fully developed values at $x^+ = 0.08, 0.085, 0.09$ respectively. These results were compared with the results of Wiginton & Dalton (1970) and the agreement is good. The entrance length is shorter for smaller aspect ratio. For tubes of elliptic cross section with aspect ratio 0.2, 0.5 and 1.0 (circle) the flow becomes (99%) developed at $x^+ =$ 0.0535, 0.0550, 0.06 respectively, thus the entrance length in a tube of elliptic cross section is shorter than that in a tube of circular cross section. For elliptic cross sections of aspect ratios 0.2 and 0.5 and 1 (circle), the course of development of the centerline velocity is very close in all three cases. This is consistent with the result that in the corresponding fully developed flows the ratio of maximum to mean velocity is the same in all three cases. The centerline velocities in a tube of crescent-shaped cross section and a tube whose cross section is an oval of Cassini were found to attain 99% of their fully developed values at $x^+ = 0.065$ and 0.053 respectively.

6.4 Suggestions for Future Work

In engineering applications, flow in tubes of non-circular cross sections occurs most frequently in conjunction with heat transfer, thus a study of thermally developing and fully developed flow in tubes of non-circular cross sections would be a natural direction in which to continue this work.

Another important application of some of this work, particularly in relation to the developing aspects of the flow, and particularly in elliptic and oval cross sections, may occur in blood flow where blood vessel under pressure assume the shape of tubes of non-circular cross sections. In this case a natural direction in which to continue the work of this thesis would be to consider pulsatile flow in tubes of non-circular cross sections.

REFERENCES

[1] Aggarwala, B.D. & Gangal, M.K. Laminar Flow Development in Triangular Ducts, *Trans. Can. Soc. Mech. Eng.*, 3, pp. 231-233, 1975.

[2] Beavers, G.S., Sparrow, E.M. & Magnuson, R.A. Experiments on Hydrodynamically Developing Flow in Rectangular Ducts of Arbitrary Aspect Ratio., *Int. J. Heat Mass Transfer*, 13, pp. 689-702, 1970.

[3] Becker, E.B., Carey, G.F. & Oden, J.T. *Finite Elements: An Introduction*, Vol.1, Prentice Hall Inc., Englewood Cliffs, New Jersy, 1981.

[4] Berker, R. *Mouvement d'un Fluide Visqueux Incompressible. in Handbuch der Physik* (ed. Flugge, S.), Springer-Verlag, New York, pp. 69-71, 1963.

[5] Bodoia, J.R. & Osterle, J.F. Finite Difference Analysis of Plane Poiseuille and Couette Flow Developments, *Appl. Sci. Res.*, Sect. A, 10, pp. 265-276, 1961.

[6] Boussinesq, J. Memoire on the Influence of Friction in the Regular Motions of Fluids, *J. Math. Pure Appl.*, 13(2), pp. 374-424, 1868.

[7] Boussinesq, J. *J. Math. Pure Appl.*, 16(2), 1871.

[8] Boussinesq, J. Hydrodynamique, *C.R. Acad. Sci.*, 110, pp. 1160-1170, 1238-1242, 1890, Vol.113, pp. 9-15, 49-51, 1891.

[9] Briley R. A Numerical Method for Predicting Three-Dimensional Viscous Flows in Ducts, *J. Comput. Phys.*, 14, pp. 8-28, 1974.

[10] Camiletti, S.E. & Zamir, M. Entry Length and Pressure Drop for Developing Poiseuille flows, *Aero. J. of the Royal Aero. Soc.*, pp. 265-269, 1984.

[11] Campbell, W.D. & Slattery, J.C. Flow in the Entrance of a Tube, *J. Basic Eng.* 85, pp. 41-46, 1963.

[12] Carlson, G.A. & Hornbeck, R.W. A Numerical Solution for Laminar Entrance Flow in a Square Duct., *J. Appl. Mech.*, 40, pp. 25-30, 1973.

[13] Chen, R.Y. Flow in the Entrance Region at Low Reynolds Numbers, *J. Fluids Eng.*, **95**, pp. 153-158, 1973.

[14] Christiansen, E.B. & Lemmon, H.E. Entrance Region Flow, *AIChE J.*, **11**, pp. 995-999, 1965.

[15] Chorlton, F. *Textbook of Fluid Dynamics*, D.Van Nostrand Company, London, pp. 332-337, 1967.

[16] Clark, S.H. & Kays, W.M. Laminar Flow Forced Convection in Rectangular Tubes, *Trans. ASME*, **75**, pp. 859-866, 1953.

[17] Collins, M. & Schowalter, W.R. Laminar Flow in the Inlet of a Straight Channel, *Phys. Fluids*, **5**, pp. 1122-1124, 1962.

[18] Curr, R.M., Sharma, D. & Tatchell, D.G. Numerical Predictions of Some Three Dimensional Boundary Layers in Ducts, *Comput. Methods. Appl. Mech. Eng.*, **1**, pp. 143-158, 1972.

[19] Dryden, H.L., Murnaghan, F.D. & Bateman, H. *Hydrodynamics*, Dover Publications Inc., New York, pp. 177-202, 1956.

[20] Duncan, W.J., Thom, A.S. & Young, A.D. *Mechanics of Fluids*, Edward Arnold (Publishers) Ltd., London, pp. 402-403, 1970.

[21] Fargie, D. & Martin, B.W. Developing Laminar Flow in a Pipe of Circular Cross Section, *Proc. R. Soc. London*, Series A, **321**, pp. 461-476, 1971.

[22] *FIDAP Theoretical Manual*, Fluid Dynamics International, Inc. Illinois, U.S.A., Revision 4.0, September, 1987.

[23] Fleming, D.P. & Sparrow, E.M., Flow in the Hydrodynamic Entrance Region of Ducts of Arbitrary Cross Section, *J. Heat Transfer*, **91**, pp.345-354, 1969.

[24] Fletcher, C.A.J. *Computational Techniques for Fluid Dynamics*, Vol. 1 & 2, 2nd ed., Springer Series in Computational Physics, Springer-Verlag, New York, 1991.

[25] Friedmann, M., Gillis, J. & Liron, N. Laminar Flow in a Pipe at Low and Moderate Reynolds Numbers, *Appl. Sci. Res.*, **19**, pp. 426-438, 1968.

[26] Galerkin, B.G. Torsion of a Triangular Prism, *Petrograd Acad. Sci. Bull.*, **13**, pp. 111-118, 1919.

[27] Garg, V.K. Developing Flow in a Rectangular Duct. in *Numerical Methods in Laminar and Turbulent Flow* (eds. Taylor, C., Johnson, J.A. and Smith, W.R.), pp. 58-68, Proc. of 3rd Int. Conf. ,Seattle, Pineridge Press, U.K., 1983.

[28] Gillis, J. & Shimshoni, M. Initial Flow in the Entrance of a Straight Circular Pipe, *J.R.Aeronaut. Soc.*, **70**, pp. 368-369, 1966.

[29] Gillis,J. & Brandt, A. The Numerical Integration of the Equations of Motion of a Viscous Fluid, *Sci. Rep. No 63-73*, Air Force Eur. Off. Aerosp. Res., Rehovoth, Israel, 1964.

[30] Goldstein, R.J. & Kreid, D.K. Measurement of Laminar Flow Development in a Square Duct Using a Laser-Doppler Flowmeter, *J. Appl. Mech.*, **35**, pp. 813-818, 1967.

[31] Goldstein, S. *Modern Development of Fluid Dynamics*, Vol.I, Oxford Univ. Press, London, 1938.

[32] Govinda Rao, N.S., Ramamoorthy, M.V. & Sarma, K.V.N., Study of Transition Zone of Laminar Flow at the Entrance to a Pipe Based on Varying Friction, *Proc. Natl. Inst. Sci. India*, Part A, **32**, pp. 266, 1966.

[33] Graetz, L., On the Motion of Fluids in Tubes, *Z. Math. Phys.*, **25**, pp. 316-334, 375-404, 1880.

[34] Greenhill, A.G. On the Flow of Viscous Liquid in a Pipe or Channel, *Proc. London Math. Soc.*, **13**, pp. 43-46, 1881.

[35] Griffith, A.A. The Use of Soap Films in Solving Stress Problems. *J. Am. Soc. Mech. Eng.*, **40**, pp. 276-277, 1918.

[36] Gubin, V.E. & Levin, V.S. Fluid Flow in the Entrance Region of a Circular Tube, *J. Eng. Phys. (USSR)*, **15**, pp. 635-637, 1968.

[37] Gupta, R.C. Flow Development in the Hydrodynamic Entrance Region of a Flat Duct, *AIChE J.*, **11**, pp. 1149-1151, 1965.

[38] Gupta, R.C. Laminar Flow in the Entrance of a Tube, *Appli. Sci. Res.* **33**, pp. 1-10, 1977.

[39] Hagen, G. Movement of Water in a Narrow Cylindrical Tube, *Ann. Phys. Chem.*, **46**, pp. 423-442, 1839.

[40] Han, L.S. & Cooper, A.L. Approximate Solutions of Two Internal Flow Problems-Solution by an Integral Method, *Proc. U.S. Natl. Congr. Appl. Mech.*, 4th, pp. 1269-1278, 1962.

[41] Han, L.S. Hydrodynamic Entrance Lengths for Incompressible Laminar Flow in Rectangular Ducts, *J. Appl. Mech.*, **27**, pp. 403-409, 1960.

[42] Han, L.S. Simultaneous Developments of Temperature and Velocity Profiles in Flat Ducts, *Int. Dev. Heat Transfer*, pp. 591-597, Proc. Heat Transfer Conf., Boulder Colorado, Part III, 1961.

[43] Hood, P. & Taylor, C., Navier-Stokes Equations Using Mixed Interpolation, *Proc. 1st Int. Conf. on Finite Element Method in Flow Problems*, Swansea, 1974.

[44] Hornbeck, R.W. Laminar Flow in the Entrance Region of a Pipe, *Appl. Sci. Res.*, Sect. A, **13**, pp. 224-232, 1964.

[45] Kapila, A.K., Ludford, G.S.S. & Olunloyo, V.O.S. Entry Flow in a Channel. Part 3, Inlet in a Uniform Stream, *J. Fluid Mech.*, **57**(4), pp. 769-784, 1973.

[46] Kolossoff, M.C. Sur la Torsion Des Prismes Ayant pour Base un Triangle Rectangle, *Comptes Rendus, Academic des Sciences, Paris*, **178**, pp. 2057-2060, 1924.

[47] Langhaar, H.L. Steady Flow in the Transition Length of a Straight Tube, *J. Appl. Mech.*, **9**, pp. A55-A58, 1942.

[48] Langlois, W.E. *Slow Viscous Flow*, The Macmillan Company, New York, pp. 118-119, 1964.

[49] Lees, C.H On the Effect of the Form of the Transverse Section on the Frictional Resistance to the Motion of an Elongated Body Parallel to Its Length through a Fluid, *Proc. Roy. Soc. London*, **92**, Series A, pp. 144-157, 1916.

[50] Leite, R.J. An Experimental Investigation of the Stability of Axially Symmetric Poiseuille Flow, *Univ. of Michigan Report IP-188*, 1956.

[51] Love, A.E.H. *A Treatise on the Mathematical Theory of Elasticity*, Dover Publications, New York, pp.311-323, 1944.

[52] Lundgren, T.S., Sparrow, E.M. & Starr, J.B. Pressure Drop Due to the Entrance Region in Ducts of Arbitrary Cross Section, *J. Basic Eng.*, **86**, pp. 620-626, 1964.

[53] Manohar, R. Analysis of Laminar Flow Heat Transfer in the Entrance Region of Circular Tubes, *Int. J. Heat Mass Transfer*, **12**, pp. 15-22, 1969.

[54] Maslen, S.H. Transverse Velocities in Fully Developed Flows. *Quart. Appl. Math.*, **16**, pp. 173-175, 1958.

[55] McComas, S.T. Hydrodynamic Entrance Lengths for Ducts of Arbitrary Cross Section, *J. Basic Eng.*, **89**, pp. 847-850, 1967.

[56] McDonald, J.N., Denny, W.E. & Mills, A.F. Numerical Solutions of the Navier-Stokes Equations in the Inlet Regions, *J. Appl. Mech.*, **39**, pp. 873-878, 1972.

[57] Miller, J.A. Laminar Incompressible Flow in the Entrance Region of Ducts of Arbitrary Cross Section, *J. Eng. Power.*, **93**, pp. 113-118, 1971.

[58] Miller, R.W. & Han, L.S. Pressure Loses for Laminar Flow in the Entrance Region of Ducts of Rectangular and Equilateral Triangular Cross Section, *J. Appl. Mech.*, **38**, pp. 1083-1087, 1971.

[59] Morihara, H. & Cheng, R.T. Numerical Solution of the Viscous Flow in the Entrance Region of Parallel Plates, *J. Comput. Phys.*, **11**, pp. 550-572, 1973.

[60] Muchnik, G.F., Solomonov, S.D. & Gordon, A.R. Hydrodynamic Development of a Laminar Velocity Field in Rectangular Channels, *J. Eng. Phys. (USSR)*, **25**, pp. 1268-1271, 1973.

[61] Narang, B.S. & Krishnamoorthy, G., Laminar Flow in the Entrance Region of Parallel Plates, *J. Appl. Mech.*, **43**, pp. 186-188, 1976.

[62] Natio, E. & Hishida, M. Laminar Boundary Layers in the Entrance Regions of Two Parallel Plates and a Circular Tube. *Nagoya Kogyo Daigaku Gakuho (In Japanese)*, **24**, pp. 143-151, 1972.

[63] Natio, E. Laminar Heat Transfer in the Entrance Region between Parallel Plates-the Case of Uniform Heat Flux, *Heat Transfer-Jpn. Res.*, **4**(2), pp. 63-74, 1975.

[64] Navier, C.L.M.H. On the Laws of Motion of Fluids Taking into Consideration the Adhesion of the Molecules. *Ann. Chem. Phys.*, **19**, pp. 234-245, 1821.

[65] Olson, M.D. Comparison of Various Finite Element Solution Methods for the Navier-Stokes Equations, *Proc. Int. Conf. on Finite Elements in Water Resources*, Princeton Univ., 1976.

[66] Prandtl, L. On the Torsion of Prisms, *Physik, Z.*, **4**, pp. 758-759, 1903.

[67] Prandtl, L. & Tietjens, O.G. *Applied Hydro and Aerodynamics*, Dover Pubilications Inc., New York, pp. 25, Fig.13, 1957.

[68] Paschoud, M. On the Problem of Uniform Regime in a Cylindrical Tube Whose Section is a Right Angled Isosceles Triangle, *Compt. Rend. Academic des Sciences, Paris*, **179**, pp. 379-381, 1924.

[69] Paschoud, M. Calculation by Means of Polynomials of the Velocities for Uniform Regime in Cylindrical Tubes Whose Sections are Regular Polygons, *Compt. Rend. Academic des Sciences, Paris*, **179**, pp. 451-454, 1924.

[70] Patankar, S.V. & Spalding, D.B. A Calculation Procedure for Heat, Mass and Momentum Transfer in Three-Dimensional Parabolic Flows, *Int. J. Heat Mass Transfer*, **15**, pp. 1787-1806, 1972.

[71] Pfenninger, W. Experiments with Laminar Flow in the Inlet of a Tube at High Reynolds Numbers with and without Boundary Layer Suction, Northrop Aircraft, Inc. Hawthorne, Calif, 1952.

[72] Poiseuille, J.L.M. Researches on the Causes of the Motion of the Blood in Capillary Vessels, *Mem. Acad. Roy. Sci*, **7**, pp. 105-175, 1840.

[73] Poisson, S.D. Memoir on the General Equations of the Equilibrium and Motion of Elastic Solid Bodies and Fluids, *J. Ecole Polytech.*, **13**, pp. 1-174, 1831.

[74] Polya, G. Torsional Rigidity, Principal Frequency, Electrostatic Capacity and Symmetrization, *Quart. Appl. Math.*, **6**, pp. 267-277, 1948.

[75] Reshotko, E. Experimental Study of the Stability of Pipe Flow, Jet Propulsion Laboratory, California Institute of Technology Progress Report No. 20-364, 1958.

[76] Roidt, M. & Cess, R.D. An Approximate Analysis of Laminar Magnetohydrodynamic Flow in the Entrance Region of a Flat Duct, *J. Appl. Mech.*, **29**, pp. 181-187, 1962.

[77] Rubin, S.G., Khosla, P.K. & Saari, S. Laminar Flow in Rectangular Channels, *Computers and Fluids*, **5**, pp. 151-173, 1977.

[78] Saint-Venant, B.de. Friction Coefficient of Fluids in Channels or Prismatic Tubes, *Compt. rend.*, **17**, pp. 1240-1243, 1843.

[79] Saint-Venant, B.de. Memoires Savants Etrangers, **14**, 1855.

[80] Schlichting, H. Laminare Kanaleinlaufstromung, *Z. Angew. Math. Mech.*, **14**, pp. 368-372, 1934.

[81] Schlichting, H. *Boundary-Layer Theory*, McGraw-Hill Book Company, New York, 1968.

[82] Schiller, L. Die Entwiklung der Laminaren Geshwindigkeitsverteilung und ihre Bedeutung fur Zahigkeitmessungen, *Z. Angew. Math. Mech.*, **2**, pp. 96-106, 1922.

[83] Schmidt, F.W. & Zeldin, B. Laminar Flow in Inlet Sections of Tubes and Ducts. *Proc. Fluids Intern. Flows, Dept. Mech. Eng.*, The Pennsylvania State Univ. Park, Part II, pp. 211-251, 1968.

[84] Schmidt, F.W. & Newell, M.E. Heat Transfer in Fully Developed Laminar Flow through Rectangular and Isosceles Triangular Ducts, *Int. J. Heat Mass Transfer*, **10**, pp. 1121-1123, 1967.

[85] Schmidt, F.W. & Zeldin, B. Laminar Flow in Inlet Sections of Tubes and Ducts., *AIChE J.*, **15**, pp. 612-614, 1969.

[86] Shah, R.K. & London, A.L. *Laminar Flow Forced Convection in Ducts, Supplement to Advances in Heat Transfer*, Academic Press, New York, 1978.

[87] Shapiro, A.H., Siegel, R. & Kline, S.J. Friction Factor in the Laminar Entry Region of a Smooth Tube, *Proc. U.S. Natl. Congr. Appl. Mech.*, 2nd, Am. Soc. Mech. Eng., New York, pp. 733-741, 1954.

[88] Shepperd, W.M. The Torsion of a Cracked Shaft, *Engineering*, **128**, pp. 39, 1929.

[89] Siegel, R. The Effect of Heating on the Boundary Layer Transition for Liquid Flow in a Tube, DSc thesis, Massachusetts Institute of Technology, 1953.

[90] Sokolnikoff, I.S. *Mathematical Theory of Elasticity*, Ist ed., McGraw-Hill Book Company, New York, pp. 127-150, 1946.

[91] Sparrow, E.M., Hixon, C.W. & Shavit, G. Experiments on Laminar Flow Development in Rectangular Ducts, *J. Basic Eng.*, **89**, pp. 116-124, 1967.

[92] Sparrow, E.M., Lin, S.H. & Lundgren, T.S. Flow Development in the Hydrodynamic Entrance Region of Tubes and Ducts, *Phys. Fluids*, **7**, pp. 338-347, 1964.

[93] Stokes, G.G. On the Theories of the Internal Friction of Fluids in Motion and of the Equilibrium and Motion of Elastic Solids, *Trans. Camb. Phil. Soc.*, **8**, pp. 287-319, 1845.

[94] Stroud, A.H. & Secrest, D. *Gaussian Quadrature Formulas*, Prentice Hall Inc., Englewood Cliffs, New Jersy, 1966.

[95] Tao, L.N. On Some Laminar Forced Convection Problems, *J. Heat Transfer*, **83**, pp. 466-471, 1961.

[96] Tao, L.N. Heat Transfer of Laminar Forced Convection in Indented Pipes, *Developments of Mechanics*, Vol.1 (eds. Lay, J.E. and Malvern, L.E.), pp. 511-525, Proc. of the 7th Midwestern Mechanics Conference held at Michigan State Univ., Sept. 6-8, 1961.

[97] Tao, L.N. Mehtod of Conformal Mapping in Forced Convection Problems., Int. Dev. Heat Transfer, *Proc. Heat Transfer Conf.*, Boulder, Colorado, Part 3, pp. 598-606, 1961.

[98] Targ, S.M. *Osnovnye Zadachi Teorii Laminarnykh Techenyi*, Gostekhizdat Press, Moscow, 1951.

[99] Taylor, G.I. The Determinations of Stresses by means of Soap Films. in *The Mechanical Properties of Fluids*, Blackie and Son, London, 1923.

[100] Taylor, J.L. The Torsion of a Cracked Shaft, *Engineering*, **128**, pp. 150, 1929.

[101] Timoshenko, S.P. & Goodier, J.N. *Theory of Elasticity*, McGraw-Hill Book Company, New York, pp. 294-313, 1970.

[102] Van Dyke, M. Entry Flow in a Channel, *J. Fluid Mech.*, **44**, pp. 813-823, 1970.

[103] Vrentas, J.S., Duda, J.L. & Bargeron, K.G. Effect of Axial Diffusion of Vorticity on Flow Development in Circular Conduits: Part I. Numerical Solutions, *AIChE J.*, **12**, pp. 837-844, 1966.

[104] Wang, Y.L. & Longwell, P.A. Laminar Flow in the Inlet Section of Parallel Plates, *AIChE J.*, **10**, No. 3, pp. 323-329, 1964.

[105] Wiginton, C.L. & Dalton, C. Incompressible Laminar Flow in the Entrance Region of Ducts, *J. Appl. Mech.*, **37**, pp. 854-856, 1970.

[106] Wiginton, C.L. & Wendt, R.L. Flow in the Entrance Region of Ducts, *Phys. Fluids*, **12**, pp. 465-466, 1969.

[107] Wiginton, C.L. Flow in the Entrance Region of Noncircular Ducts, *Phys. Fluids*, **18**, pp. 488-490, 1975.

[108] Williamson, J.W. Decay of Symmetrical Laminar Distorted Profiles between Flat Parallel Plates, *J. Basic Eng.*, **91**, pp. 558-560, 1969.

[109] Wilson, S.D.R. Entry Flow in a Channel. Part 2, *J. Fluid Mech.*, **46**(4), pp. 787-799, 1971.

[110] Yadoff, O. Sur les ecoulements a la Poiseuille, *Compt. Rend. Academic des Sciences, Paris*, **223**, pp. 192-193, 1946.

[111] Yadoff, O. Sur le Calcul des debis dans les ecoulements permanents a la Poiseuille, *Compt. Rend. Academic des Sciences, Paris*, **224**, pp. 374-376, 1947.

[112] Zamir, M. Similarity and Stability of the Laminar Boundary Layer in a Streamwise Corner, *Proc. Roy. Soc. London*, **377**, Series A, pp. 269-288, 1981.

[113] Zamir, M. & Camiletti, S.E. Characteristics of Poiseuille Flow in a Divided Channel, *Aero. Quart*, **33**, pp. 59-72, 1982.

[114] Zienkiewicz, O.C. *The Finite Element Method*, McGraw Hall Book Company, London, 1977.